

University of Cincinnati

Date: 6/26/2020

I, **Jing Liu**, hereby submit this original work as part of the requirements for the degree of Doctor of Philosophy in Chemistry.

It is entitled:

Application of Novel ROS sensitive Prodrug on Sunscreen

Student's name: **Jing Liu**

This work and its defense approved by:

Committee chair: Edward Merino, Ph.D.

Committee member: Ana Luisa Kadekaro, Ph.D.

Committee member: David Smithrud, Ph.D.

Committee member: Peng Zhang, Ph.D.



36736

Application of Novel ROS sensitive Prodrug on Sunscreen

A dissertation submitted to the
Graduate School
of the University of Cincinnati
in Partial Fulfillment of the
Requirements for the Degree of

DOCTOR OF PHILOSOPHY (Ph.D.)

In the Department of Chemistry
of McMicken College of Arts and Sciences by

Jing Liu

M.S., Chemistry,
University of Cincinnati, McMicken College of Arts & Science, 2015

B.S., Chemistry,
NanKai University, College of Chemistry, 2012

Dissertation Advisor: Edward J. Merino, Ph.D.

Abstract

Reactive oxygen species(ROS) are a family of radical and non-radical byproducts of aerobic metabolism. It plays essential roles as secondary signaling molecules in cell proliferation, differentiation, senescence, and apoptosis. Ultraviolet radiation (UVR) overexposure can upregulate ROS in skin cells and results in further damage to deoxyribonucleic acid (DNA), protein, and lipid. As UVR is an essential risk factor for the development of premalignant skin lesions as well as of melanoma and nonmelanoma skin cancer, sunscreen agent was developed to prevent it.

The chemoprevention strategy is found and developed since 1976, which is being developed to present. It includes two different types: one is applying the chemical which can absorb or reflect UVR to prevent UVR radiation on the skin surface, the other type affects the metabolism of skin cells to stop the cell damage and malignant initiation. The second category is developing fast in the most recent 20 years to meet the need of human beings. A series of antioxidants and natural products prove to effectively prevent UVR by reducing the ROS level by ROS scavenging or as an inhibitor of the ROS generator. And a ROS-activated prodrug strategy is developed to enhance the selectivity of chemoprevention.

The first project was finished by designing a novel ROS-activated moiety attached with apocynin, which is not only an antioxidant but a nicotinamide adenine dinucleotide phosphate oxidase(NOX) inhibitor. Releasing manner about it was studied by high-performance liquid chromatography (HPLC) and mass spectrometry (MS). The skin protection function of it was further proved by gel electrophoresis, dichlorofluorescein diacetate(DCFDA) assay, MTT assay, western blot, and

cyclobutane pyrimidine dimers (CPD) quantification. To sum, this prodrug was proved to release the NOX1 inhibitor and protect the DNA from UVR radiation by lowering the ROS level.

Considering the drug attached has a controversial mechanism to inhibit ROS generation after releasing it. In the second project, I designed two ROS-activated moieties and attached them with a natural antioxidant and a NOX1 inhibitor. Then releasing manners of each was verified with HPLC and MS. They show the potential to be tested by cells to be further evaluated in the future.

In the last project, a new ROS-quantification assay was designed base on the gas chromatography-headspace-mass spectrometry (GCHSMS) system. The probes were designed by attaching a diethylamine to a ROS-active moiety as an analyte. Limit of detection (LOD) and limit of quantification (LOQ) were verified by GCHSMS. Releasing behavior of two different probes were tested by HPLC and GCMS. It proves the potential of them to be further evaluated by cell assay.

To sum up, all three projects I worked on the aim to prevent UVR radiation-induced melanoma by lowering ROS. Base on a ROS-active strategy, selectivity, and stability of them are improved. A new quantification assay of ROS is being developed to provide another simple method for further ROS study.

Acknowledgment

I would like first to express my sincere gratitude to my committee chair and my research advisor Dr. Edward Merino. His patient help and wisely guidance motivate and enlighten me to finish all the research and thesis. Dr. Merino is not only a perfect mentor but also a wise senior to me for working with. Then I would like to extend my gratitude to my other committee member Dr. David Smithrud, Dr. Peng Zhang, and Dr. Kadekaro Ana Luisa for the hard question but which is thought-refreshing and motivative encouragement that they offered year by year. Thanks for Kadekaro Ana Luisa, Dr. Julio Landero-Figueroa, and Dr. Stephen Macha for the help they provide in all parts of my experiments as collaborators. Thanks to the Department of Chemistry at the University of Cincinnati for the opportunity I provided to pursue knowledge and exciting life. My sincere thanks also go to Dr. Stephen Macha, Dr. Larry Sallans, and Dr. Keyang Ding, who trained me for the instrument use and authorized me to the research facilities.

I am grateful for the love, encouragement, and tolerance of Tingyu Zhao, the woman who has made my life different. Without her support, I could not have completed this journey. She is always there when I need it most.

For the present and past labmates; of Merino lab, Dr. Anish K Vadukoot, Dr. Purujit Gurjar, Dr. Kaylin Earnest, Dr. Safnas Abdulsalam, Dr. F. Shazna Thowfeik, Gurdatt Premnauth, Senevirathne Priyangika, Alyssa Sterling and Nazanin Mokhtarpour: thanks all for the support and encouragement you gave me. The moment we share thought and food is the memory I will keep for my life. I would also like to thank to the undergraduate researchers I worked with, I also

learned a lot from you when we are working together. Thanks to my friends at UC: you are all supportive and motive for my daily life.

Finally, I'm extremely grateful to my family, who give me life as the biggest present. Father showed me the sprite and morale to be a good man. Mother nurture me with consideration and empathy. That's made me today as a man who stands with courage and sympathy.

Table of Contents

Chapter 1	10
Introduction.....	10
1.1 The role of reactive oxygen species (ROS) in cells	11
1.2 ROS, DNA damage, and UVR induced melanoma	12
1.3 Chemoprevention strategies to prevent melanoma.....	13
1.3.2 ROS reduction: direct antioxidant treatments to reduce UVR induced ROS.....	16
1.3.3 Natural products to reduce UVR induced ROS: mechanisms and effects.....	16
1.4 NOX inhibitor as a chemoprevention strategy	17
1.4.1 NOX Biochemistry	17
1.4.2 Known NOX inhibitors.....	18
1.4.3 Why target NOX	20
1.5 ROS activated prodrug strategies	20
1.5.1 The Merino lab strategy	21
1.5.2 Other Strategies	23
1.6. Goals of this Dissertation.....	24
1.7. Overview of Chapter 2.....	24
1.8. Overview of Chapter 3.....	25
1.9. Overview of Chapter 4.....	25
Chapter 2 UV cell stress induces oxidative cyclization of a protective reagent for DNA damage reduction in skin explants	27
2.1 Introduction.....	28
2.2 Experiment section.....	31
2.2.1 Synthesis and characterization of compounds	31
2.2.2 Oxidation study	51
2.2.3 HPLC condition for oxidation studies.....	52
2.2.4 pUC19 ASSAY	53
2.2.5 ABTS Assay	53
2.2.6 Cell Culture	54
2.2.7 Efficacy of RIP Reagent in Cellular Environment.....	54
2.2.8 Quantifying Damage by LC-MS.....	54
2.2.9 DCFDA assay by flow cytometry.....	55
2.3 Results and Discussion.....	56

2.3.1 Compound 1 could release apocynin as a prodrug.	56
2.3.2 Compound 1 could protect skin cells from UVR irradiation without damaging health cells.	59
2.3.3 Application of Compound 1 in skin explants.....	62
2.4 Conclusions.....	64
Chapter 3.....	65
UV cell stress-induced protective reagent based on natural product and NOX inhibitor.....	65
3.1 Introduction.....	66
3.2 Experiment section.....	68
3.2.1 Synthesis and characterization of compounds.....	68
3.2.2 Oxidation study.....	79
3.2.3 HPLC condition for oxidation studies.....	79
3.2.4 DCFDA assay by flow cytometry.....	80
3.3 Results and Discussion.....	80
3.3.1 Compound SA1 could release sesamol as a prodrug.	80
3.3.2 Compound RIP2 could release ML171 as a prodrug.	82
3.3.3 RIP2 could reduce the ROS level in the cell.	83
3.4 Conclusions.....	85
Chapter 4:.....	86
Novel ROS quantification technique based on GCMS.....	86
4.1 Introduction.....	87
4.2 Experiment section.....	89
4.2.1 Synthesis and characterization.....	89
4.2.2 Oxidation study.....	97
4.2.3 HPLC condition for oxidation studies.....	97
4.2.4 GCMS assay.....	98
4.3 Results and Discussion.....	98
4.3.1 Diethylamine shows a good LOQ on GCMS.....	98
4.3.2 Oxidation study of DEASOR-OH.....	99
4.4 Conclusions.....	102
Reference.....	103
Abbreviations List.....	113
Appendices.....	108
Appendices S1: Reagent 1 reaction with Fenton generated hydroxyl radical is diffusion controlled.	108

Appendices S2: ABTS Inhibition Study	109
Appendices S3: The effect of compound 2 and a compound lacking apocynin release on viability and UVR rescue	110
Appendices S4: Compound releasing in Neonatal human keratinocytes cell (NHKC) after irradiation	111
Appendices S5: Uptake of 1 and apocynin by cells	112
Appendices S6: Western blot for Apocynin	113

List of Figures

Chapter 1:

Figure 1.1 The ROS production produced and how it leads the cancer initiation.	11
Scheme 1.1 Small molecule NOX inhibitors.....	19
Scheme 1.2 Mechanism of MA14 oxidation.....	21
Figure 1.2 Design of novel ROS-active prodrug.....	22
Figure 1.3 Mechanism of ROS-active linkers.....	23
Figure 2.1 ROS (brown) are normally present, but UV radiation enhances the formation of highly toxic species (underlined) that damage DNA. RIP reagents, such as the apocynin-linked compound 1 shown, eject an oxidase inhibitor in high oxidative stress environments. Apocynin (red) binds NADPH oxidase-associated factors NCF1 and NCF2 to limit further ROS production. Structure from PDB 1K4U in reference 21.....	30
Scheme 2.1 Compound 1 self cyclizes and oxidizes to form final product 1^{OX}	31
Scheme 2.2 The synthesis route of compound 1	32
Scheme 2.3 The Synthesis route for 2	43
Figure 2.2 (A) Proposed reaction of 1 to release apocynin and generate 1^{OX} . The control compound 2 lacks an oxidizable phenol. (B) HPLC analysis of 1 incubated in phosphate buffer (gray trace) and under Fenton conditions (black trace); the organic (left) and aqueous (right) layers were analyzed. Pure Apo was also analyzed (red trace), and peak corresponding to 1^{OX} and Fenton reagent are indicated. (C) MS of isolated products. (D) Sensitivities of 1 (black) and 2 (purple) to various ROS forms. (E) Antioxidant capacity as measured by ABTS assay. The obtained EC ₅₀ values are shown. (F) Fraction of 1 in solution not subjected to irradiation and irradiated with 10 SED.	57
Figure 2.3 (A) Gel electrophoretic separation of supercoiled and nicked plasmid in the presence and absence of Fenton reagent and compound 1 . (B) Viability of primary keratinocytes in a range of concentrations of 1 . (C) Production of Apo in skin cells treated with 50 μ M 1 with and without irradiation with 10 SED. (D) Viability of primary keratinocytes without (gray bars) and with 10 SED UVR (red bars) in the presence of the indicated antioxidants. (E) Relative LCMS quantification of 8-oxo-7,8-dihydro-2'-deoxyguanosine under UVR and 1 treatment. (F) Dichlorodihydrofluorescein diacetate fluorescence measurements under UVR and 1 treatment.	60
Figure 2.4 (A) Representative image of skin explant. (B) Western blot analysis of p53 production in skin explants treated or not with 1 and subjected or not to UVR. Actin protein shown as a control. (C) Representative immunofluorescence images of skin explants treated with DMSO or 1 and subjected to 10 SED irradiation. Red indicates the presence of CPDs; nuclei were stained with DAPI (blue). (D) Quantification of CPD-positive cells per mm ² of non-irradiated (black bars) and irradiated (red bars) skin treated with DMSO (-), compound 1 , or catalase (CAT).....	63
Figure 3.1 UVR induced ROS upregulation leads to skin cancer.....	67

Figure 3.2 ROS activated prodrug base on natural products.....	68
Scheme 3.3 The synthesis route of compound SA1	69
Scheme 3.4 The Synthesis route for RIP2	76
Figure 3.3 (A) Proposed reaction of SA1 to release sesamol and generate SA1^{OX} . (B) HPLC analysis of SA1 incubated in phosphate buffer (black trace) and under HRP conditions (blue trace). Pure sesamol sample was also analyzed (mint trace). (D) Sensitivities of SA1 to various ROS forms.	81
Figure 3.4 (A) Proposed reaction of RIP2 to release ML171 and generate RIP2^{OX} . (B) HPLC analysis of RIP2 incubated in phosphate buffer (black trace) with H ₂ O ₂ (red trace) and under HRP conditions (blue trace). (C) MS of isolated products.	82
Figure 3.5 H ₂ O ₂ inhibitor of RIP2 as a NOX1 inhibitor under Dichlorodihydrofluorescein diacetate fluorescence measurements.....	84
Figure 4.1 Dichlorodihydrofluoresceindiacetate (DCFHDA)intracellular reaction to release fluorescence	88
Figure 4.2 ROS quantification assay designed base on GCHSMS and a volatile amine.....	89
Scheme 4.3 The synthesis route of compound DEASOR-OH	90
Scheme 4.4 The synthesis route of compound BDEASOR	93
Figure 4.3 (A) Exact mass of Diethylamine (B) GCMS of Diethylamine (C) LOD and LOQ with the calibration curve.....	99
Figure 4.4 (A) Proposed reaction of DEASOR-OH to release diethylamine as the probe. (B) HPLC analysis of DEASOR-OH degradation on time scale in phosphate buffer under HRP conditions. (C) Reaction order of DEASOR-OH	100
Figure 4.5 (A) Proposed mechanism of BDEASOR to release diethylamine as the probe. (B) GCHSMS analysis of BDEASOR under H ₂ O ₂ condition (purple trace). Also, the pure Diethylamine is analyzed under the same condition (pink trace).....	101

Chapter 1

Introduction

1.1 The role of reactive oxygen species (ROS) in cells

Reactive oxygen species (ROS) have been found and studied for the most recent century. ROS stands for a family consist of non-radical and radical species. Non-radical species are hydrogen peroxide (H_2O_2) and singlet oxygen. Free radicals in redox biology are superoxide radical ($\text{O}_2^{\bullet-}$) and hydroxyl radical ($\bullet\text{OH}$). The first ROS form, H_2O_2 , was discovered in the 1800s and widely used in disinfecting products as its active oxidative function. Then the superoxide radical was discovered based on the theory of quantum mechanics in 1933. Hydroxyl radical was discovered by Haber and Weiss by analyzing a reaction containing H_2O_2 with $\text{O}_2^{\bullet-}$ in 1934. What is more, their new roles in the cells as a second signaling messenger is being elucidated.¹

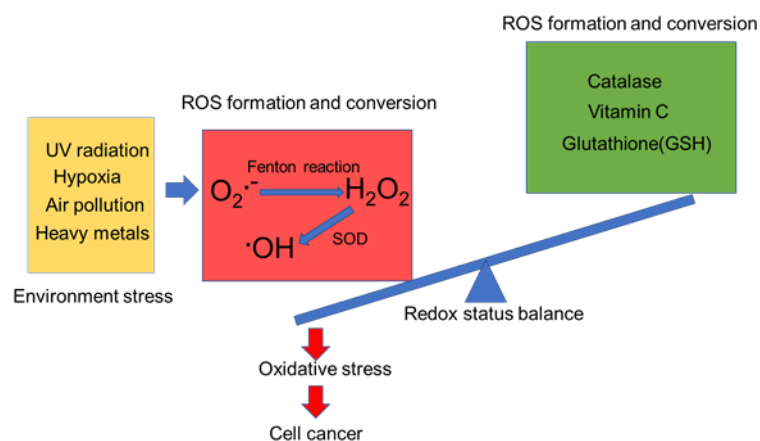


Figure 1.1 The ROS production produced and how it leads the cancer initiation.

Endogenous ROS are mainly produced from oxygen-containing pathways such as mitochondrial respiration, NOX haloenzyme complexes, peroxysomes, and within the endoplasmic reticulum (ER).²⁻³ In addition signaling cascades used in cellular metabolism force cells to keep a specific amount of ROS to exist that is subtly balanced by antioxidant capacity.⁴⁻⁵ The three different ROS forms can interconvert in cells (**Figure1.1**). Moreover, cells have different tolerance for each ROS form from evolution. ROS signaling plays an essential role in the proliferation, differentiation,

senescence, and apoptosis of the cell. ROS is a cellular signal messenger to sustain the proliferation and differentiation of the cell at a low level by reacting with thiols to form disulfides and thioethers to form sulfoxides. However, a high level of ROS leads to oxidative stress by reacting with protein, DNA, or lipids.⁶ Thus, the balance of ROS and antioxidants is pivotal to cell survival. There are many causes for increasing the ROS level and induce cell damage. **(Figure1.1)**

1.2 ROS, DNA damage, and UVR induced melanoma

Ultraviolet radiation(UVR) is one of the sources which increases the levels of ROS when cells are exposed.⁷ UVR stress happens naturally and ubiquitously all over the world on a daily base. UVR can be further divided into three bands: UVA (320 to 400 nm), UVB (290-320 nm), and UVC (200-290 nm). The solar emitted UVR will only reach the earth with at the following percentages: 95-98% for UVA; 2-5% for UVB; 0% for UVC. UVC is absorbed by ozone. Once UVR reaches skin the stratum corneum and epidermis will absorb most of the UVB.⁸ However, UVA will penetrate the skin and deliver radiation deep into the dermis.⁹ It is inevitable that each individual will get exposed to the UVR since it is necessary for normal physiological function. However, UVR leads to skin cancer and malignant melanoma upon overexposure.¹⁰

UVR radiation will damage the DNA and lead to cell apoptosis or cancer by several different mechanisms.¹¹ ROS generated during UVR exposure is one of the primary reasons.¹² Direct ROS formation occurs when oxygen reacts with a UVR excited molecule and accepts an electron and then is protonated, forming superoxide. First, catalase is known to be able to degrade hydrogen peroxide in normal cells¹³. However, the UVR will excite the heme iron, which is the binding site of hydrogen peroxide after epidermis penetration. The excitation will alter the binding site of

hydrogen peroxide to allow the water to access the heme iron to produce the protons, which can interact with molecular oxygen to produce ROS. Then, UVR can increase the ROS levels in cells¹⁴, and it will turn to react with iron-sulfur proteins to disrupt their structure, which releases reducing ferrous iron to elevate the production of ROS further. Alternatively, UVR may also indirectly elevate the ROS level by affecting the signaling pathway like protein kinase C(PKC).¹⁵ It shows that UVR will depress the expression of PKC δ and level up the ROS generation.

ROS generation could lead to DNA lesions upon exceeding the antioxidant capacity.¹⁶ Upregulated ROS production proceeds the oxidation of the DNA base. Then the oxidation at the ribose leads to strand breaks, which are primarily repaired by nucleotide excision repair(NER). At last, the carcinogenesis happen because of replication of DNA damage as lacking efficient repair by The Furthermore, Guanine is the primary target as its favorable potential(-1.3V) to be oxidized to be guanine cation radical. It will catch the oxygen and oxidized further to 8-oxo-7,8-dihydro-2'deoxyguanosine(8-oxo-dG) lesion which generally used as promising tumor marker.¹⁷

Human skin is the primary organism exposed to UVR heavily since its significant surface area day by day. It takes a high chance to undertake UV-induced oxidative stress. The accumulated ROS may lead to the upregulation of the melanin, cell apoptosis, and even malignant melanoma as the increase in DNA damage. It is vital to protect the skin from exceeding UVR exposure considering the pathological UV-induced ROS production.

1.3 Chemoprevention strategies to prevent melanoma

1.3.1 Sunscreens: how they work and their current issues

It is considering the pronounced acute and chronic effects on the skin. What is more, the depletion of the atmospheric ozone layer may induce the increasing level of the UVB and UVC irradiation. The increasing risk of overexposed to UVR contributes to a higher risk of skin cancer. Melanoma widely exists with a fast rate of 95830 cases from previous year.¹⁸ It is a malignancy skin cancer and known for its aggressive type and high lethality. Because of the truth that it is inevitable to avoid UVR exposure for human daytime activities and the manner of solar bath for tan skin, the growth of the anti-melanoma strategy is an inner need for the human being.

The sunscreen can be classified as organic sunscreens and inorganic reagents. Organic sunscreen reagents include derivatives of anthranilates¹⁹, benzophenones²⁰, camphor, cinnamates, dibenzoyl methane, *p*-aminobenzoates, and salicylates.²¹ They can absorb UV radiations within a particular range of wavelengths, depending on their chemical structure and convert the remaining energy into low energy radiation (of a longer wavelength above 380nm). Inorganic sunscreens will physically absorb or reflect the UV radiation by molecular rearrangement (size, shape, and appearance change) without changing the internal structures.²²⁻²³ Zinc oxide (ZnO) and Titanium dioxide (TiO₂) are examples of inorganic sunscreens that are well used.²⁴ It reports that the sunscreen with an SPF of 15 provides >93% protection against UVB. Protection against UVB is increased to 97% with SPF of 30+.

However, the sunscreen has disadvantages for health concern. Organic UV sunscreen will absorb the UV and break down to intermediate, which will be directly absorbed by the skin.²⁵⁻²⁶ Many of oxidized organic molecules lead to oxidative stress by redox cycling that promotes ROS generation. Such as 4-*tert*-Butyl-4'-methoxy dibenzoyl methane, which is known as avobenzone. However, It

is widely used as a sunscreen agent. But it could degrade to allergic sources under photodegradation²⁵. Another sunscreen agent, octocrylene, proved to generate a high level of ROS in the cytoplasm of the nucleated keratinocytes²⁷. Other than the harmful effect on human health, high use of sunscreen reagents may lead to significant environmental hazards.²⁸⁻³⁰ The inorganic reagents are known to be lethal to invertebrates.³¹ The organic sunscreen reagents like oxybenzone, octocrylene, octisalate, and avobenzone may reduce the UV light penetration to the water and affect the ecosystem.³² The increased usage of sunscreen and the fact that at least 25% of applied sunscreen washes off in the water leads to poor environmental outcomes in locations with many tourists.³⁰ The stress on the aquatic ecosystem should also be a concern, especially coral reefs. Furthermore, sunscreen product lacks effectiveness on free radical prevention UVA-induced, which is recently worked out as a primary cause for skin cancer.

Chemoprevention is first used by Sporn et al. in 1976s.³³ It is a relatively new and promising strategy that generally use synthesized or natural products to slow down or stop the carcinogenesis progression.³⁴ Chemoprevention could be a better strategy compared to therapeutic agents since the skin is continuously exposed to UVR and high levels of ROS are proposed long term after the exposure.³⁵ Moreover, melanoma is known for its relative risk factors and premalignant lesion.³⁶ Novel sunscreen product was developed to be a valuable tool to protect the skin detriment from the UVR base on chemoprevention concept.

To summarize this section, conventional sunscreen products can absorb UVA and UVB. However, some of them can be absorbed by the human body and induce further effects, such as cancer. Then the increasing amount of sunscreen use also contributes to environmental pollution, especially to

the aquatic system. Furthermore, it lacks the effectiveness of UVA-induced free radical prevention. Chemoprevention strategies are increasingly needed to be developed as an improvement of the current state of affairs.

1.3.2 ROS reduction: direct antioxidant treatments to reduce UVR induced ROS

Antioxidants are known for their healthy function. Antioxidants can also contribute to the prevention of skin damage under UVR.³⁷ Although a certain amount of antioxidant capacity is possessed by the skin for dealing with the oxidative stress induced by excessive UVR exposure, an additional antioxidant is required for ROS scavenging. As a result, the antioxidant treatment is developed as one of the chemoprevention for balancing the redox status in cellular.

A series of enzymatic antioxidants like glutathione peroxidase, superoxide dismutase (SOD), and catalase and small molecule antioxidants like Vitamin C, Vitamin D, glutathione (GSH) are able to be reduced to protect against oxidative stress.³⁸⁻⁴⁰ Under the UVR exposure, the depletion of the small molecule antioxidants and reduction in enzymatic function may not be enough to prevent large increases in oxidative protein and DNA lesions. The exogenous antioxidant can be used as a treatment on photoaging or melanoma prevention are widely reported. For example, ascorbic acid is defined as a ROS scavenger during the oxidation from ascorbate to dehydroascorbate to maintain the physiologic status. The long term topical application of the ascorbic acid daily can effectively improve the photodamaged facial skin.⁴¹

1.3.3 Natural products to reduce UVR induced ROS: mechanisms and effects

Many natural products are used for preventing the initiation of melanoma by decrease the ROS level with various mechanisms. They are discovered from the UVR defense system of plants and animals and show high potential for its low cost and low toxicity.

Carotenoids are a type of pigments plants produced to protect themselves from UVR. Carotenoids are reported as being a good scavenger of singlet oxygen upon UVA-induced skin damage.⁴² With pretreatment of 10 μ M of the carotenoids astaxanthin, ROS formation can be reduced to 70% comparing to the control. Resveratrol is also a natural product that shows the ability to quenching the oxidative stress produced during melanoma initiation, promotion, and even progression.³⁸It not only suppresses the formation of ROS, such as hydroxyl radical, hydrogen peroxide, nitric oxide and inducible nitric oxide synthase as an antioxidant but also downregulates COX-2 and inhibits the mTORC2 pathway linked to carcinogenesis of the skin.⁴³ Then, Epigallocatechin-3-gallate (EGCG) is a compound found in green tea.⁴⁴ It can indirectly reduce the ROS level by affecting the signaling pathway. Inhibition of the epidermal growth factor receptor (EGFR) and p38 proteins of the MARK family will depress the ROS production. The further developed EGCG nanoparticles show 63.14% protection against DNA damage.⁴⁵

1.4 NOX inhibitor as a chemoprevention strategy

1.4.1 NOX Biochemistry

To quench the excessive ROS and lower the oxidative stress, a strategy to inhibit the ROS production effectively is needed. There are many different enzymes that exist in the cells that

should respond to ROS generation. Such as mitochondrial electrons transport chain (ETC)⁴⁶, nitric oxide synthase (NOS)⁴⁷, cytochrome P450 oxidases⁴⁸, xanthine oxidase (XO)⁴⁹, and NADPH oxidase (NOX)⁵⁰. Among them, NADPH oxidase is widely distributed through different cell types and tissues.⁵⁰ Many oxidative stress-induced pathologies have a relationship with NOX enzymes. Considering the importance of NADPH oxidase (NOX) on ROS production, research about inhibition of NOX to reduce the ROS generation has developed to be a promising chemoprevention approach.

The NADPH oxidase is an enzyme family that contains a catalytic subunit, NOX, as the critical structure. It concludes seven members which are different from each other on activation trigger, enzymatic composition, and their product. However, the seven members share the a six trans-membrane helical domain containing two iron-heme prosthetic groups. Then the cytosolic c-terminus consists of the NADPH binding domain and a flavin adenine dinucleotide (FAD).⁵¹

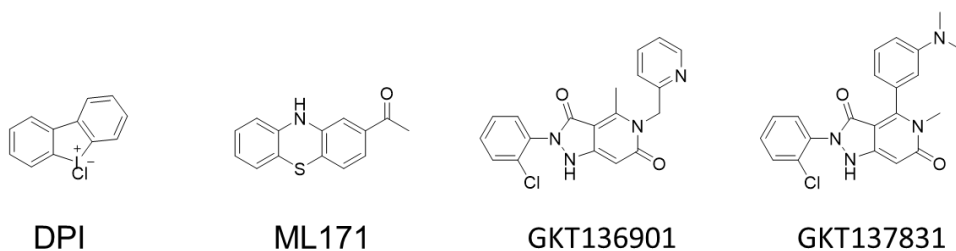
Base on the two iron-heme prosthetic groups and FAD domain, NOX family can catalyze the transfer of two electrons from NADPH to the molecular oxygen in cellular. However, the enzymatic product differs. NOX1, NOX2, NOX3, and NOX5 produce superoxide because of the single electron transfer from the iron-heme group.⁵²⁻⁵³ While NOX4, DUOX1, and DUOX2 primarily generate hydrogen peroxide during the procedure may because of the superoxide was trapped and reacted to hydrogen peroxide by superoxide dismutase(SOD).⁵⁴

1.4.2 Known NOX inhibitors

NOX inhibitors have been shown to effectively lower the ROS levels inside cells. There are many small molecules found or synthesized as NOX inhibitors for recent decades. The NOX inhibitor is evolving from non-specific molecular to selective enzymatic agents fast these recent years.

In the early stage, some of the molecules are used as NOX inhibitor with some side effect on enzymes other than NOX, like diphenylene iodonium DPI.⁵⁵ DPI is used as a reference for measuring the inhibition of NOX. It can widely inhibit NOX isoforms.

Next inhibitors that were more specific to NOX isoform were developed. For example, 2-acetylphenothiazine (ML171)(**Scheme 1.1**) was identified as strong NOX inhibition potential among 16000 commercially available phenothiazine derivatives by Scripps Research Institute.⁵⁶ ML171 showed IC₅₀ values of 130–250 nM for NOX1, and of 3–5 μM for NOX2–4 well as for xanthine oxidase. ML171 has already been widely used as a NOX1 inhibitor in vivo base on the pharmacokinetics and safety data.



Scheme 2.1 Small molecule NOX inhibitors

There are two NOX inhibitors termed GKT136901 and GKT137831(**Scheme 1.1**) that are found in among a series of pyrazolopyridine dione derivatives by GenKyoTex.⁵⁷ They show the best inhibition on NOX1 and NOX4 (110 nM-170nM) while shows 1530 μM for NOX2 inhibition.

Biological drugs can also be developed to NOX inhibitors. The NOX2ds-tat is designed as an 18-amino-acid peptide.⁵⁷⁻⁵⁹ It consists of a nine-amino-acid sequence as and p47_{phox}. p47_{phox} is one of the required protein going to bind with the NOX2 during the activation. After the binding of p47_{phox} with NOX2, the peptide sequence will block the other activation site on the NOX2 to interfere with the regular action of NOX2. It shows 80% inhibition of superoxide generation with IC50 as 0.7uM. The modification of the peptide sequence could change the selectivity of those drugs to make them more potential in the future.

1.4.3 Why target NOX

Some enzymes will generate the ROS only after any oxidative stress has occurred. Such enzymes include xanthine oxidase and nitric oxide synthase. Compared to these enzymes, NADPH oxidase is a primary ROS producer.⁵⁰ To the skin cells, NOX1 is the target researchers are focusing on. Research in the lab of Antonio Valencia has shown that increases in [Ca²⁺] and ceramide are upregulated by superoxide formation. These changes then activate Rac1 in human keratinocytes.⁶⁰ Then, Rac1 activates NOX1 by relocating to the plasma membrane and binding with preassembled NOX1, NOXO1, and NoxA1 to produce ROS.⁶¹ The excessive ROS will induce the synthesis of prostaglandin E2 (PGE2), which is an inflammatory mediator after UVA radiation. It proves that the UVA-induced skin damaged could be stopped by inhibition of the NOX1 isoform. The agents can interfere with the activation of NOX1 to slow it down or stop it have the potential to be studied as an anti-cancer drug by reducing the ROS generation *in vivo*.

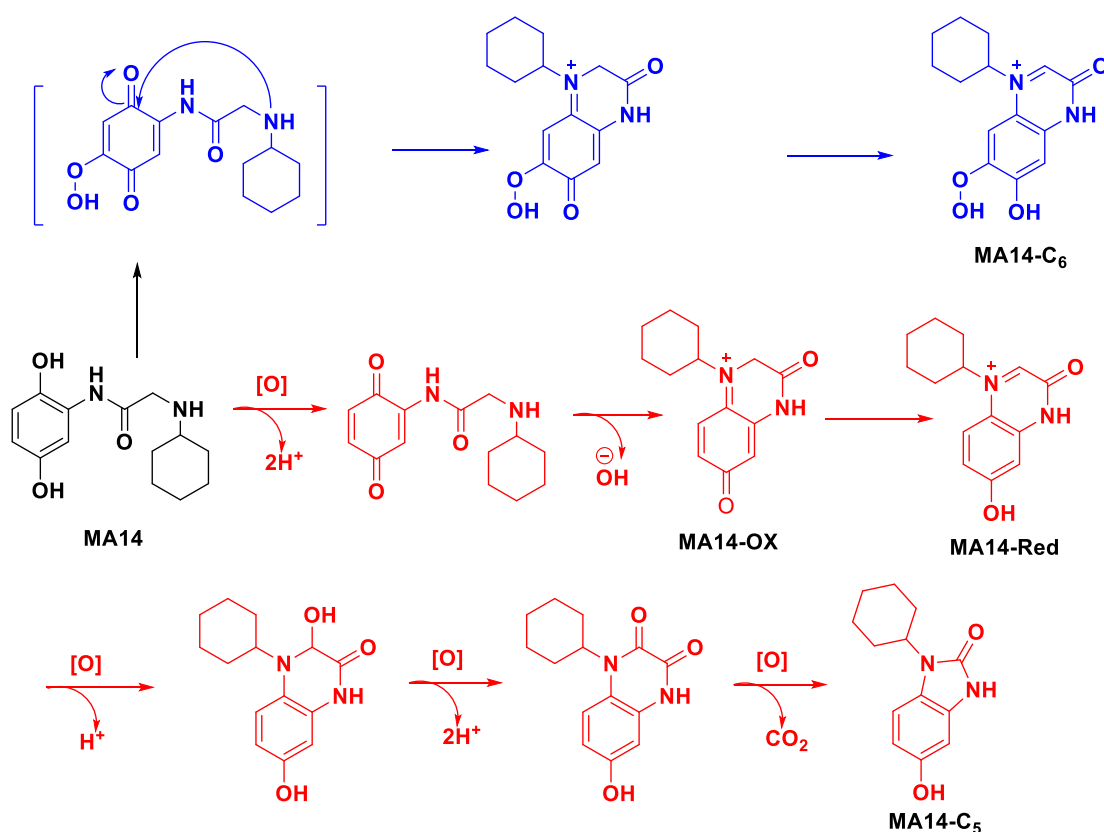
1.5 ROS activated prodrug strategies

ROS scavenger was developed as chemotherapies for skin cancer.⁶² However, the lack of selectivity to tumor cells may also affect the healthy cells to make drug toxic to the normal cell by

reductive stress.^{63c} Alternatively, loaded drugs will be consumed before reaching the target cells. Using the different oxidative load between tumor and healthy cells to create the prodrugs can improve the selectivity and long-lasting life span of them for extending the application potential.⁶⁴

1.5.1 The Merino lab strategy

Based on the previous research of Dr. Merino's lab, novel self-cyclizing moieties were designed.⁶⁵



Scheme 3.2 Mechanism of MA14 oxidation.

The mechanistic studies of MA14 led to an enlightening design observation that identified a novel strategy to design a ROS sensitive and long-lasting prodrug (**Scheme 1.2**). Compound MA14 readily oxidizes in the presence of Fenton conditions that generate hydroxyl radicals. MA14 is oxidized to the quinone form intermedia by ROS forms, and then this intermedia will go through

an inter-molecular nucleic attack by the secondary aliphatic amine at the end of side-chain to obtain two isomers MA14-Ox and MA14-Red. MA14-Red will be further oxidized by three consecutive steps, followed by CO₂ loss and ring closure/oxidation to give the main product MA14-C₅. Also, the quinone form intermedia could be oxidized to MA14-C₆ under the Michael addition mechanism.

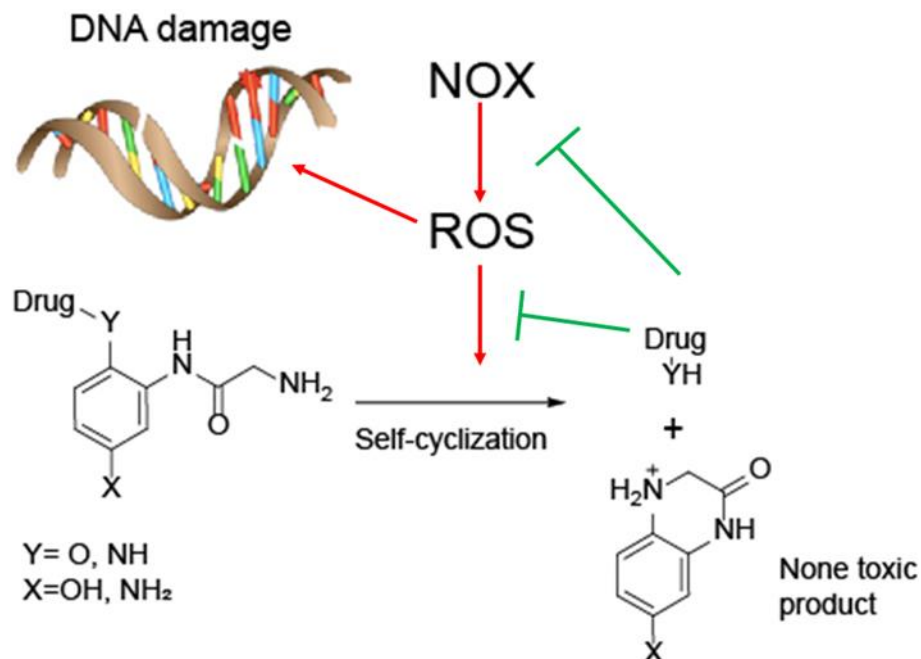


Figure 4.2 Design of novel ROS-active prodrug

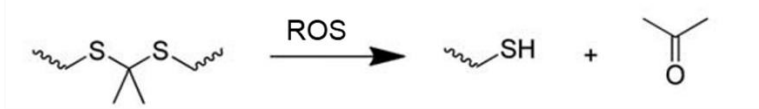
One of the hydroxyl group is eliminated by oxidation activated and self-cyclization. It importantly indicates a way to design a drug cargo system by conjugating a ROS sensitive moiety with a drug. (Figure 1.2) The cyclohexylamine is removed to low the cytotoxicity. Then the Y position will be conjugated with the drug with a hydroxyl group or aniline group as the activation site. The X position allows various substituents to modulate the oxidation rate. This novel self-cyclizing drug will be delivered to the target cell without degradation because of the different ROS volumes between healthy cells from damaged cells. Then DNA damage-induced high-level ROS would

activate the compound to release the drug under a self-cyclization reaction and be reduced by direct elimination or indirect inhibition.

1.5.2 Other Strategies

There are many other ROS-activated prodrug strategies that were developed to selectively target the DNA-damaged cells base on its higher ROS level than the healthy cells.

A. Thioketal linkers



B. Boronic acids and esters



Figure 5.3 Mechanism of ROS-active linkers

Thioketal linkers: Thioether linkers(**Figure1.3**) are sensitive to the ROS, especially the hydroxyl radical.⁶⁶ The central carbon (RS-C(CH₃)₂-SR) is attacked by the free radicals to release acetone and other oxidation products. A thioketal shows the potential to be used as a ROS-responsive nanocarrier. The nanoparticles function by transitioning from hydrophobic (alkylene sulfide) to hydrophilic (alkylene sulfoxide) states under oxidative stress in cells. This leads to the opening of the particle and release of the particles contents (usually anticancer drugs).

Boronic acids and esters: Aryl boronic acids(**Figure1.3**) and their esters is another well known ROS active linker. It could be cleaved by the ROS form, especially the hydrogen peroxide (H₂O₂) in vivo. The peroxide anion from the hydrogen peroxide will attack and attach on the empty p-

orbital or the boron to form a tetrahedral boronate intermediate. Then the intermediate will lose a alkoxide via a 1,2-metallate rearrangement, which will rearrange the Cobon-Boron σ -bond to the neighbor oxygen. At last, hydrolysis will happen to cut the oxygen-boron bond and produce alcohol. The boronic acid is widely used in the anti-cancer drug area for designing the ROS-active probe and drug. PCL-1 is a boronic acid-caged firefly luciferin molecule designed by the Howard Hughes Medical Institute.⁶⁷ It can selectively react with H_2O_2 to release firefly luciferin, which triggers a bioluminescent release response in the presence of firefly luciferase. Then this bioluminescent signal will be imaged in real-time by a CCD camera.

1.6. Goals of this Dissertation

This dissertation aims to improve the applications of a novel ROS activated self-cyclizing agents as a series of chemoprevention prodrug for skin cancer/melanoma prevention. Furthermore, the use of it could be extended to oxidative stress quantification.

1.7. Overview of Chapter 2

UV irradiation is a significant driver of DNA damage and, ultimately, skin cancer. UV exposure leads to persistent radicals that generate ROS over prolonged periods. Toward the goal of developing long-lasting antioxidants that can penetrate the skin, we have designed a ROS-initiated protective (RIP) reagent that, upon reaction with ROS (antioxidant activity), self-cyclizes and then releases the natural product apocynin. Apocynin is a known antioxidant and inhibitor of NOX oxidase enzymes. An essential phenol on the compound **1** controls ROS-initiated cyclization and makes **1** responsive to ROS with a lower EC_{50} compared to common antioxidants in an ABTS assay. In an *in vitro* DNA nicking assay, the RIP reagent prevented DNA strand breaks. In cell-

based assays, the reagent was not cytotoxic, apocynin was released only in cells treated with UVR, and the reagent prevented UV-induced cell death. Finally, topical treatment of human skin explants with the RIP reagent reduced UV-induced DNA damage as monitored by quantification of cyclobutane dimer formation and DNA repair signaling via TP53. The reagent was more effective than the administration of a catalase antioxidant on skin explants. This chemistry platform will expand the types of ROS-activated motifs and enable inhibitor release for potential use as a long-acting sunscreen.

1.8. Overview of Chapter 3

Two new chemoprevention prodrugs named SA1 and RIP2 of melanoma are designed base on the ROS-active scaffold developed in chapter2 and another new p-phenylenediamine ROS sensitive moiety. An antioxidant named sesamol and a NOX1 inhibitor is attached on the ROS sensitive scaffold to develop better stability and selectivity to only high ROS level cells, such as melanoma. Pharmacokinetics includes stability and half-life in vitro and in vivo are perform under HPLC and LCMS. Cytotoxicity and ROS inhibition are tested by MTT assay and DCFDA assay in a keratinocyte cell line.

1.9. Overview of Chapter 4

ROS plays a critical role in the pathology of the skin by suppressing the immune response, oxidization of lipids and proteins, initiation of the generation of proinflammatory cytokines,

damaging DNA. Two primary questions are not answered clearly for now. Where and how much of ROS are formed after the UVR treatment. These are critical questions since the quantification of ROS level is the fundamental data for research about ROS induced cell change to make progress. A compound DEASor is designed by conjugating a versatile small molecule with aryl boronate ester to release the small molecule as a probe under oxidative stress in the cells. Then the probe released during the cell culture will be quantitated by GCHSMS. With the calibration curve of the multiple cell assay, oxidative stress could be worked out.

Chapter 2 UV cell stress induces oxidative cyclization of a protective reagent for DNA damage reduction in skin explants

Parts of this chapter have already been published UV cell stress induces oxidative cyclization of a protective reagent for DNA damage reduction in skin explants. Liu, J., Zhu, H., Premnauth, G., Earnest, K.G., Hahn, P., Gray, G., Queenan, J.A., Pevette, L.E., AbdulSalam, S.F., Kadekaro, A.L. and Merino, E.J., 2019. *Free Radical Biology and Medicine*, 134, pp.133-138.

2.1 Introduction

Prolonged exposure to ultraviolet radiation (UVR) generates reactive oxygen species (ROS) forms that are highly toxic. [1] UVR-mediated excitation of melanin and ROS imbalance are important biochemical contributors to melanoma risk. [2] Counterintuitively, skin cells, especially melanocytes, have benign biochemistry that generates and utilizes ROS (**Figure 2.1**) such as hydrogen peroxide. These normal biochemical functions include melanin production and protein signaling. [3] Recently, it has been found that UVR not only causes direct DNA damaging events but also results in the generation of “dark” cyclobutane pyrimidine dimers (CPDs), which derive from radicals long after exposure. [4] Melanin-based radicals, observed using electron paramagnetic resonance experiments, can generate the more toxic hydroxyl radical (**Figure 2.1**) long after UVR exposure. These radicals lead to the production of exotic DNA damage products that are both lethal and mutagenic. [5] Currently available sunscreens, which are comprised of UVR blocking and UVR absorbing compounds, combat excessive UV exposure but do not stop these dark damaging events. In addition, marine life toxicity issues surrounding the use of UVR-blocking compounds like oxybenzone and the finding that repetitive sunburns are strongly associated with poor prognosis melanoma mean that new sun-protection agents are needed. There are two design requirements: (I) minimal activity against benign ROS biochemistry and (II) a non-stoichiometric or catalytic cellular effect to enhance activity. In this manuscript, we detail our first molecular design that satisfies these criteria. The ROS-initiated protective (RIP) reagent reported here releases the natural product apocynin, an inhibitor of NADPH oxidases, upon oxidative reactions with ROS generated in cells by UVR and later forming “dark” damage events (**Figure 2.1**).

We were among the first to report ROS-activated chemotherapeutic agents. [6, 7] The most common ROS-responsive chemistries are boron-based. Boron-based antioxidants, [8, 9] modified gene-targeting agents, [10] and inhibitor pro-drugs have been reported. [11, 12] Alternatives are needed for several reasons. First, aryl boronate esters readily oxidize in the presence of hydrogen peroxide or other ROS forms in a Chan-lam-like reaction. [13] Given that the steady-state concentration of peroxide in blood and cells is between 200 nM and 2 μ M, [14] reported aryl boronate esters are likely activated rapidly in vivo. We have used a much different approach in this work that spans several molecular designs. [15] We designed a cytotoxic molecule a few years back. [16] This molecule had an unusual mechanism in that it underwent intramolecular cyclization and dehydrated in the presence of hydrogen peroxide. Then we designed an antioxidant that was not cytotoxic, but this molecule had modest cell effects. [17, 18] In this work, we hypothesized that biologically relevant effects could be achieved by taking advantage of this oxidative reaction pathway to eject a bioactive inhibitor of ROS-producing enzymes for UVR induced protection (**1**, **Figure 2.1**). We reasoned if we could release an inhibitor of cellular oxidases, like apocynin (red, **Figure 2.1**), then selectively initiated cellular protection would be possible. This manuscript details our first investigations into addition of a bioactive molecule to generate catalytic antioxidants.

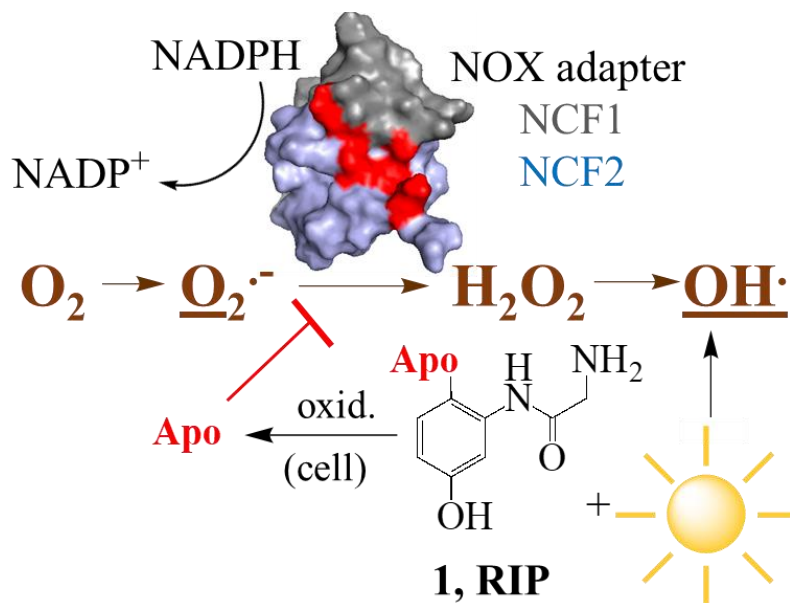
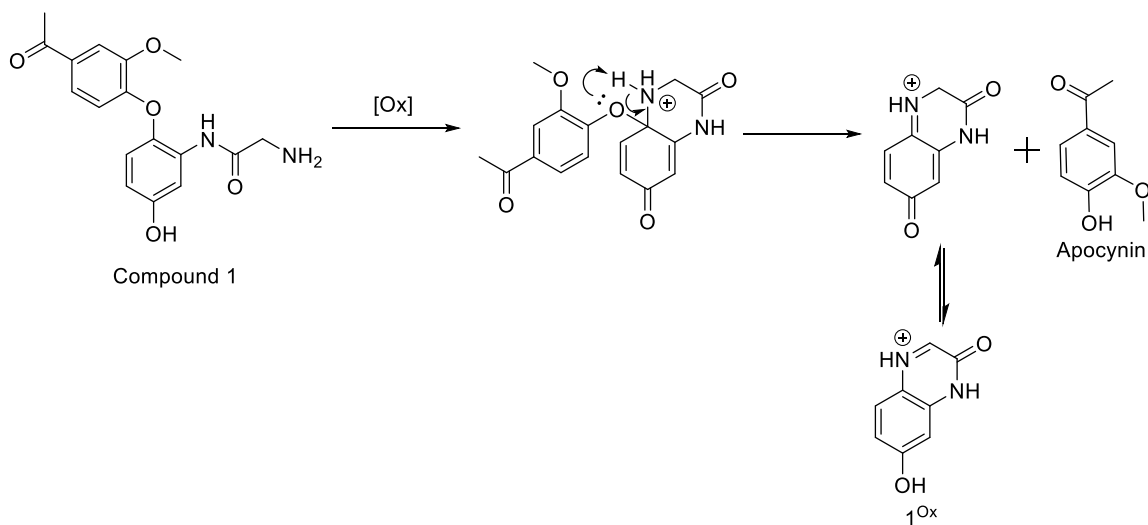


Figure 1.1 ROS (brown) are normally present, but UV radiation enhances the formation of highly toxic species (underlined) that damage DNA. RIP reagents, such as the apocynin-linked compound **1** shown, eject an oxidase inhibitor in high oxidative stress environments. Apocynin (red) binds NADPH oxidase-associated factors NCF1 and NCF2 to limit further ROS production. Structure from PDB 1K4U in reference 21

We sought to design a RIP reagent that would activate and release a bioactive molecule that could globally lower ROS selectively (**Scheme 2.1**). This is important because unselective ROS reduction can be harmful. [19] A survey of literature identified several NADPH oxidase inhibitors that act as general ROS reducers. We focused on a natural product called apocynin (**Figure 2.1**), a ketone version of vanilla that has been used in traditional medicines. Its promiscuous biological properties are ascribed to the ability to inhibit oxidases in the monomeric and multimeric states. [20, 21] Oxidases are major generators of cell ROS, [22] and recent literature suggests that melanocytes and keratinocytes have high levels of NOX oxidases such as NADPH oxidase 1. [23] The NADPH oxidase 1 holoenzyme is a major producer of UV-induced ROS. [20] The oxidase is

involved in activation of the PI3K/Akt signal pathway. [24] Apocynin may inhibit activity of other oxidases as well. Despite this poorly understood and likely complex mechanism, its biological effects in ROS reduction are exceptional. [25] Thus, despite the complex biological profile of apocynin it presented the best possible chance for functioning *in vivo*.



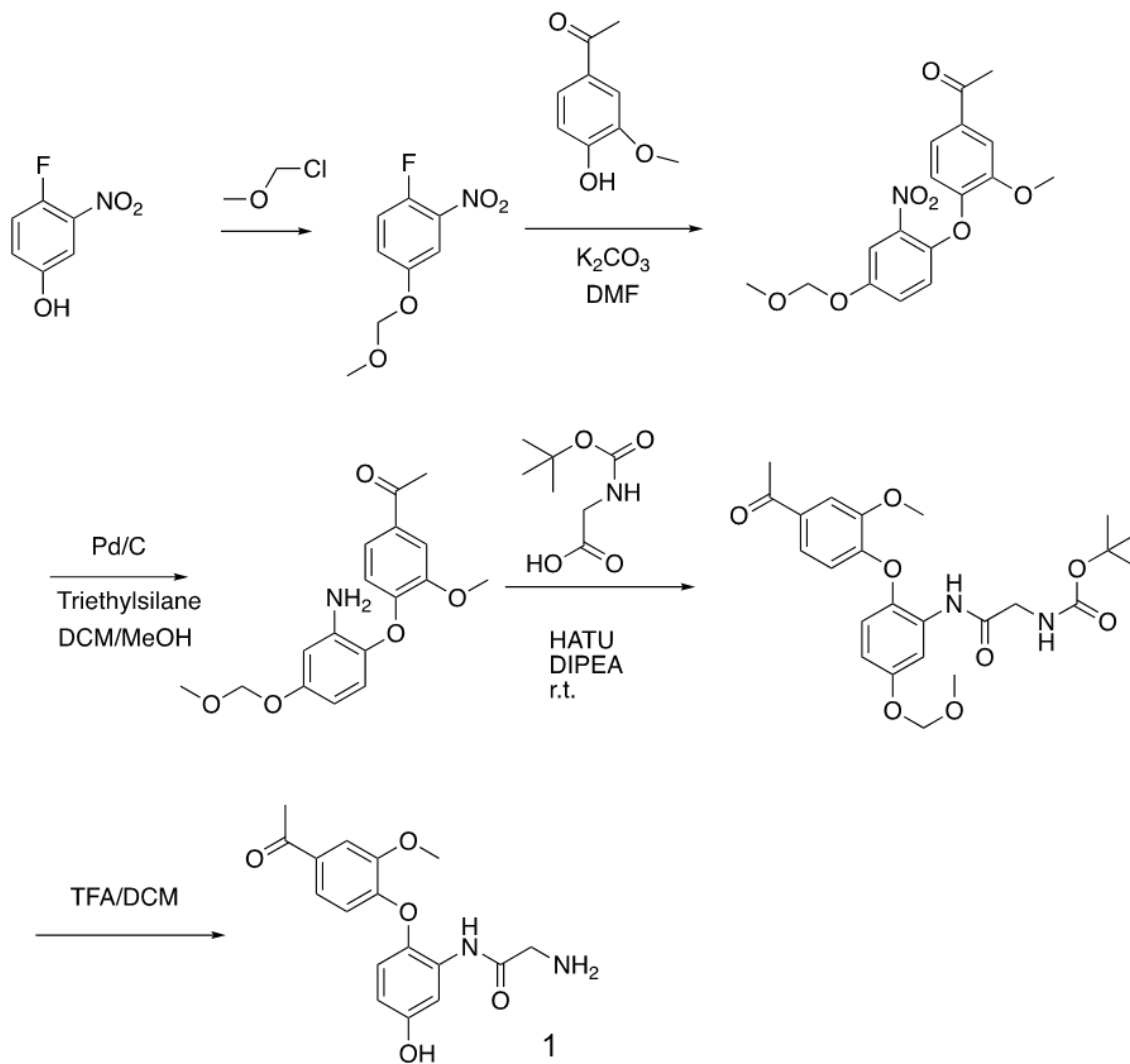
Scheme 2.1 Compound 1 self cyclizes and oxidizes to form final product **1^{Ox}**

2.2 Experiment section

2.2.1 Synthesis and characterization of compounds

Boc-sarcosine, trifluoroacetic acid (TFA) and dimethylformamide, chloromethyl methyl ether were purchased from Sigma-Aldrich Chemical Co. (St. Louis, MO, USA). Apocynin, 4-floro-3nitro phenol, pladium on carbonyl, 4'-Hydroxyacetophenone, 1-Fluoro-2-nitrobenzene, Triethylsilane, HATU were purchased from Fisher scientific international, Inc. All solutions were prepared with water purified by a Milli-Q system (Millipore, Bedford, MA, USA). All reagents used for buffer preparation were of analytical grade.

2.2.1.1 Synthesis of compound 1



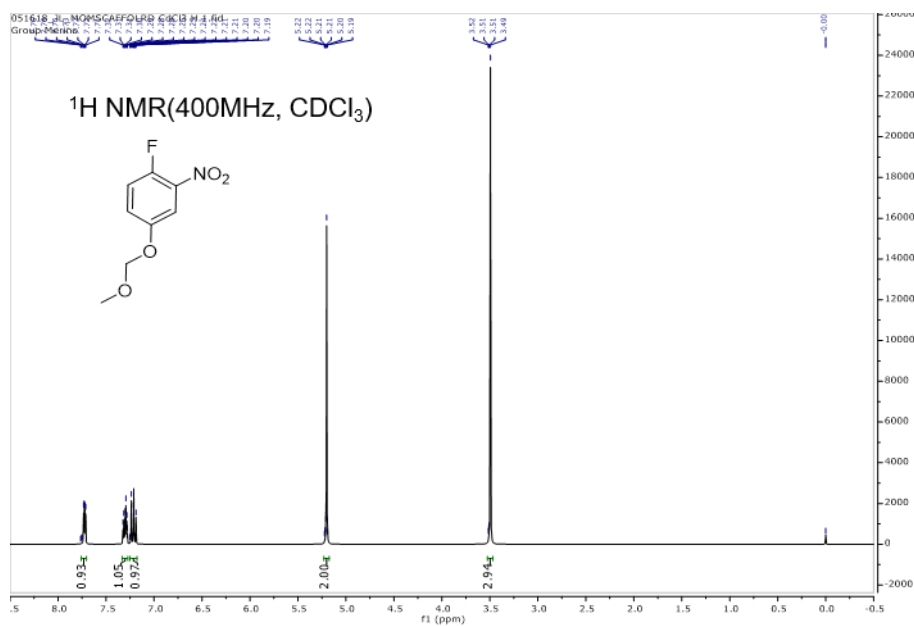
Scheme 3.2 The synthesis route of compound 1.

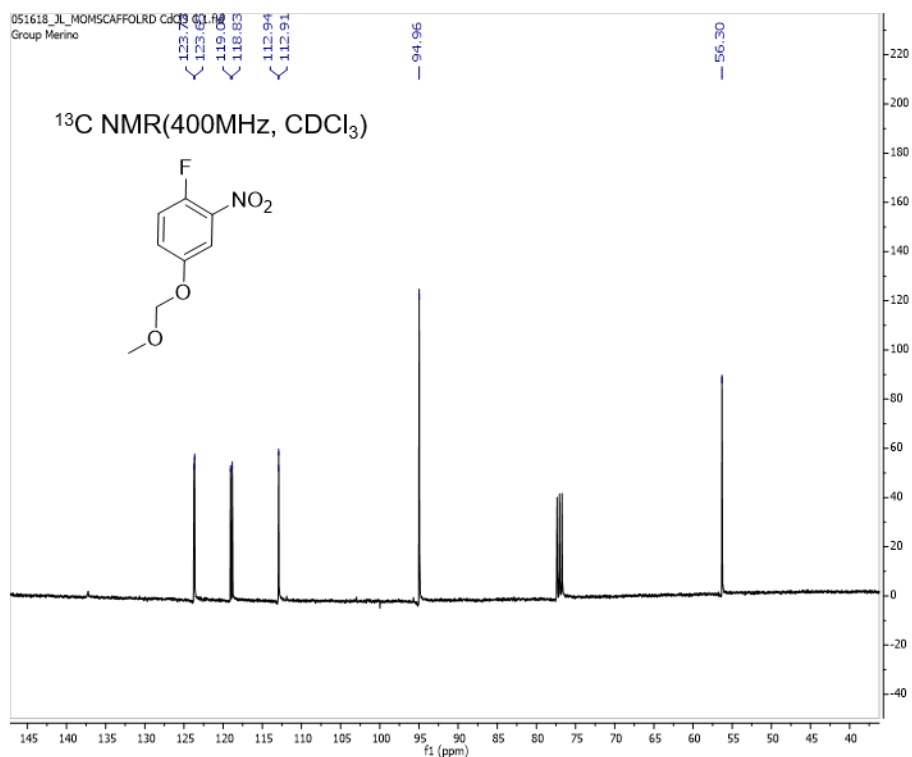
Synthesis of 1-Fluoro-4-(methoxymethoxy)-2-nitrobenzene:

Dissolve the 4-Fluoro-3-nitrophenol (1g, 6.36mmol) into the dichloromethane (20mL) at ice bath. Then Add methoxymethyl chloride (966.12ml, 12.72mmol) twice with half amount every five minutes. After 10 minutes, add N, N-Diisopropylethylamine (3,1ml, 17.81mmol). The resulting

mixture was stirred at RT for 1h, after which time the solvent was diluted with H₂O and extracted with EtOAc. The organic layer was dried (Na₂SO₄) and concentrated in vacuo to provide the product as a brownish liquid. [1.28g, yield: 99%] ¹H NMR (400 MHz, Chloroform-*d*) δ 7.72 (dd, *J* = 6.1, 3.1 Hz, 1H), 7.30 (dt, *J* = 9.1, 3.5 Hz, 1H), 7.21 (dd, *J* = 10.4, 9.1 Hz, 1H), 5.20 (s, 2H), 3.49 (s, 3H). ¹³C NMR (101 MHz, CDCl₃) δ 123.73, 123.65, 119.06, 118.83, 112.94, 112.91, 94.96, 56.30.

NMR for 1-Fluoro-4-(methoxymethoxy)-2-nitrobenzene

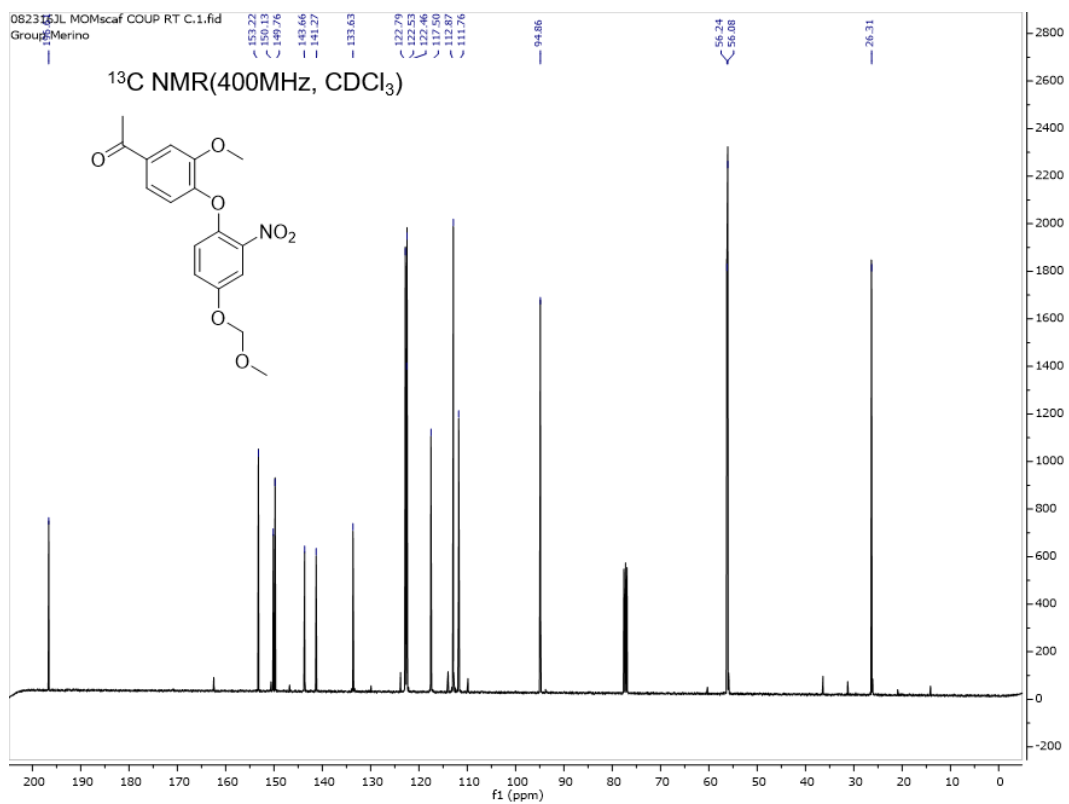
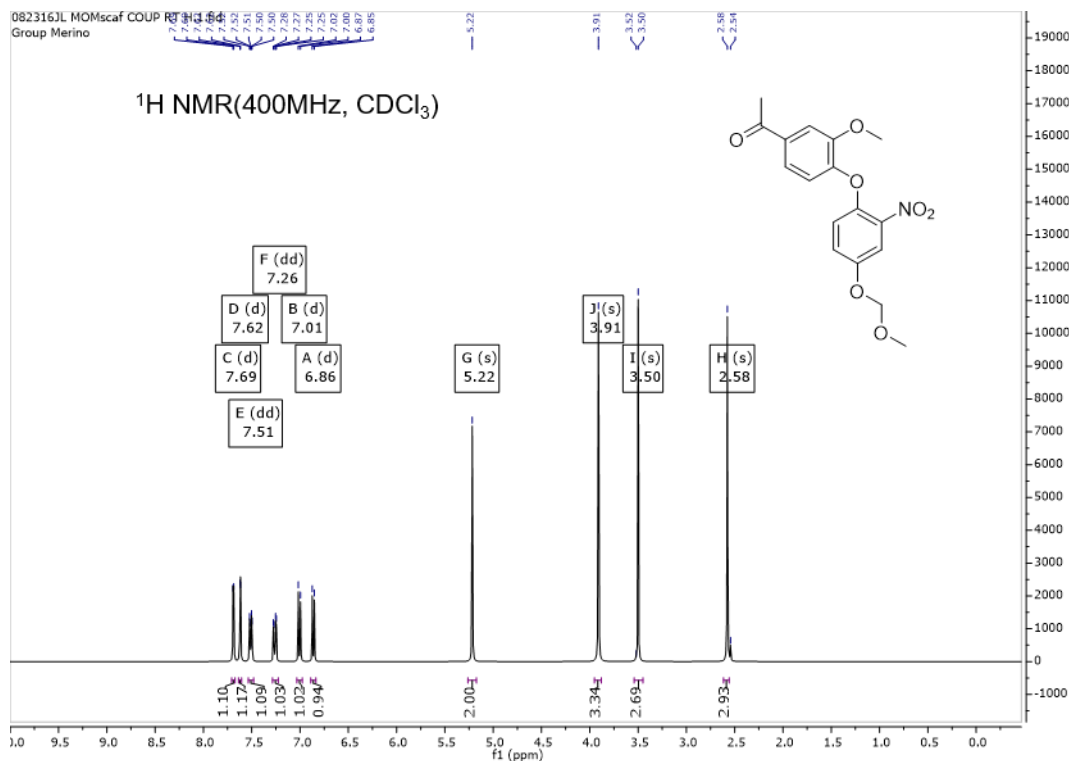




Synthesis of 1-(3-methoxy-4-(4-(methoxymethoxy)-2-nitrophenoxy)phenyl)ethanone:

To a solution of apocynin (1.05g, 6.36mmol) in dimethylformamide (8mL) was added potassium carbonate (0.9g, 6.55 mmol) and then 1-Fluoro-4-(methoxymethoxy)-2-nitrobenzene (1.28g, 6.36mmol). The resulting mixture was stirred at 45°C for 12hours. The reaction was then diluted with H₂O and extracted with EtOAc. The organic layer was dried (Na₂SO₄) and concentrated in vacuo. The resulting material was purified by flash chromatography using ethyl acetate/hexane (1:2) as eluent to provide the product as a yellowish solid. [yield:60%]¹H NMR (400 MHz, Chloroform-*d*) δ 7.69 (d, *J* = 2.9 Hz, 1H), 7.62 (d, *J* = 2.1 Hz, 1H), 7.51 (dd, *J* = 8.3, 2.1 Hz, 1H), 7.26 (dd, *J* = 9.1, 3.0 Hz, 1H), 7.01 (d, *J* = 9.0 Hz, 1H), 6.86 (d, *J* = 8.3 Hz, 1H), 5.22 (s, 2H), 3.91 (s, 3H), 3.50 (s, 3H), 2.58 (s, 3H). ¹³C NMR (101 MHz, CDCl₃) δ 196.61, 153.22, 150.13, 149.76, 143.66, 141.27, 133.63, 122.79, 122.53, 122.46, 117.50, 112.87, 111.76, 94.86, 56.24, 56.08, 26.31.

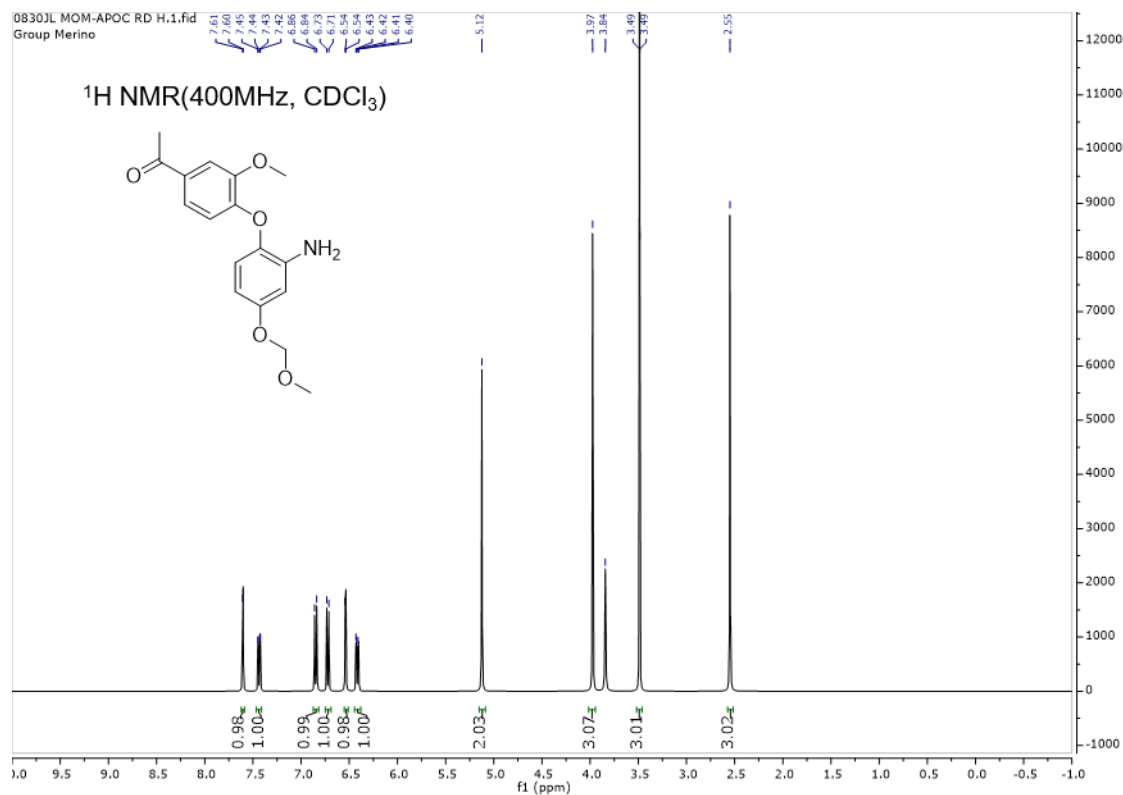
NMR for 1-(3-methoxy-4-(4-(methoxymethoxy)phenyl)ethoxy)phenyl)ethanone

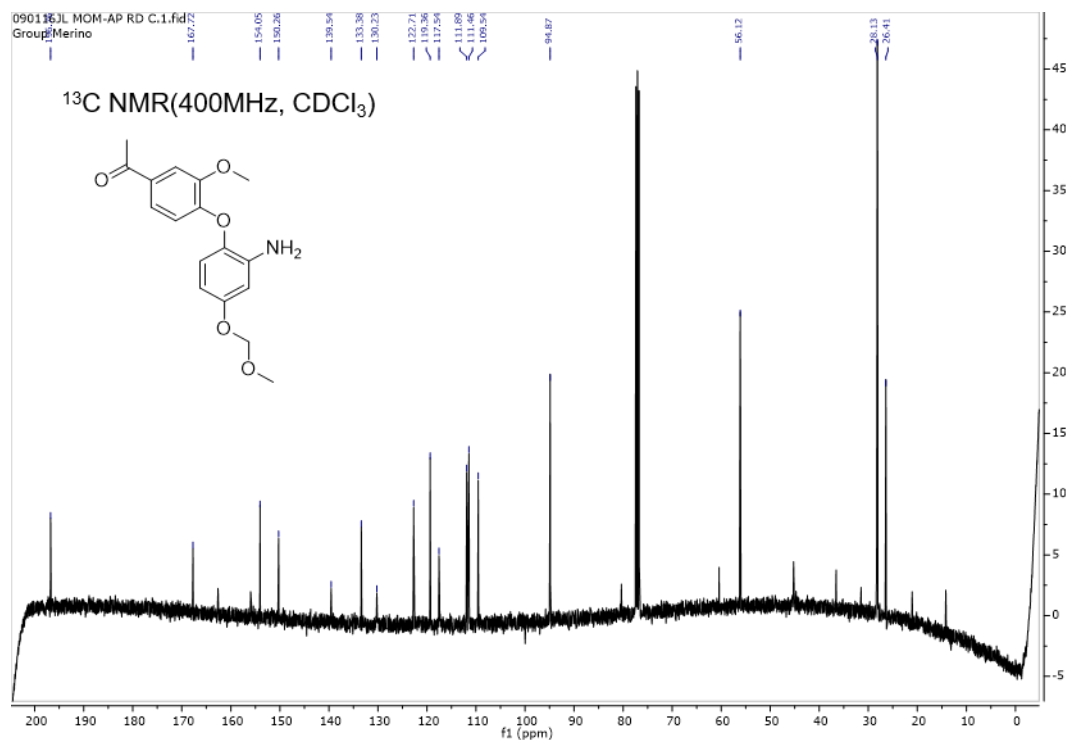


Synthesis of 1-(4-(2-amino-4-(methoxymethoxy)phenoxy)-3-methoxyphenyl)ethanone:

To a solution of 1-(3-methoxy-4-(4-(methoxymethoxy)-2-nitrophenoxy)phenyl)ethanone (0.7g, 2mmol) in dichloromethane under Argon atmosphere was added 10% Pd-C (70mg) and MeOH (0.45mL, 10mmol), followed by the addition of Neat triethylsilane (1.6mL, 10mmol.) dropwise from a syringe. When the reaction was complete (TLC), typically complete within 3h, the mixture was filtered off and the solvent was removed under reduced pressure. The resulting material was purified through flash chromatography acetate/hexane (2:1) to provide the product as a yellowish solid. [580mg, 50%.] ¹H NMR (400 MHz, Chloroform-d) δ 7.60 (d, J = 2.1 Hz, 1H), 7.44 (dd, J = 8.5, 2.1 Hz, 1H), 6.85 (d, J = 8.8 Hz, 1H), 6.72 (d, J = 8.5 Hz, 1H), 6.54 (d, J = 2.8 Hz, 1H), 6.42 (dd, J = 8.8, 2.8 Hz, 1H), 5.12 (s, 2H), 3.97 (s, 3H), 3.49 (s, J = 0.6 Hz, 3H), 2.55 (s, 3H). ¹³C NMR (101 MHz, CDCl₃) δ 196.76, 167.72, 154.05, 150.26, 139.54, 133.38, 130.23, 122.71, 119.36, 117.54, 111.89, 111.46, 109.54, 94.87, 56.12, 28.13, 26.41.

NMR for 1-(4-(2-amino-4-(methoxymethoxy)phenoxy)-3-methoxyphenyl)ethanone

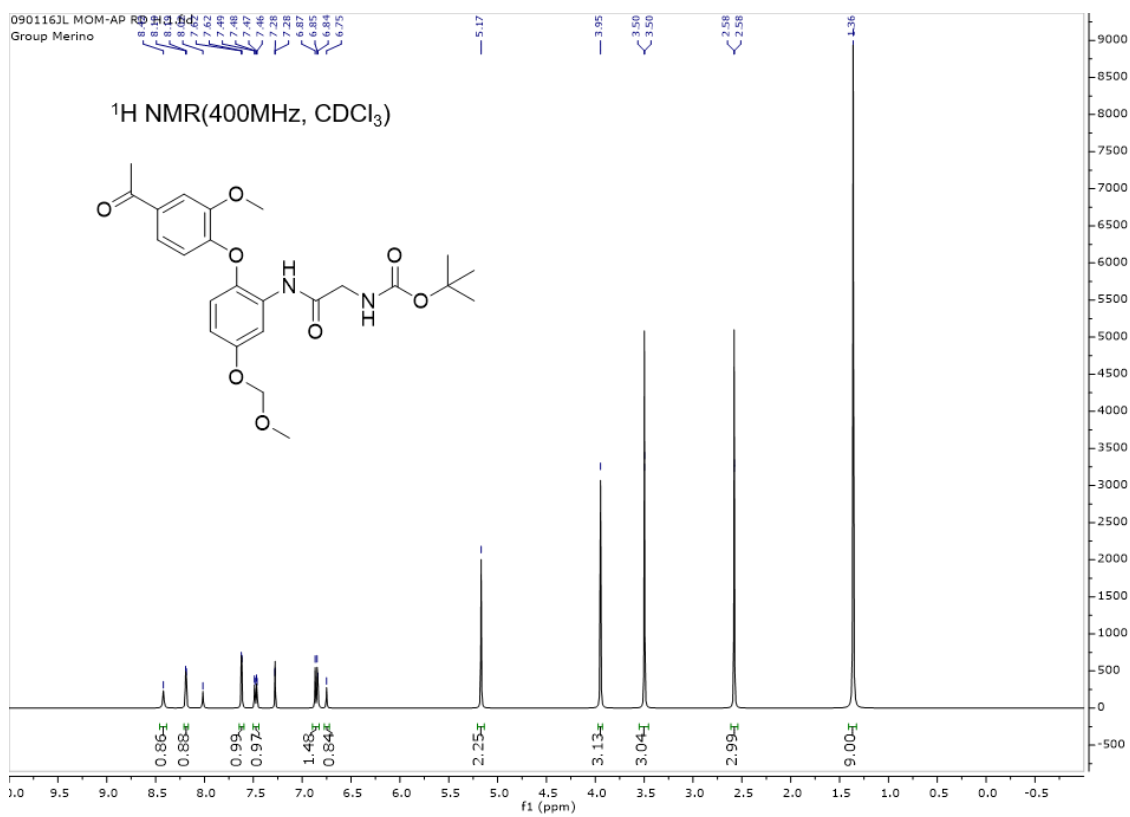


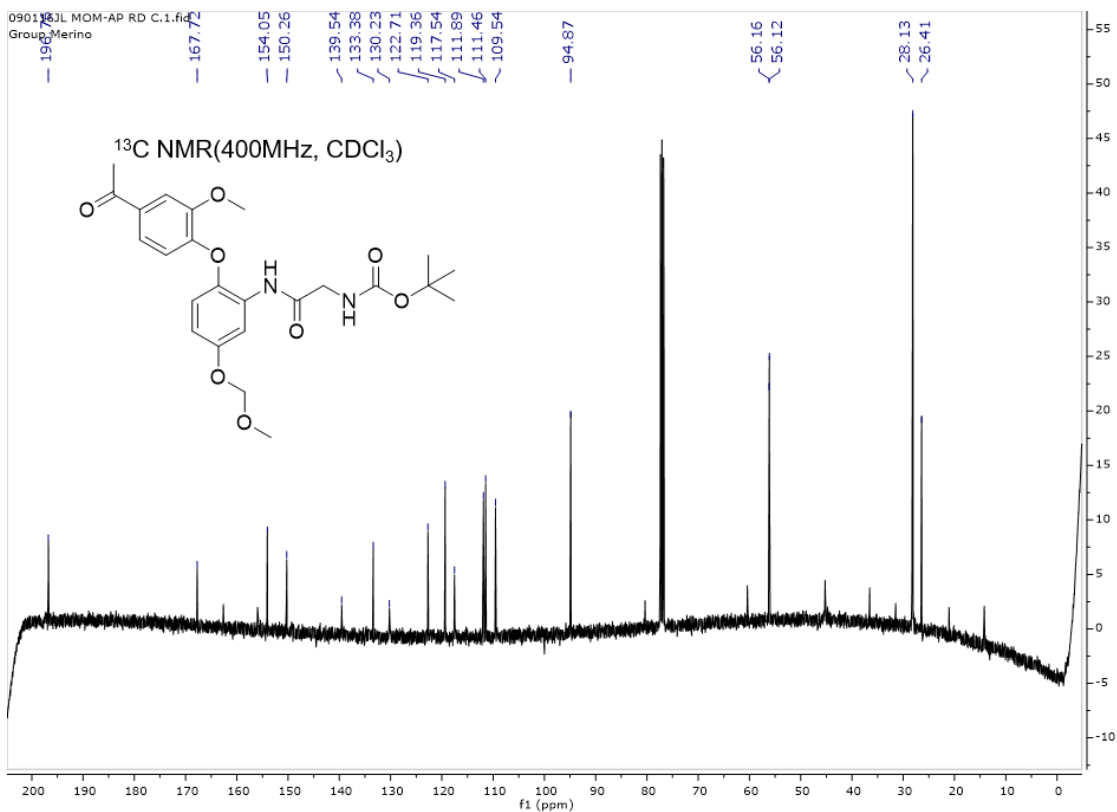


Synthesis of Tert-butyl 2-(-2-(4-acetyl-2-methoxyphenoxy)-5-(methoxymethoxy)phenylamino)-2-oxoethylcarbamate:

To a solution of the 2-(tert-butoxycarbonylmethylamino) acetic acid (0.95g, 5mmol) in DMF (5.0 mL) at room temperature was added HATU (2.1g, 5.5 mmol) and 1-(4-(2-amino-4-(methoxymethoxy)phenoxy)-3-methoxyphenyl)ethanone (0.91g, 5 mmol), after 30 mins, followed by the addition of DIPEA (1.8 mL, 10mmol). The resulting mixture was stirred at RT for 8 h, after which time the reaction mixture was diluted with H₂O and extracted with EtOAc. The organic layer was dried (Na₂SO₄) and concentrated in vacuo. The resulting material was purified by flash chromatography using ethyl acetate/hexane (1:1) as eluent to provide the product as a yellowish solid. [1.6g, 93%] ¹H NMR (400 MHz, Chloroform-d) δ 8.42 (s, 1H), 8.19 (d, J = 3.0 Hz, 1H), 8.02 (s, 1H), 7.62 (d, J = 2.5 Hz, 1H), 7.47 (dd, J = 8.3, 2.8 Hz, 1H), 7.28 (d, J = 0.9 Hz, 1H), 6.96 – 6.82 (m, 1H), 5.17 (s, 2H), 3.95 (s, 3H), 3.50 (s, J = 0.8 Hz, 2H), 2.58 (s, J = 0.8 Hz, 3H), 1.36 (s, 9H). ¹³C NMR (101 MHz, CDCl₃) δ 196.61, 153.22, 150.13, 149.76, 143.66, 141.27, 133.63, 122.79, 122.53, 122.46, 117.50, 112.87, 111.76, 94.86, 56.24, 56.08, 26.31.

NMR for Tert-butyl 2-(2-(4-acetyl-2-methoxyphenoxy)-5 (methoxymethoxy)phenylamino)-2-oxoethylcarbamate

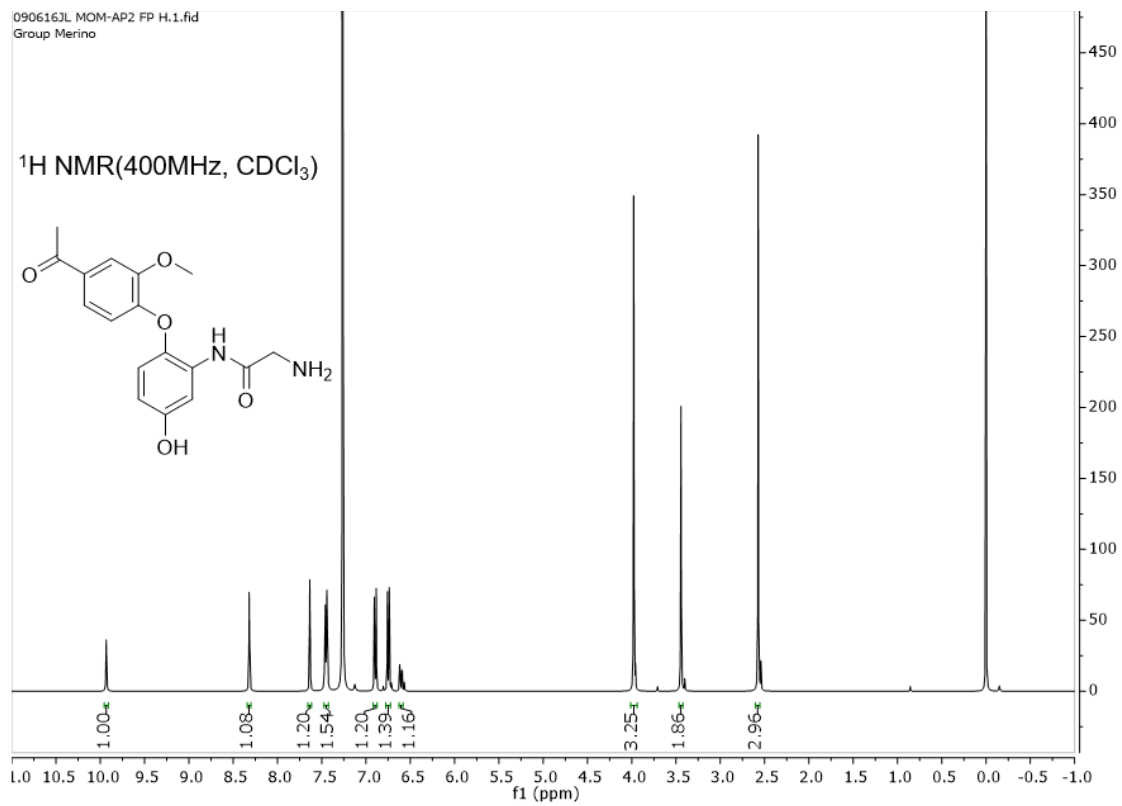


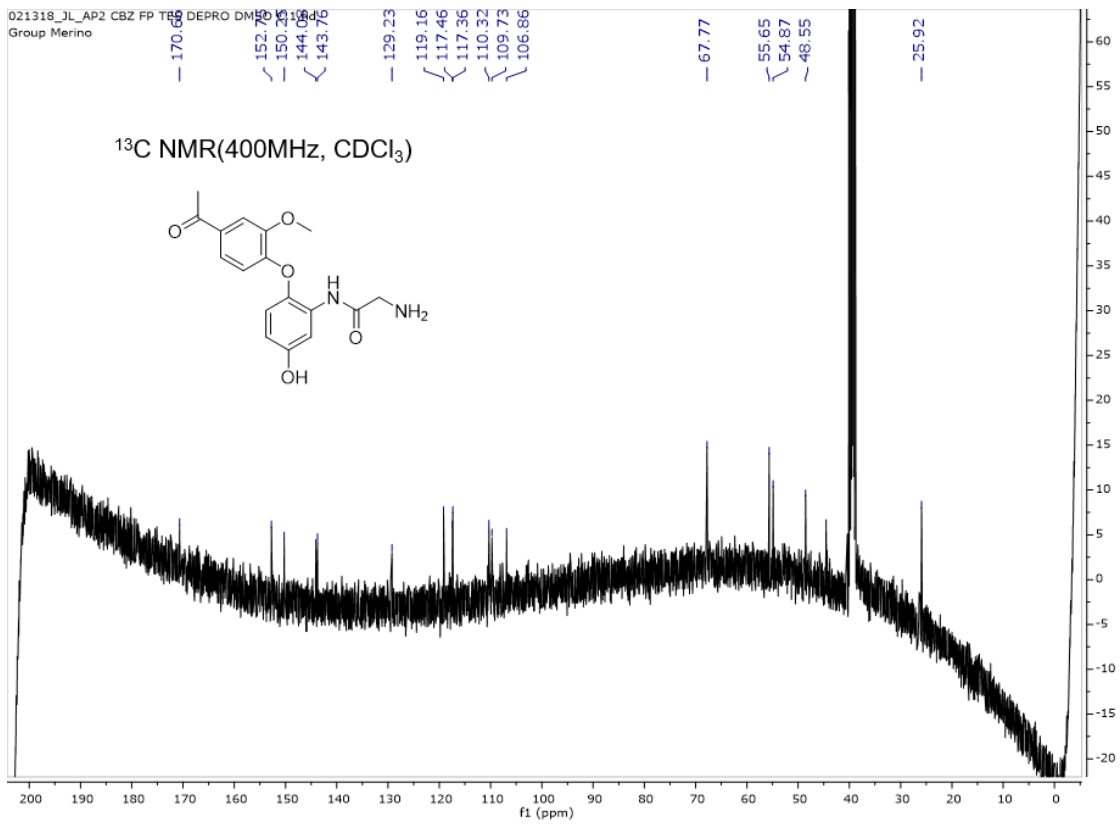


Synthesis of N-(2-(4-acetyl-2-methoxyphenoxy)-5-hydroxyphenyl)-2-aminoaceamide(1):

To a solution of Tert-butyl 2-(2-(4-acetyl-2-methoxyphenoxy)-5-(methoxymethoxy)phenylamino)-2-oxoethylcarbamate (500mg, 1.55mmol) in dichloromethane (5mL) was added trifluoroacetic acid (0.5mL). The resulting mixture was stirred at RT for 4 h with argon protection, after which time the reaction mixture was neutralized with saturated Na₂CO₃ solution and extracted with EtOAc. The organic layer was dried (Na₂SO₄) and concentrated in vacuo. The resulting material was obtained without any purification to provide the product as a yellowish solid. [345mg yield:99%] ¹H NMR (400 MHz, Chloroform-d) δ 9.88 (s, 1H), 8.35 – 8.12 (m, 1H), 7.69 – 7.52 (m, 1H), 7.49 – 7.38 (m, 1H), 6.96 – 6.88 (m, 1H), 6.80 – 6.70 (m, 1H), 6.64 – 6.54 (m, 1H), 4.00 (s, 3H), 3.50 (s, 2H), 2.61 (s, 3H). HRMS (ESI) for [MH]⁺ calculated: 331.1288, observed: 331.1289. ¹³C NMR (101 MHz, DMSO) δ 170.67, 152.75, 150.25, 144.08, 143.76, 129.24, 119.16, 117.46, 117.36, 110.32, 109.73, 106.86, 67.77, 55.65, 54.87, 48.55, 25.92. LRMS (ESI) m/z for C₁₇H₁₈N₃O₂ observed [M + H⁺] 331.1289.

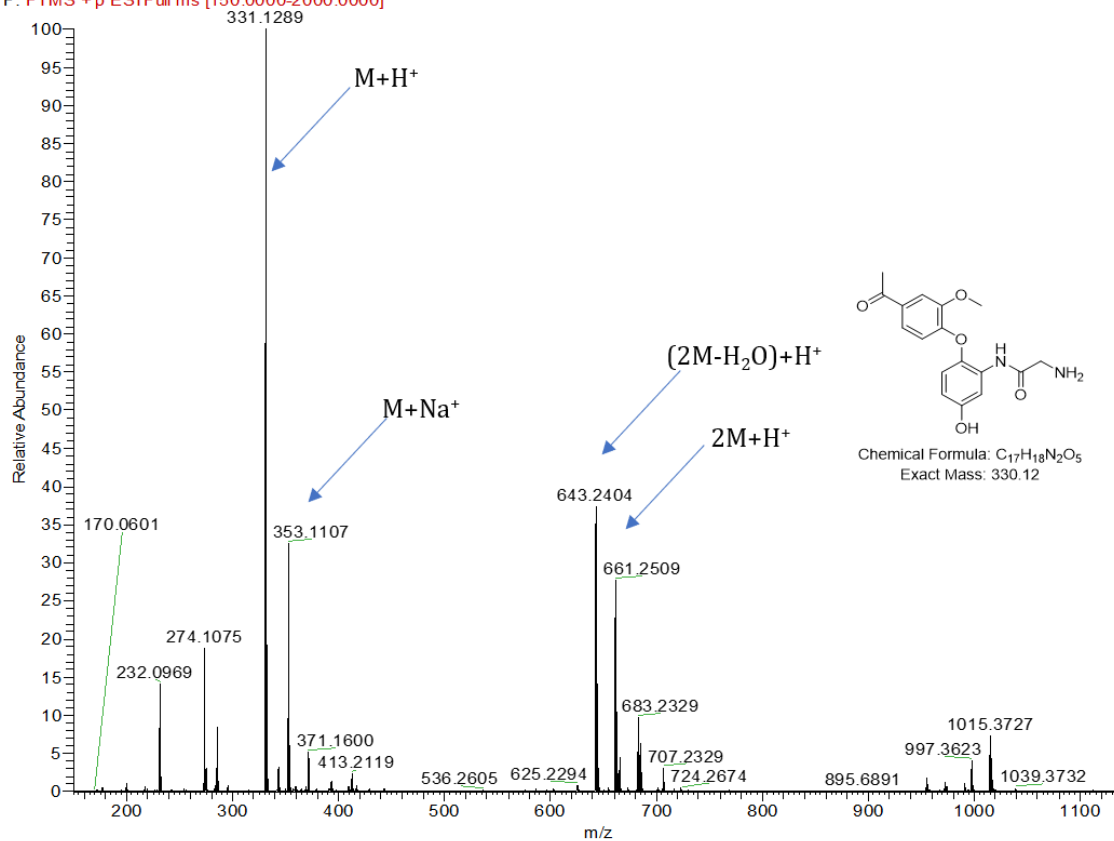
NMR for N-(2-(4-acetyl-2-methoxyphenoxy)-5-hydroxyphenyl)-2-aminoacetamide(1)



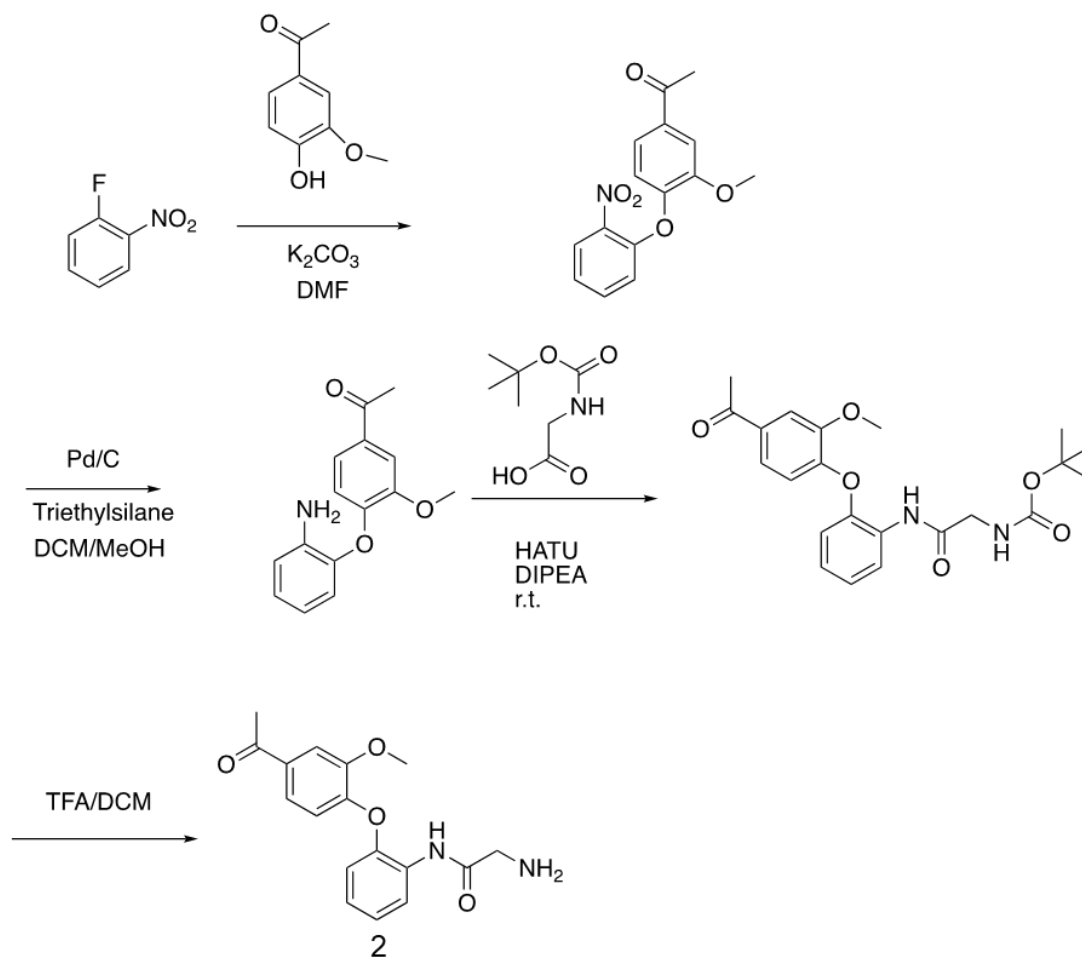


MS for N-(2-(4-acetyl-2-methoxyphenoxy)-5-hydroxyphenyl)-2-aminoacetamide(1)

Rawdata #140-216 RT: 0.35-0.59 AV: 46 NL: 1.66E9
F: FTMS + p ESI Full ms [150.0000-2000.0000]



2.2.1.2 Synthesis of compound 2



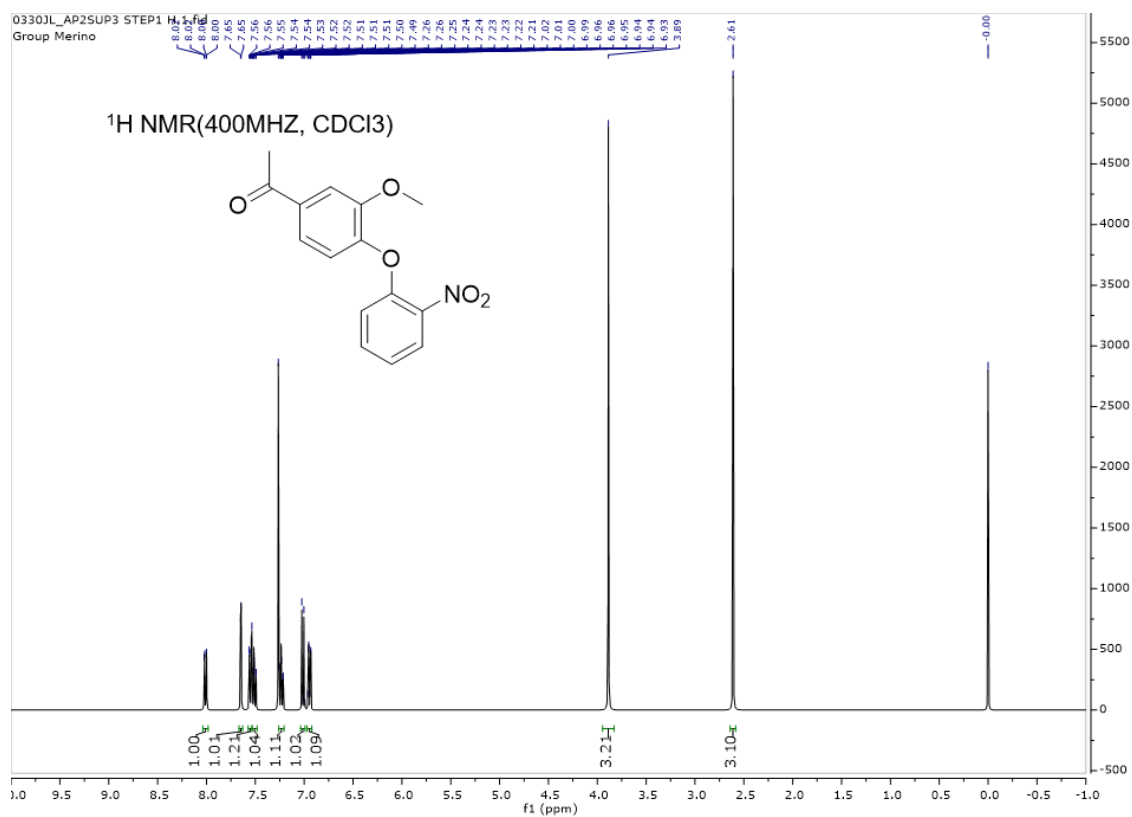
Scheme 4.3 The Synthesis route for **2**.

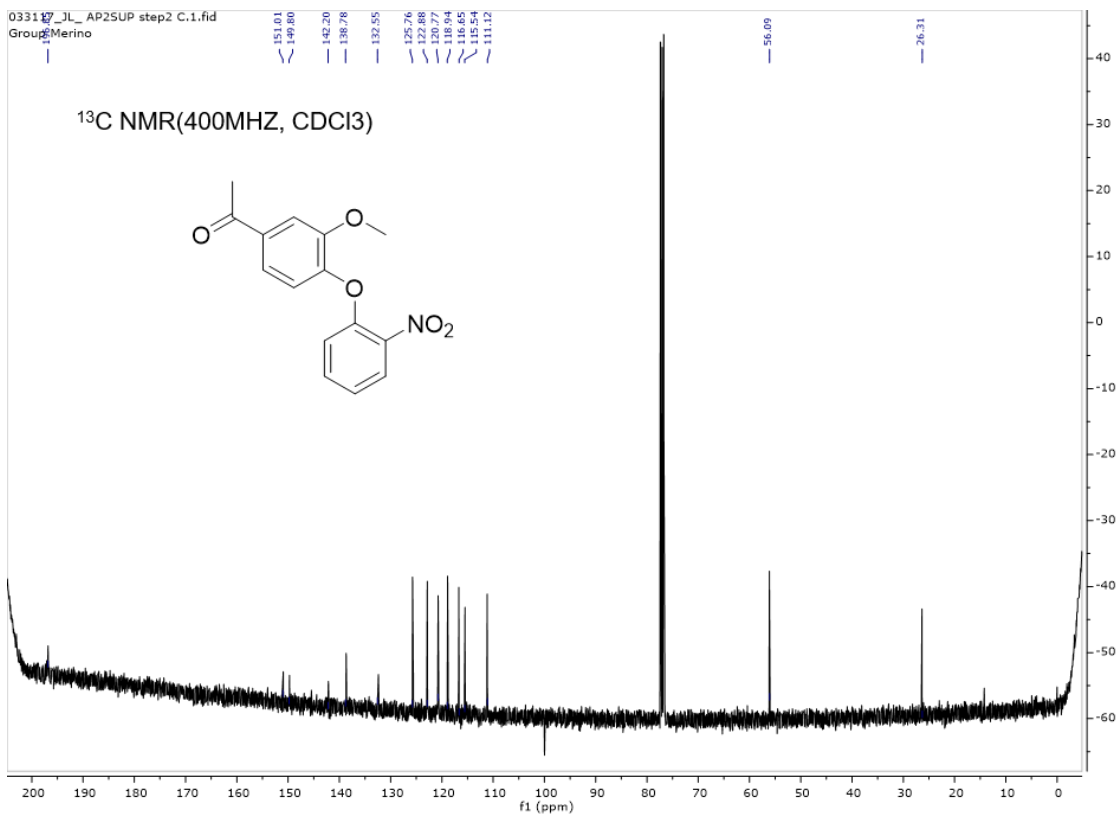
Synthesis of 1-(3-methoxy-4-(2-nitrophenoxy)phenyl)ethanone:

To a solution of apocynin (1.67g, 10mmol) in dimethylformamide (8mL) was added potassium carbonate (1.52g, 11mmol) add 1-Fluoro-2-nitrobenzene (1.41g, 10mmol) . The resulting mixture was stirred at 45°C for 12hours, after which time the reaction mixture was diluted with H₂O and extracted with EtOAc. The organic layer was dried (Na₂SO₄) and concentrated in vacuo. The resulting material was purified by flash chromatography using ethyl acetate/hexane (1:2) as eluent to provide the product as a yellowish solid. [2.58g yield:90%] ¹H NMR (400 MHz, Chloroform-d) δ 8.01 (dd, J = 8.2, 1.6 Hz, 1H), 7.65 (d, J = 2.0 Hz, 1H), 7.59 (m, 1H), 7.29 (m, 1H), 7.01 (d, J = 8.2 Hz, 1H), 6.98 (m, 1H), 3.89 (s, 3H), 2.61 (s, 3H). ¹³C NMR (101

MHz, CDCl₃) δ 196.85, 151.01, 149.80, 142.20, 138.78, 132.55, 125.76, 122.88, 120.77, 118.94, 116.65, 115.54, 111.12, 56.09, 26.31.

NMR for 1-(3-methoxy-4-(2-nitrophenoxy)phenyl)ethanone



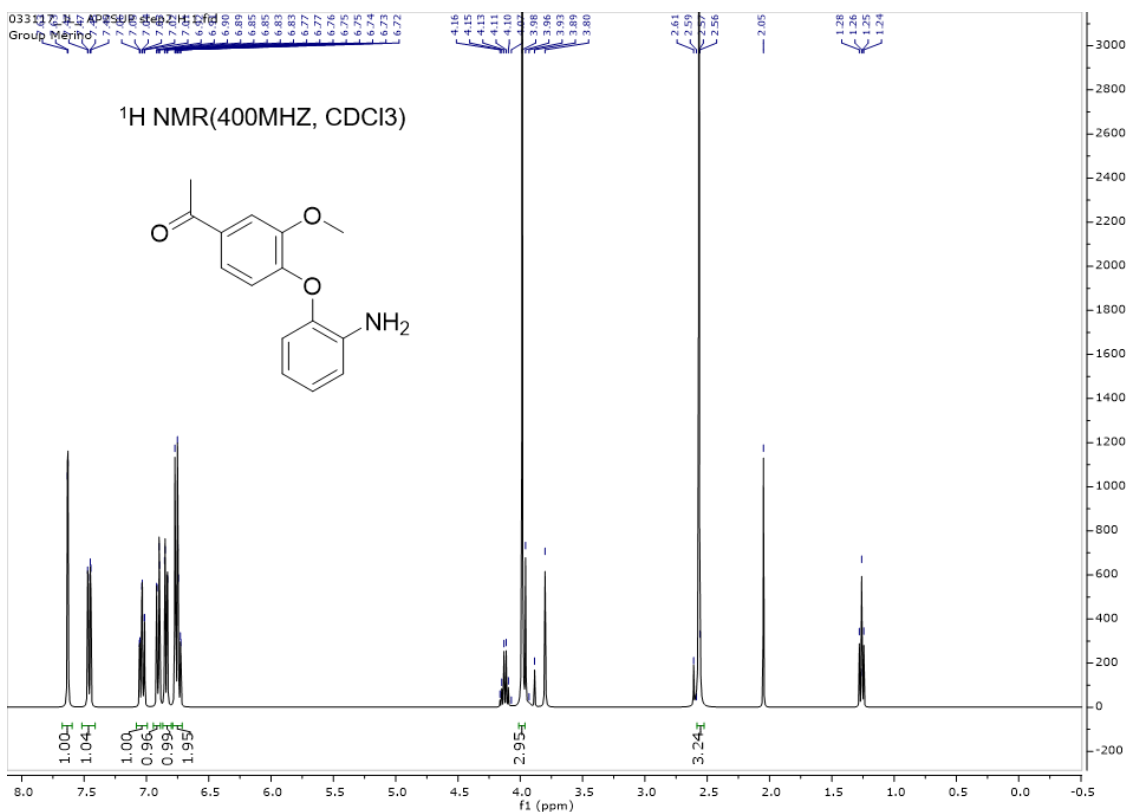


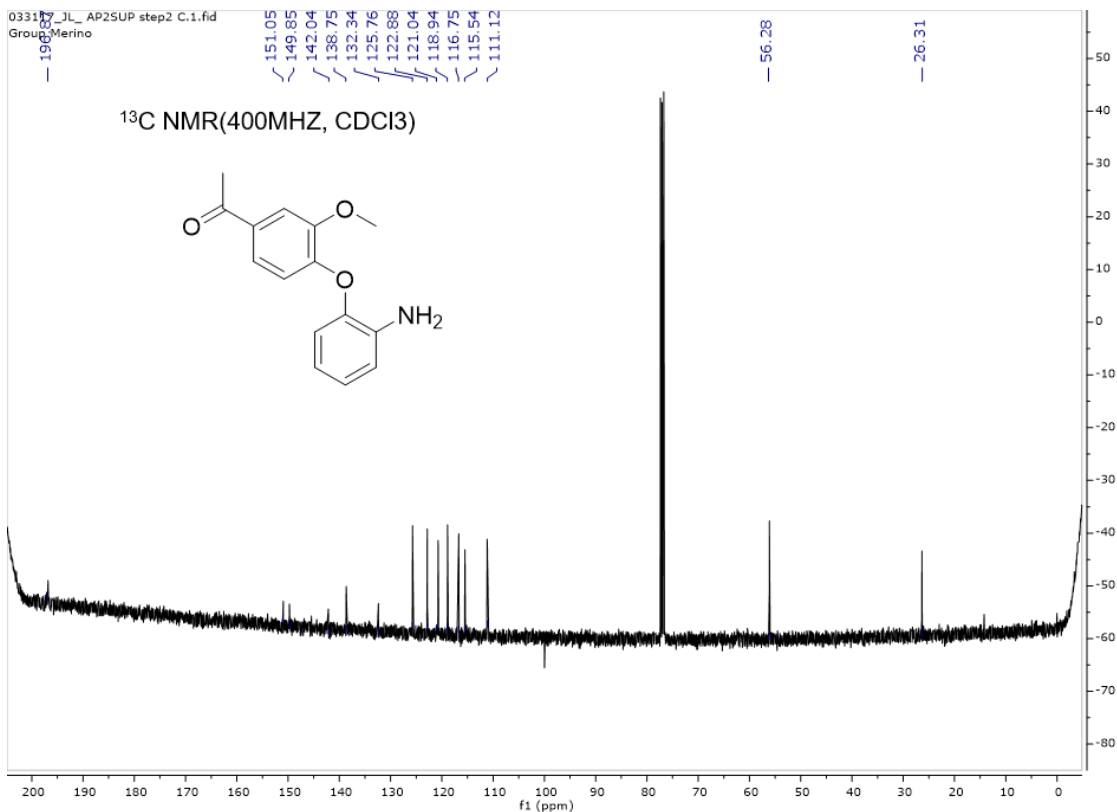
Synthesis of 1-(4-(2-aminophenoxy)-3-methoxyphenyl)ethanone:

To a solution of 1-(3-methoxy-4-(2-nitrophenoxy)phenyl)ethanone (1.72g, 6mmol) in dichloromethane which protected with Argon was added 10% Pd-C (172mg) and MeOH (13.5mL, 30mmol), followed by the addition of Neat triethylsilane (4.8mL, 30mmol) dropwise from a syringe. When the reaction was complete (TLC), typically complete within 3h, the mixture was filtered off and the solvent was removed under reduced pressure. The resulting material was purified through flash chromatography acetate/hexane (2:1) to provide the product as a yellowish solid. [1.38g, 90%]. ¹H NMR (400 MHz, Chloroform-*d*) δ 7.63 (d, *J* = 2.0 Hz, 1H), 7.46 (dd, *J* = 8.3, 2.0 Hz, 1H), 7.04 (td, *J* = 7.6, 1.5 Hz, 1H), 6.91 (dd, *J* = 8.1, 1.5 Hz, 1H), 6.84 (dd, *J* = 8.0, 1.5 Hz, 1H), 6.80 –

6.69 (m, 2H), 3.98 (s, 3H), 2.57 (s, 3H). ¹³C NMR (101 MHz, CDCl₃) δ 196.87, 151.05, 149.85, 142.04, 138.75, 132.34, 125.76, 122.88, 121.04, 118.94, 116.75, 115.54, 111.12, 56.28, 26.31.

NMR for 1-(4-(2-aminophenoxy)-3-methoxyphenyl)ethanone



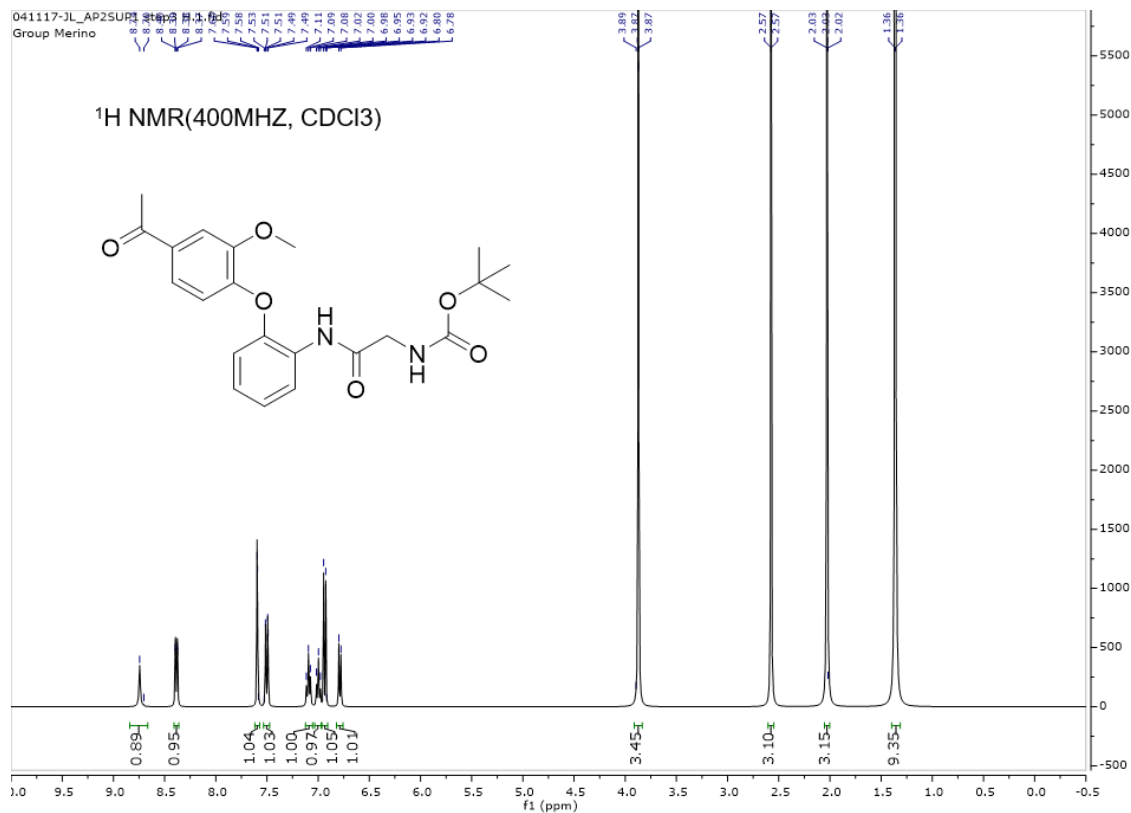


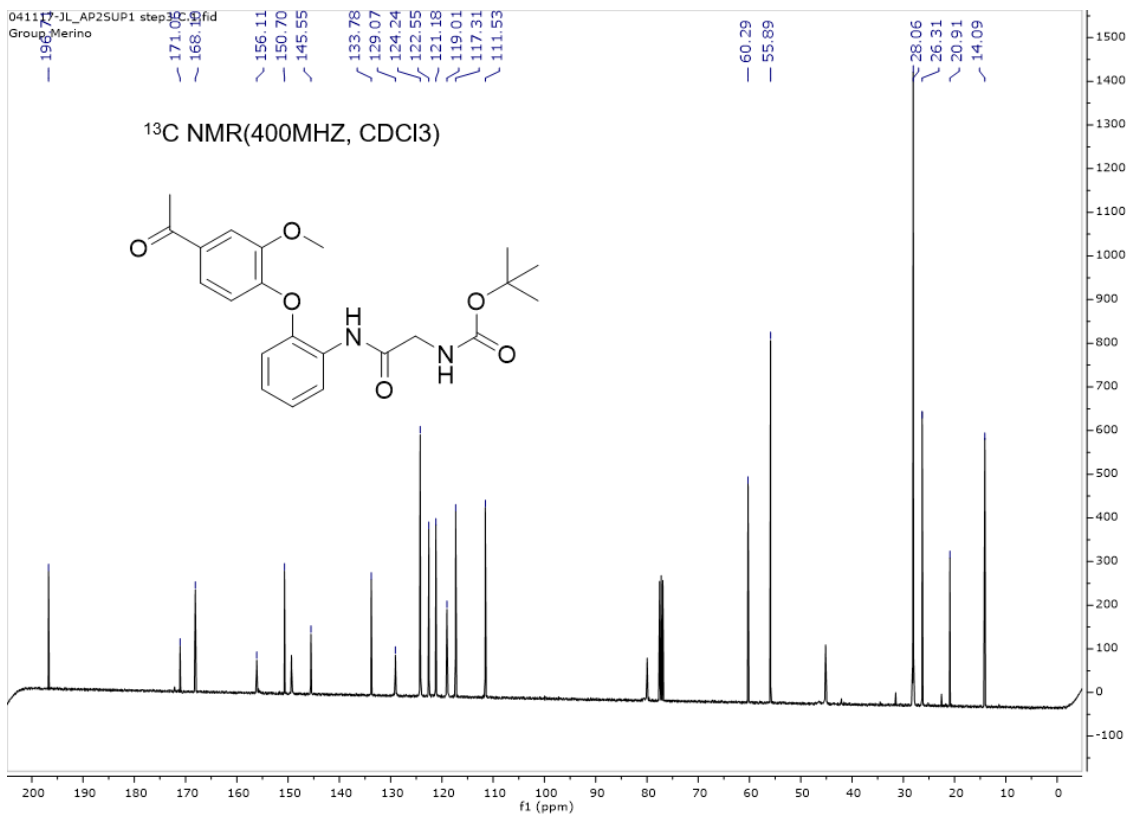
Synthesis of Tert-butyl 2-(2-(4-acetyl-2-methoxyphenoxy)phenylamino)-2-oxoethylcarbamate:

To a solution of the 2-(tert-butoxycarbonylmethylamino) acetic acid (0.875g, 5mmol) in DMF (5.0 mL) at room temperature was added HATU (2.1g, 5.5 mmol) and 1-(4-(2-aminophenoxy)-3-methoxyphenyl)ethanone (1.28g, 5 mmol), after 30 mins, followed by the addition of DIPA (1.8 mL, 10mmol). The resulting mixture was stirred at RT for 8 h, after which time the reaction mixture was diluted with H₂O and extracted with EtOAc. The organic layer was dried (Na₂SO₄) and concentrated in vacuo. The resulting material was purified by flash chromatography using ethyl acetate/hexane (1:1) as eluent to provide the product as a yellowish solid. [1.65g, 80%] ¹H NMR (400 MHz, Chloroform-d) δ 8.74 (s, 1H), 8.38 (d, J = 8.1, 1.5 Hz, H), 7.59 (d, J = 2.0 Hz, H), 7.50 (d, J = 8.3, 2.0 Hz, 1H), 7.09 (t, J = 7.8 Hz, 1H), 7.01 (t, J = 8.0 Hz, 1H), 6.94 (d, J = 8.3 Hz, 1H),

6.79 (d, J = 8.1 Hz, 1H), 3.92 (s, 3H), 2.61 (s, 3H), 2.09 (s, 3H), 1.45 (s, 9H). ¹³C NMR (101 MHz, CDCl₃) δ 196.71, 171.06, 168.10, 156.11, 150.70, 145.55, 133.78, 129.07, 124.24, 122.55, 121.18, 119.01, 117.31, 111.53, 60.29, 55.89, 28.06, 26.31, 20.91, 14.09.

NMR for Tert-butyl 2-(2-(4-acetyl-2-methoxyphenoxy)phenylamino)-2-oxoethylcarbamate



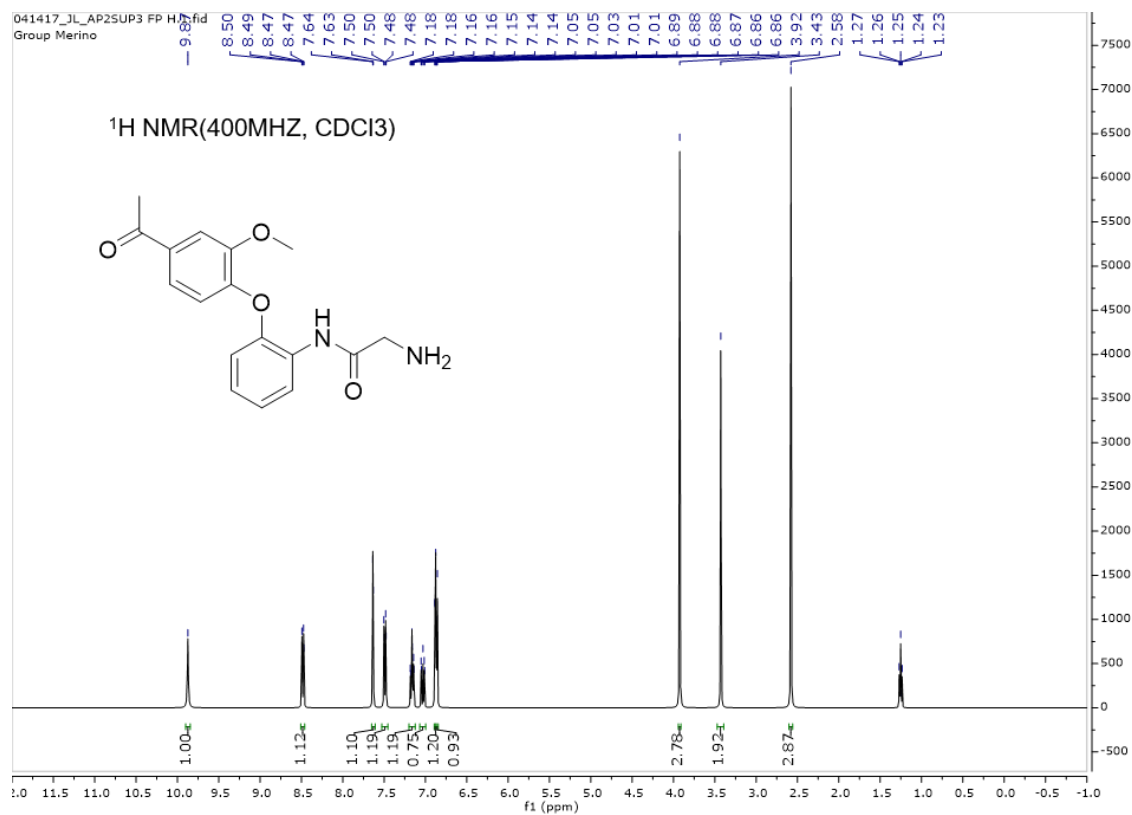


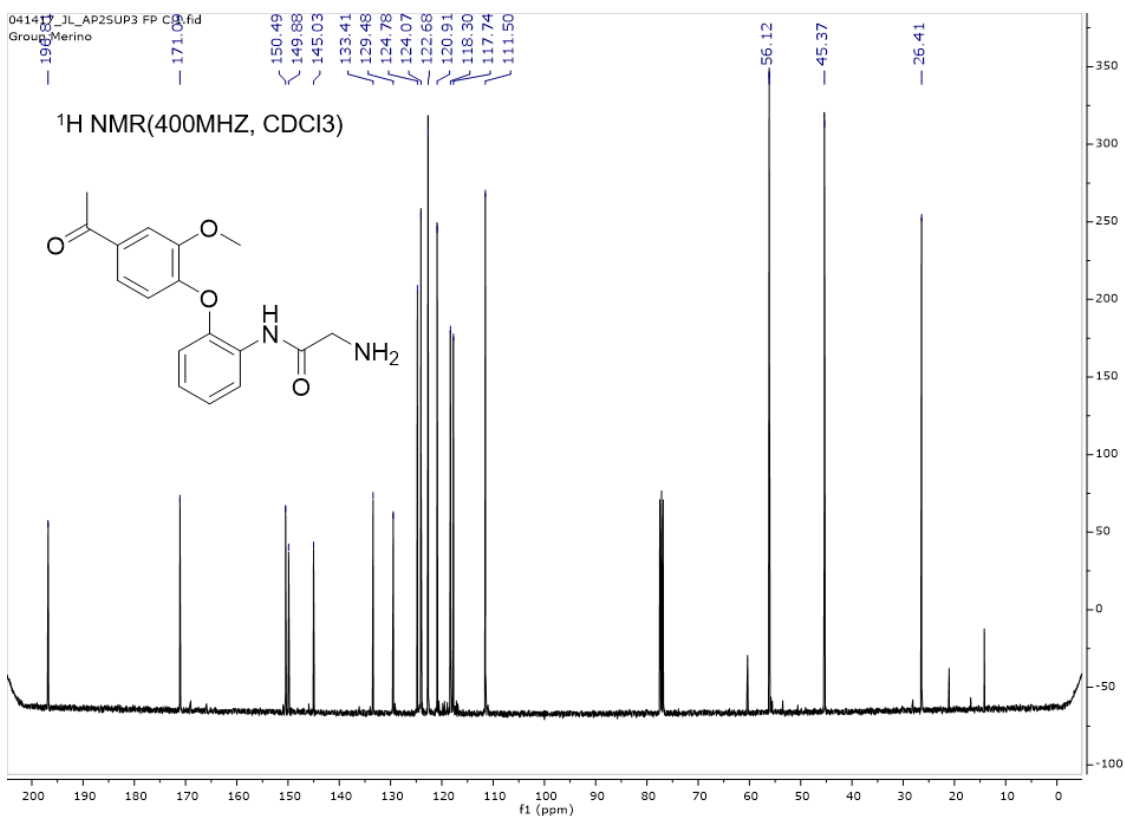
Synthesis of N-(2-(4-acetyl-2-methoxyphenoxy)phenyl)-2-aminoacetamide:

To a solution of Tert-butyl 2-(2-(4-acetyl-2-methoxyphenoxy)phenylamino)-2-oxoethylcarbamate (1.24g, 3mmol) in dichloromethane (5mL) was added trifluoroacetic acid (0.5mL). The resulting mixture was stirred at RT for 4 h with argon protection, after which time the reaction mixture was neutralized with saturated Na₂CO₃ solution and extracted with EtOAc. The organic layer was dried (Na₂SO₄) and concentrated in vacuo. The resulting material was purified by flash chromatography using DCM/MeOH (9:1) as eluent to provide the product as a yellowish solid. [847mg yield:90%] ¹H NMR (400 MHz, Chloroform-d) δ 9.87 (s, 1H), 8.48 (dd, J = 8.1, 1.7 Hz, 1H), 7.63 (d, J = 2.0 Hz, 1H), 7.49 (dd, J = 8.3, 2.0 Hz, 1H), 7.16 (td, J = 7.8, 1.5 Hz, 1H), 7.08 – 6.97 (m, 1H), 6.91 – 6.85 (m, 1H), 3.92 (s, 3H), 3.43 (s, 2H), 2.58 (s, 3H). ¹³C NMR (101 MHz, CDCl₃)

δ 196.81, 171.09, 150.49, 149.88, 145.03, 133.41, 129.48, 124.78, 124.07, 122.68, 120.91, 118.30, 117.74, 111.50, 56.12, 45.37, 26.41.

NMR for N-(2-(4-acetyl-2-methoxyphenoxy)phenyl)-2-aminoacetamide





2.2.2 Oxidation study

HRP oxidation: A working solution (1mg **1** was dissolved in 30mL 0.08 mM hydrogen peroxide in 25 mM phosphate buffer, pH=7.0) was made. A 1mL sample was used as the no enzyme control. The reaction was 1mL of working solution and 0.1U HRP. After 60 mins, 1mL ethyl acetate was added, shaken, and extraction performed. The organic layer was analyzed by HPLC to quantify the relative amounts of **1** and apocynin. Moles were calculated using a standard of each compound and yields were calculated using integration. All determinations were carried out in triplicate on different days. On each occasion and new standards and samples were made.

Fenton reagent oxidation: The above working solution was mixed with 10 μ L Fe-solution (10 mM Fe(NH₄)₂(SO₄)₂•6 H₂O, 10 mM EDTA, pH 8) by centrifugation of Fe-solution placed on the cap

of an Eppendorf tube. After 60mins of reaction, the reaction was processed as before.

KO₂ oxidation: 1mg **1** was dissolved in 30mL 25 mM phosphate buffer, pH=7. Solid KO₂ was premeasured into an 15mL falcon to give a final concentration of KO₂. After 60mins analysis proceeded as before.

UV Sensitivity of **1**: 1mg **1** was dissolved in 30mL 25 mM phosphate buffer, pH=7. 1mL was irradiated for 10 SED (10 min) using an Oriel Sol-UV-6 Solar Simulator, Oriel Instruments. After irradiation, analysis proceeded as before.

Oxidation studies of compound **2** were performed following the same procedure as **1**.

2.2.3 HPLC condition for oxidation studies

A Beckman Coulter's HPLC system consisting of a dual pump Model 126 with 32 Karat Software, a System Gold 168 detector and a System Gold 508 Auto Sampler was used. A reverse phase C-18 column (Synergi™ 4μm Hydro-RP 80Å, LC Column 100×4.6mm, Ea.) was used. The mobile phase consisted of HPLC grade Acetonitrile (Fisher Scientific), LCMS grade formic acid (Fisher scientific) and distilled water filtered through a Millipore Milli-Q water purification system. Solvent A for the mobile phase was 95% water, 5% Acetonitrile for oxidation study of **1** and 95% water, 5% Acetonitrile for oxidation studies of 1a-c. Solvent B is 95% acetonitrile and 5% water. The gradient was 0% B for 4 minute and 95% B over 16 minutes. Flow was 1ml/min. A detection wavelength of 250nm and 285nm was used for oxidation of **1**.

2.2.4 pUC19 ASSAY

Reaction mixture were prepared with 1 $\mu\text{g}/\mu\text{L}$ pUC19, and 0.5 mM 2'-deoxyguanosine in 20mM pH 7.4 phosphate buffer. Reactions with **1** had a final concentration of 50 μM . Fenton conditions were as described above. After 20 minutes reactions were stopped by addition of 10 μL quench solution (0.5 M EDTA and 0.75M 2-mercaptoethanol in 6X agarose gel loading buffer). A 1% agarose gel was prepared containing 0.75 $\mu\text{g}/\text{mL}$ ethidium bromide. From each reaction, 12 μL of quenched reaction was loaded per well. Gel electrophoresis was performed at 120 mV for 45 mins. Agarose gel images were analyzed by ImageQuant 6.0 software to determine the intensity of each band. Percentage of non-damaged DNA was calculated in each sample, by comparing the band intensity corresponding to super-coiled pUC19 in each sample, with DNA only control.

2.2.5 ABTS Assay

ABTS was dissolved in water to a 7 mM concentration. ABTS radical cation ($\text{ABTS}^{\bullet+}$) was produced by reacting ABTS stock solution with 2.45 mM potassium persulfate (final concentration) and allowing the mixture to stand in the dark at room temperature for 24 h before use. For the study, the $\text{ABTS}^{\bullet+}$ working solution was diluted with PBS, pH 7.4, to an absorbance of 0.70 (± 0.05) at 734 nm. Then 100 μL working solution was mixed with 100 μL of various concentrations of each solution in a 96 well microplate. After 6 minutes of incubation the plate was read at 743nm for absorbance. Appropriate solvent blanks were also run in each assay. All determinations were carried out at least three times including the standards and controls. The percentage inhibition of absorbance at 734 nm is calculated by: $(A_c - A_t)/A_c \times 100\%$. The EC50 based on the Concentration-response curve for the absorbance at 734 nm for $\text{ABTS}^{\bullet+}$ as a function of concentration of antioxidant solution.

2.2.6 Cell Culture

In these studies neonatal human keratinocytes were plated at a density of 0.60×10^6 cells/100 mm dish in EpiLife® supplemented medium (Gibco) and grown to a density of 80% confluence. The following experimental groups: 1) Control; 2) ssUVR; 3) 50 μ M **1**; and 4) ssUVR+50 μ M **1** were used unless otherwise noted.

2.2.7 Efficacy of RIP Reagent in Cellular Environment

Cells were allowed to attach for 24 h and incubated with **1** for 18 h before irradiation with 8 SED using an Oriel Sol-UV-6 Solar Simulator set to maximum power. Immediately after irradiation, fresh medium was replaced, and cells were kept in 5% CO₂ humidified incubator at 37°C for 1.5 hr. After 1.5hr, cells were washed in cold PBS and detached from the dish with cell scraper in 1ml of cold PBS. Ethyl acetate was added 1:1 (v/v) to the cell suspension. Organic layer was then extracted and dried. Samples were resuspended in 100 μ L of acetonitrile and analyzed by direct injection into the HPLC as described above. All determinations were carried out at least three times.

2.2.8 Quantifying Damage by LC-MS

Fibroblast cells (8×10^6 per sample) in PBS were treated with **1** or PBS for 18 h at 37 °C. Then, sample cells were irradiated at 10 SED using an Oriel Sol-UV-6 Solar Simulator operating at 24 °C. All treatments were performed in quadruplicate. To isolate genomic DNA cells were trypsinized, washed, and lysed by freeze/thaw for four cycles. Then, DNA isolated using a Wizard Genomic DNA Purification Kit (Promega Corp) per kit instructions. DNA yield for each sample was quantified by A₂₆₀ in triplicate. Digestion of DNA occurred using, the following procedure. DNA was denatured, placed on ice, and incubated 0.2 U of bovine pancreas DNase I (Millipore

Sigma) in 0.03 M ammonium acetate (pH 5.) at 45 °C for 2 h. The enzyme was then precipitated and spun down using ammonium bicarbonate (pH 8.0). Next, 5 mU of phosphodiesterase I (Worthington Biochemical Corp.) and 0.2 U of calf intestinal alkaline phosphatase (Thermo Fisher) were incubated at 37 °C for 2 h. Finally, enzymes were again precipitated. and samples resuspended in 200 µL of LC-MS mobile phase.

LC-MS analysis was performed with a SCIEX 4000 QTRAP triple quad mass spectrometer with a turbo spray ion source interfaced with an Agilent 1260 HPLC. Injection volume was 5 µL onto an Agela Technologies Optimix C18/amide column (2.1 x 50 mm, 5 µm) flowing at 0.2 mL/min in HILIC mode at 20 °C. Solvent A was 95:5 water: acetonitrile and Solvent B was 95:5 acetonitrile:water, both with 0.1% formic acid. The following gradient was used: 0 min, 100% B; 2.5 min, 100% B; 7.6 min, 70% B; 9.4 min, 70% B; 10.4 min, 100% B. Selected ion monitoring in positive ion mode to detect 8-oxo-7,8-dihydro-2'-deoxyguanosine ($[M+H]^+$; $m/z = 284.1$). Peak areas were normalized per µg of DNA.

2.2.9 DCFDA assay by flow cytometry

Cells were grown in 25 cm² tissue culture plates to 50% confluence. Then each plate was incubated with the listed compound for 18 hours. Cells were trypsinized and washes with HBSS twice. Each sample was irradiated and then 5µM DCF-DA (Sigma Aldrich) was added. Incubation for 30 min, washing, and DCF fluorescence was obtained in using BD FACS Canto flow cytometer by exciting at 485 nm and emission at 535nm after eliminating 7AAD positive cells. Percentage of cells with high DCF fluorescence were compared among different treatments. Data shown are the average of three biological replicates.

2.3 Results and Discussion

2.3.1 Compound 1 could release apocynin as a prodrug.

We envisioned that the ROS-initiated release of apocynin would occur, as shown in **Figure 2.2** and a more detailed mechanism is shown in SI Scheme 1. Because the phenol of apocynin is essential to its unique biochemical mechanism, the covalent attachment through the ether to the ROS-sensitive motif would block activation except under oxidative stress conditions. To examine the reaction, two derivatives were synthesized: the RIP reagent (**1**, structure shown) and a control molecule (**2**) where the phenol is not present to prevent oxidation and subsequent cyclization. Compound **1** was made in five steps with a net 25% yield, and **2** was made in four steps in 45% yield.

The oxidation reaction of **1** was examined (**Figure 2.2A**) under Fenton conditions, which generate hydroxyl radical. The Fenton conditions were 0.1 mM $\text{Fe}(\text{NH}_4)_2(\text{SO}_4)_2 \cdot 6\text{H}_2\text{O}$, and 0.08 mM H_2O_2 in pH 7.0 phosphate buffer and the concentration of **1** was 0.1 mM. Extraction was performed since apocynin is not soluble in buffered solutions. After extraction with ethyl acetate, aqueous and organic layers were analyzed by HPLC. Under our conditions, **1** eluted near 10 min, whereas apocynin eluted near 12 min (**Figure 2.2B**). Apocynin, which is observed in the organic layer, has a retention time of 13 min. The second reaction product, **1^{ox}**, is observed in the aqueous layer and has a characteristic absorbance at 375 nm as does a variant of **1^{ox}** identified in a previous manuscript. [17] Exposure to Fenton conditions in phosphate buffer led to formation of products **1^{ox}** and apocynin, whereas in the absence of Fenton reagent no reaction was observed (**Figure 2.2B**). Quantitative analysis of the organic layer indicated that under these Fenton conditions, 85% (+/- 2%) of **1** was converted to products (**Figure 2.2C**). This is close to the expected yield based

on the concentrations of **1** and H₂O₂, indicating that the first oxidative equivalent of Fenton reagent reacts with **1** completely. Both products were collected, and MS analysis confirmed expected product identities (**Figure 2.2C**).

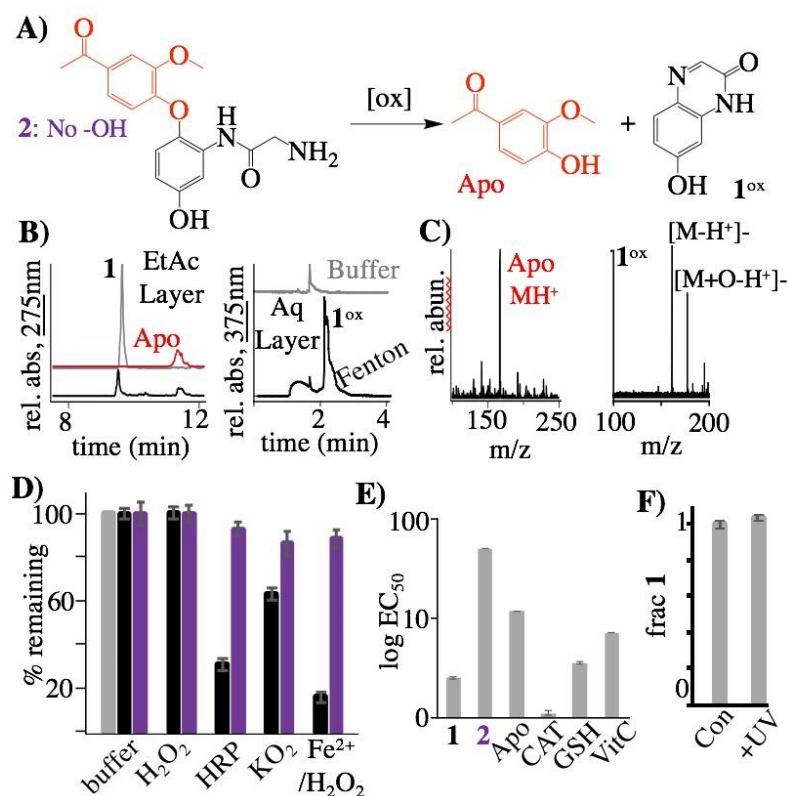


Figure 5.2 (A) Proposed reaction of **1** to release apocynin and generate **1^{ox}**. The control compound **2** lacks an oxidizable phenol. (B) HPLC analysis of **1** incubated in phosphate buffer (gray trace) and under Fenton conditions (black trace); the organic (left) and aqueous (right) layers were analyzed. Pure Apo was also analyzed (red trace), and peak corresponding to **1^{ox}** and Fenton reagent are indicated. (C) MS of isolated products. (D) Sensitivities of **1** (black) and **2** (purple) to various ROS forms. (E) Antioxidant capacity as measured by ABTS assay. The obtained EC₅₀ values are shown. (F) Fraction of **1** in solution not subjected to irradiation and irradiated with 10 SED.

We next examined the reaction of **1** with various ROS forms encountered under cellular conditions **Figure 2.2D**. After 1 hr in Fenton conditions, 15% (+/- 2%) **1** remained. In experiments lacking $\text{Fe}(\text{NH}_4)_2(\text{SO}_4)_2$ and only containing hydrogen peroxide we find an insignificant loss of **1** after 1 hr. Importantly, the reaction is diffusional and first order in both Fenton reagents (**Appendices S 1**). This indicates that self-cyclization of **1** will be strongly correlated to the total amount present in cells. After a 1 hr exposure to 0.08 mM KO_2 63% (+/-8%) of **1** remained. Oxidase activation was examined using 0.01 mU of HRP enzyme and 0.08 mM H_2O_2 . Under these conditions 30% (+/-5%) remained after 1 h. We examined the control compound **2**, which lacks a phenol important to oxidation under the same conditions. Compound **2** was resistant to oxidation (**Figure 2.2D**, purple) under the same conditions, in all cases.

We then assessed antioxidant activity of the RIP reagent **1** (**Figure 2.2E** for EC_{50}). To determine antioxidant capacity a 2,2'-azino-bis(3-ethylbenzothiazoline-6-sulphonic acid) (ABTS) assay was performed. In the assay, green ABTS (7 mM) radicals are induced from persulfate (2 mM), and the ability of antioxidants to reduce color formation is evaluated over a concentration range to obtain an EC_{50} value (**Appendices S2**). In the presence of 10 μM **1**, rapid inhibition was observed, whereas **2** at the same concentration had limited activity. Compound **1** had an EC_{50} value of 2.4 (+/-0.1) μM , whereas the EC_{50} of **2** is 60 (+/- 1) μM . Apocynin, catalase, glutathione, and vitamin C had EC_{50} values of 11.7 (+/- 0.4), 0.7 (+/- 0.1), 3.5 (+/- 0.2), and 7 (+/- 0.1) μM , respectively. Thus, **1** has modest antioxidant ability relative to common antioxidants but these reactions are required to release the bioactive molecule.

It is important that **1** be stable to UVR exposure (**Figure 2.2F**). To test this, **1** (100 μM) in phosphate buffer (pH 7) was irradiated for a total of 10 Standard Erythemal Dose (SED) units. Under these conditions, **1** is not degraded. In summary, these data show that **1** is oxidized by various ROS, has antioxidant capacity similar to those of common antioxidants and that the oxidation liberates apocynin, a bioactive oxidase inhibitor.

2.3.2 Compound 1 could protect skin cells from UVR irradiation without damaging health cells.

Next, we analyzed the ability of **1** to prevent DNA damage in an *in vitro* DNA nicking assay. The concentration of pUC19 plasmid was 1000 ng/ μL . After 1 hr incubation under Fenton conditions, 31% (+/-3%) of the plasmids were nicked. No nicking was observed under Fenton conditions in the presence of 50 μM **1** or **1** without Fenton reagent (**Figure 2.3A**).

We then evaluated the cytotoxicity of **1** to primary keratinocytes in culture. After three days of incubation with **1** no cytotoxicity was observed except at the highest dose tested. At the high dose of 100 μM , a 15% (+/- 3%) reduction in viability was observed (**Figure 2.3B**). We also examined the effect of **2**, which is not oxidizable, and a compound that is oxidizable but does not eject apocynin (**Appendices S3**). Again, neither of have an effect on viability. To evaluate the efficacy of the RIP reagent in the cellular environment, primary keratinocytes (10 million cells) were treated with 50 μM **1** or not and irradiated. (**Appendices S4**). In cells treated with **1** but not subjected to UVR, little apocynin was detected (0.03 +/- 0.02 pmol). In cells that were treated with **1** and irradiated 0.97 (+/- 0.07) pmol of apocynin were detected (**Figure 2.3C**), thereby confirming that self-cyclization and apocynin release occurs within a cellular environment. Based on this

analysis, the concentration of apocynin within the cells is approximately 28 μM , this is a level that is known to cause inhibitory effects. We also observed **1** inside of cells at a concentration of 190 μM .

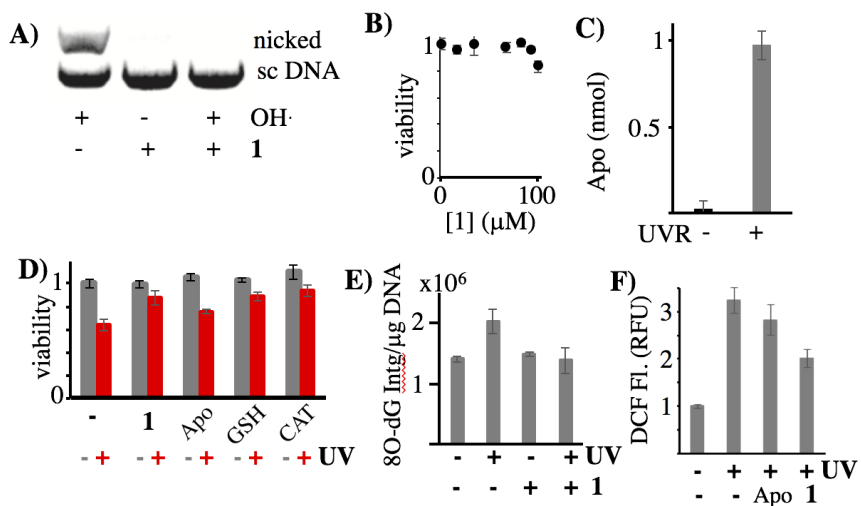


Figure 6.3 (A) Gel electrophoretic separation of supercoiled and nicked plasmid in the presence and absence of Fenton reagent and compound **1**. (B) Viability of primary keratinocytes in a range of concentrations of **1**. (C) Production of Apo in skin cells treated with 50 μM **1** with and without irradiation with 10 SED. (D) Viability of primary keratinocytes without (gray bars) and with 10 SED UVR (red bars) in the presence of the indicated antioxidants. (E) Relative LCMS quantification of 8-oxo-7,8-dihydro-2'-deoxyguanosine under UVR and **1** treatment. (F) Dichlorodihydrofluorescein diacetate fluorescence measurements under UVR and **1** treatment.

Irradiation of primary keratinocytes with 10 SED reduced viability to 63% (+/-5%) relative to DMSO-treated control cultures (**Figure 2.3D**). Cells were also treated with 50 μM **1**, 50 μM apocynin, 50 μM glutathione, or 3 U catalase without irradiation. Both apocynin and catalase slightly but significantly enhanced growth to 106% (+/-2%) and 110% (+/- 3%) relative to DMSO-treated controls ($p < 0.05$). Neither **1** nor glutathione influenced viability at this concentration (**Figure 2.3D**). Higher concentrations of apocynin, glutathione, and catalase were cytotoxic (data not shown). After the 10 SED irradiation, compound **1** increased viability to 88% (+/-5%) relative

to the control, while irradiated cells pretreated with apocynin showed a more modest rescue to 75% (+/-2%) (**Figure 2.3D**). **1** is two times better at entering a cell than apocynin (**Appendices S5**), but does not affect viability without activation. Only when UVR radicals are formed **1** will react (antioxidant function) and release apocynin. Next, we examined if **2**, which cannot be oxidized, rescued cells from UVR stress. **Appendices S3** shows little rescue in the presence of UVR. Similarly, we examined a compound that lacks apocynin and no rescue in the presence of UVR stress is observed. We validated if apocynin was inhibiting NOX enzymes (**Appendices S6**). Cells were treated with apocynin and the phosphorylation status of AKT, a downstream protein dependent on NOX1 activity quantified. An in-cell western for phosphorylation of AKT at Ser473 which is phosphorylated by NOX1. Apocynin reduced the amount of phosphorylated serine by 21 (+/-9) % in the presence of UVR. The p-value was less than 0.02. We then examined common antioxidants. At the concentrations tested, glutathione and catalase increased viability to 88% (+/-4%) and 93% (+/- 5%) respectively (**Figure 2.3D**). Extents of rescue by antioxidant treatment were not statistically different. To further confirm the ability of **1** to reduce oxidative stress in cells we examined the amount of 8-oxo-7,8-dihydro-2'-deoxyguanosine relative to non-UVR treated cells via LC-MS (**Figure 2.3E**). Because of the large quantity of cells needed primary fibroblasts were used. In this assay the integrated intensities at 284 m/z were compared to the total amount of DNA recovered. For simplicity total integrated values are reported per million. We found that UVR treatment raised the relative level of the lesion to 2.03 (+/- 0.19) from 1.41 (+/- 0.05) Int/ μ g DNA with a p-value less than 0.01. Treatment of **1** prior to UVR lead to a reduction of the lesion back to 1.39 (+/- 0.21), which is not statistically different compared to untreated cells. Finally, **1** alone does not change the amount of lesion found. Subsequent confirmatory experiments utilized the common DCF-DA oxidative stress assay (**Figure 2.3F**). Though DCF-DA has known issues,

mainly dealing with the amount of incubation time leading to indiscriminate activation of the dye[26], the same trend in the data is observed. Thus, of the compounds tested, **1** had the smallest effect on cell growth in non-irradiated cells and similar ability to protect cells from UV irradiation.

2.3.3 Application of Compound 1 in skin explants

We then used a human skin explant model to evaluate the effect of topical treatment with **1** on UV-induced damage (**Figure 2.4A**). In this model, topical treatments, mimicking use of sunscreen, can be tested without compromising the dermis. Discarded and deidentified human skin was obtained from donors undergoing elective surgical procedures. Human skin was used as rodent models do not recapitulate human biochemistry due to the amount of hair. Subcutaneous fat tissue was removed from the skin, and skin was cut into 3.5 cm diameter circles and placed into culture dishes with DMEM/F12 media without phenol red, supplemented with growth factors. The dermal side was in contact with the medium, and the epidermal was exposed to air. A solution of 50 μ M **1** or DMSO control solution was spread on the skin and allowed to dry overnight. Note that skin is much more resistant to UVR than naked cells so a 25 SED UVR exposure was used. After exposure skin was homogenized, protein was extracted, and DNA damage signaling quantified by western blotting. UVR induced strong expression of the DNA repair signaling protein p53 at 24 h post irradiation. Treatment of **1** without UVR caused no increase in expression of p53. Importantly, p53 expression was reduced by 46% (+/-5%) in skin treated topically with **1** and then irradiated (**Figure 2.4B**).

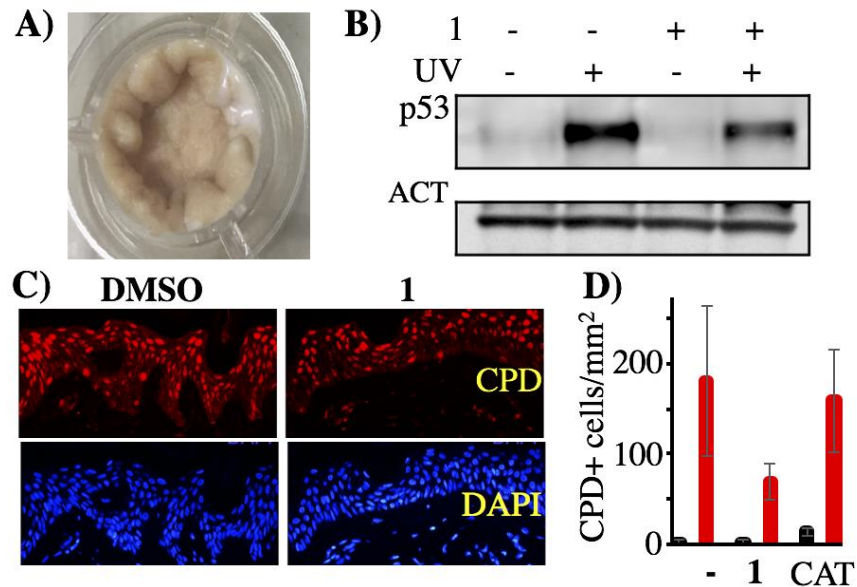


Figure 7.4 (A) Representative image of skin explant. (B) Western blot analysis of p53 production in skin explants treated or not with **1** and subjected or not to UVR. Actin protein shown as a control. (C) Representative immunofluorescence images of skin explants treated with DMSO or **1** and subjected to 10 SED irradiation. Red indicates the presence of CPDs; nuclei were stained with DAPI (blue). (D) Quantification of CPD-positive cells per mm² of non-irradiated (black bars) and irradiated (red bars) skin treated with DMSO (-), compound **1**, or catalase (CAT).

We then directly evaluated DNA damage in skin explants by staining for cyclobutane dimers (CPDs). Skin explants were treated with RIP reagent **1** (50 μ M) or catalase (3U) and dried overnight. At 24 h after 25 SED irradiation, explants were subjected to immunofluorescence imaging (**Figure 2.4C**). Experiments were performed on three separate skin explants per condition and quantification was performed using ImageJ software at 20 different locations per skin explant (**Figure 2.4D**). Cells (identified by staining with DAPI) that co-localized with CPD signal (3 fold above background) were scored as damaged. Without irradiation, few cells were positive for CPD (2 \pm 2 cells/mm²). Upon UVR exposure, 180 (\pm 82) CPD-positive cells per mm² were detected

in DMSO-treated control explants. Treatment with **1** without UVR did not have a significant effect (2 ± 2 CPD⁺ cells/mm²) but catalase treatment did (13 ± 4 CPD⁺ cells/mm²), indicating some resting reductive stress. After UVR exposure, catalase-treated samples had $160 (\pm 60)$ CPD-positive cells per mm², not significantly different from the control UVR-treated explants. In contrast, treatment with **1** significantly reduced the number of CPD-positive cells per mm² to $70 (\pm 20)$ relative to the control explants ($p < 0.0005$). Thus, the RIP reagent **1** greatly reduced DNA damage and damage signaling when applied topically to human skin explants.

2.4 Conclusions

In conclusion, we have developed an ROS-controlled antioxidant, RIP reagent **1**, that after oxidative reaction (antioxidant function) releases a NOX inhibitor known as apocynin. The ROS-activation is dependent on a key phenol in the molecule that leads to self-cyclization and release of the NOX inhibitor. The molecular design of the ROS-initiated protective reagent is an alternative to the well-known boron ester and quinone methide chemistries. Reagent **1** did not alter viability of cultured skin cells and prevented UVR-induced cell death to a similar extent as other tested antioxidants. In a human skin explant model, **1** applied topically reduced the formation of cyclobutane dimers and DNA repair signaling. Thus, the described RIP reagent is a catalytic antioxidant activated by high oxidative stress environments like UVR irradiation and these reagents have potential for uses in sunscreens.

Chapter 3
**UV cell stress-induced protective reagent
based on natural product and NOX inhibitor**

3.1 Introduction

The overdose of UV radiation leads to obvious acute and chronic consequences on the skin, such as sunburn (inflammation)⁶⁸, pigmentation, immunosuppression⁶⁹, and chronic effects such as photoaging photocarcinogenesis (melanoma progression)⁷⁰. ROS has a vital role in the metabolism of skin cells not only in a positive way, such as proliferation and differentiation⁷¹ but also negative way, like cell death or carcinogenesis⁷²⁻⁷³.

Cutaneous melanoma is a highly malignant tumor derived from pigment-producing melanocytes in the epidermis of the skin⁷⁴. ROS can be involved in both the initiation and progression of malignant melanoma⁷⁵. **(Figure 3.1)** UV irradiation induce an immediate strong activation of NOX at the beginning, a more moderate increase in NOX activation was observed from a long time after irradiation. The activation of NOX upregulates the ROS production and further leads the DNA damage². Nucleotide excision repair (NER) is the primary pathway for repairing this damage. However, defective NER is associated with cell apoptosis and carcinogenesis. ROS also contributes to cell viability of melanoma by activation of nuclear factor-kappa B⁷⁶, a transcription factor that is essentially promoting cell survival⁷⁷. What's more, it is also the first step for melanoma progression to happen.⁷⁸ Chemokines upregulated by NF- κ B can improve the growth and invasion of melanoma cells by autocrine and paracrine loops⁷⁹.

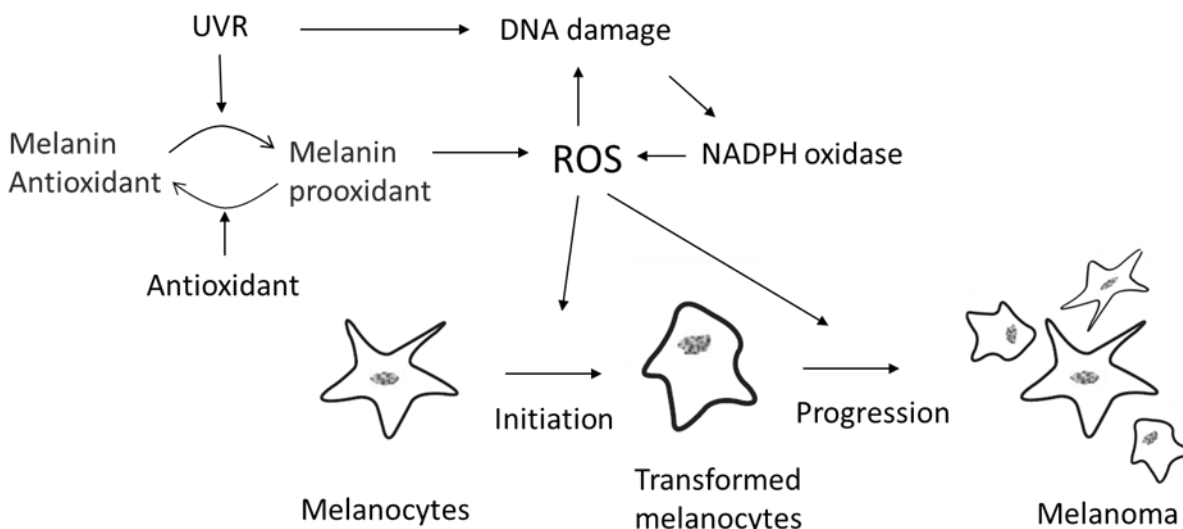


Figure 8.1 UVR induced ROS upregulation leads to skin cancer

The control of ROS may help with the prevention of melanoma from the initiation to the progression by its role. Two strategies proposed to use for the downregulation of ROS. One of them is to antioxidants uploading to quench the extra ROS produced by UV stress. Antioxidants like Vitamin C, Vitamin D are used in the daily diet for skin protection and are proven to be useful. The other one is to inhibit the NADPH oxidase, which is the primary generator of ROS. Several NOX inhibitors are already in use for melanoma prevention like apocynin, GKT137831. However, the direct use of antioxidants or NOX inhibitor has potential issues. First, the ROS and NOX exist not only in the cancer cells but also in healthy cells, and they will react and consume the volume the drug before letting the drug enter the target cancer cells. Then, the overdose of antioxidants and NOX inhibitor also induce cell stress.

The RIP1 reported in chapter2 enlight the researcher to design prodrugs conjugated an antioxidant sesamol and NOX1 inhibitor ML171 with a ROS active moiety to provide stability and selectivity

for anti-ROS drugs. Sesamol is a potent antioxidant and free radical scavenging ingredient extracted from sesame seeds.⁸⁰ Sesamol has a cell protection effect on UVB-induced cytotoxicity, intracellular ROS generation, and oxidative DNA damage in human fibroblasts.⁸¹ ML171 is reported as a potent NOX inhibitor, which showed IC50 values of 130–250 nM for NOX1, and of 3–5 μ M for NOX2–4 well as for xanthine oxidase. The ROS activated self-cyclizing linker, and a ROS sensitive oxoacetamide are designed and attached on the active site of either of the drugs. Cell test about the stability of SA1 and RIP2 and releasing manner prove their potential as an anti-cancer drug by ROS downregulation.

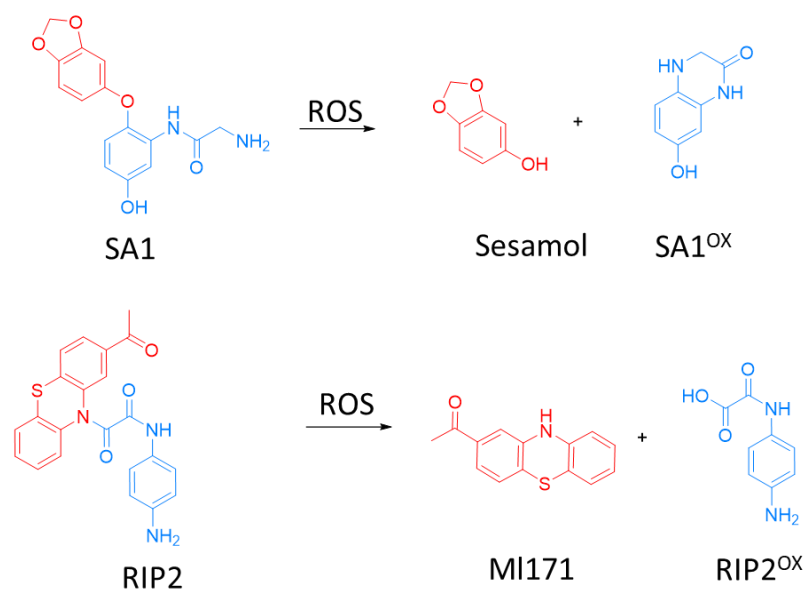


Figure 9.2 ROS activated prodrug base on natural products

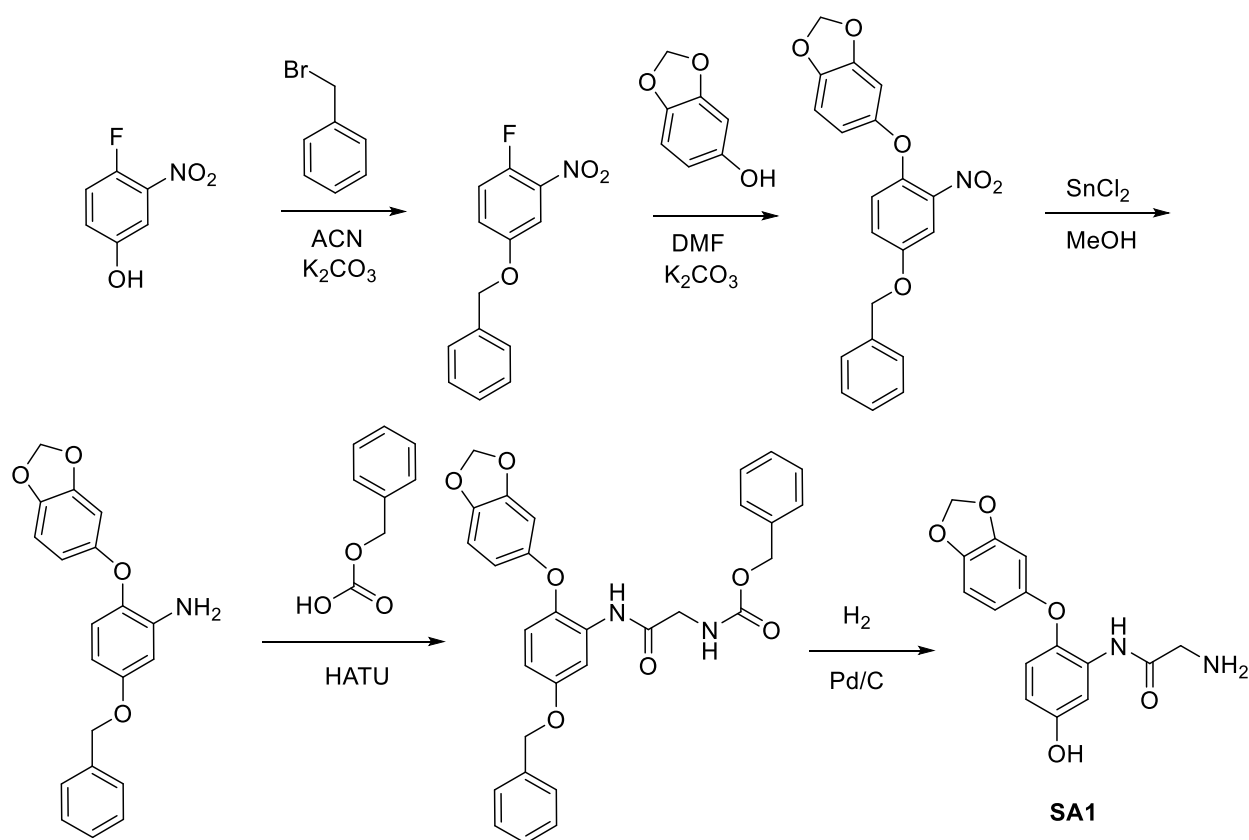
3.2 Experiment section

3.2.1 Synthesis and characterization of compounds

Boc-sarcosine, trifluoroacetic acid (TFA) and dimethylformamide, chloromethyl methyl ether were purchased from Sigma-Aldrich Chemical Co. (St. Louis, MO, USA). Sesamol, 4-floro-3nitro

phenol, pladium on carbon, 4'-Hydroxyacetophenone, 1-Fluoro-2-nitrobenzene, Triethylsilane, HATU were purchased from Fisher scientific international, Inc. All solutions were prepared with water purified by a Milli-Q system (Millipore, Bedford, MA, USA). All reagents used for buffer preparation were of analytical grade.

3.2.1.1 Synthesis of compound SA1



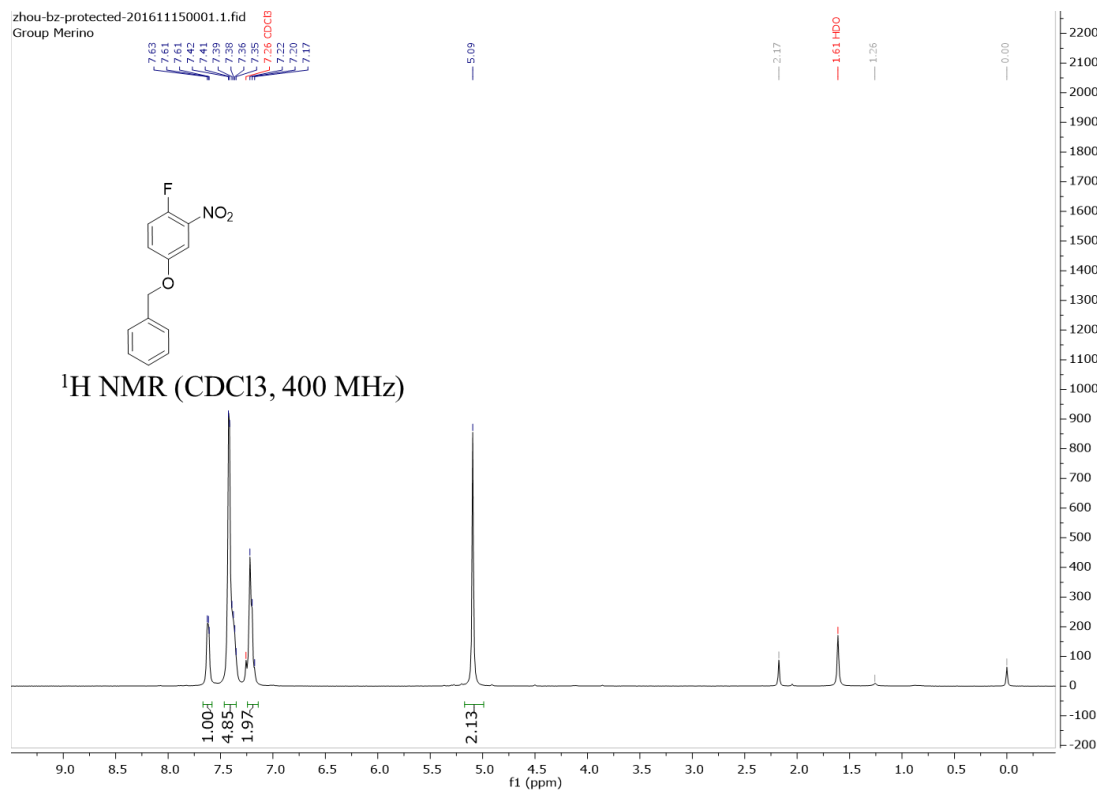
Scheme 10.3 The synthesis route of compound SA1.

Synthesis of 4-(benzyloxy)-1-fluoro-2-nitrobenzene:

Dissolve the 4-Fluoro-3-nitrophenol (1g, 6.36mmol) into the acetonitrile (20mL) at ice bath. Then Add benzyl bromide (966.12ml, 12.72mmol). Then, add potassium carbonate (2.45g,

17.81mmol). The resulting mixture was stirred at RT for 6h, after which time the solvent was diluted with H₂O and extracted with EtOAc. The organic layer was dried (Na₂SO₄) and concentrated in vacuo to provide the product as a brownish liquid. [1.57g, yield: 99%] ¹H NMR (CDCl₃, 400 MHz) δ 7.67(s, 1H), 7.42(s, 5H), 7.22(m, 1H), 5.09(s, 2H)

NMR for 4-(benzyloxy)-1-fluoro-2-nitrobenzene

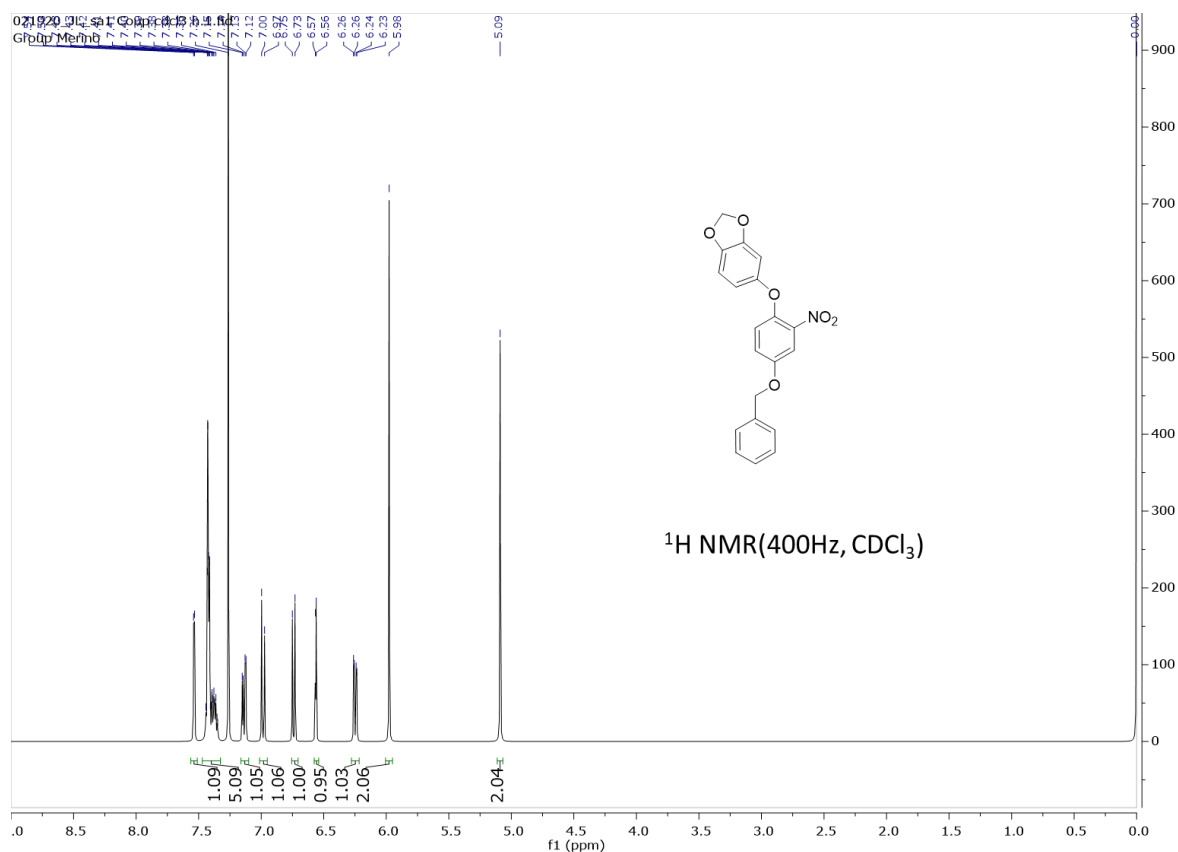


Synthesis of 5-(4-(benzyloxy)-2-nitrophenoxy)benzo[d][1,3]dioxole:

To a solution of sesamol (1.05g, 6.36mmol) in dimethylformamide (8mL) was added potassium carbonate (0.9g, 6.55 mmol) and then 4-(benzyloxy)-1-fluoro-2-nitrobenzene (1.55g, 6.36mmol). The resulting mixture was stirred at 45°C for 12hours. The reaction was then diluted with H₂O and extracted with EtOAc. The organic layer was dried (Na₂SO₄) and concentrated in vacuo. The resulting material was purified by flash chromatography using ethyl acetate/hexane (1:2) as eluent

to provide the product as a yellowish solid. [2.2g, yield:80%] ^1H NMR (400 MHz, Chloroform-*d*) δ 7.54 (d, $J = 3.0$ Hz, 1H), 7.47 – 7.32 (m, 5H), 7.14 (dd, $J = 9.1, 3.1$ Hz, 1H), 6.98 (d, $J = 9.2$ Hz, 1H), 6.74 (d, $J = 8.4$ Hz, 1H), 6.56 (d, $J = 2.5$ Hz, 1H), 6.25 (dd, $J = 8.3, 2.5$ Hz, 1H), 5.98 (s, 2H), 5.09 (s, 2H).

NMR for 5-(4-(benzyloxy)-2-nitrophenoxy)benzo[d][1,3]dioxole

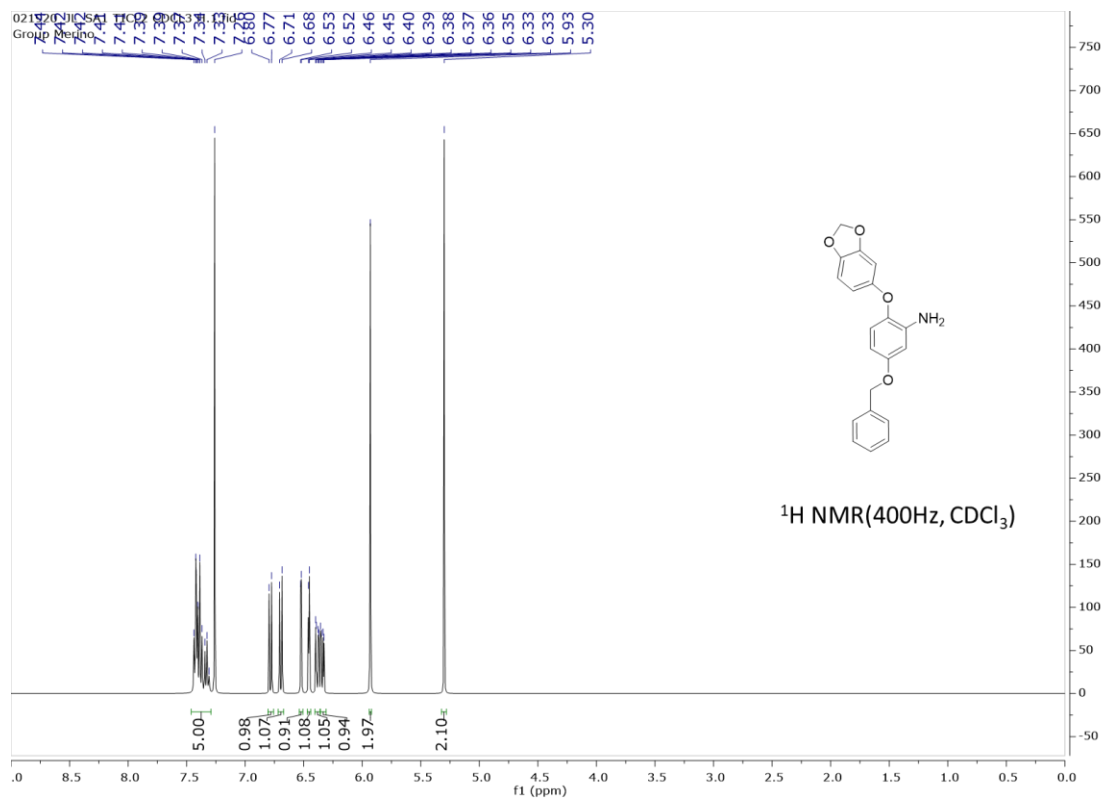


Synthesis of 2-(benzo[d][1,3]dioxol-5-yloxy)-5-(benzyloxy)aniline:

To a solution of 5-(4-(benzyloxy)-2-nitrophenoxy)benzo[d][1,3]dioxole (0.73g, 2mmol) in dichloromethane was added MeOH (0.45mL, 10mmol), followed by the addition of *tin(II) chloride* (0.19g, 10mmol). When the reaction was complete (TLC), typically complete within 6h, the mixture was filtered off and the solvent was dried under reduced pressure. The resulting material

was purified through flash chromatography acetate/hexane (2:1) to provide the product as a yellowish solid. [335mg, 50%.] ^1H NMR (400 MHz, Chloroform-*d*) δ 7.46 – 7.29 (m, 5H), 6.79 (d, $J = 8.7$ Hz, 1H), 6.70 (d, $J = 8.5$ Hz, 1H), 6.52 (d, $J = 2.5$ Hz, 1H), 6.46 (d, $J = 2.8$ Hz, 1H), 6.40 – 6.36 (m, 1H), 6.34 (dd, $J = 8.8, 2.9$ Hz, 1H), 5.93 (s, 2H), 5.30 (s, 2H).

NMR for 2-(benzo[d][1,3]dioxol-5-yloxy)-5-(benzyloxy)aniline

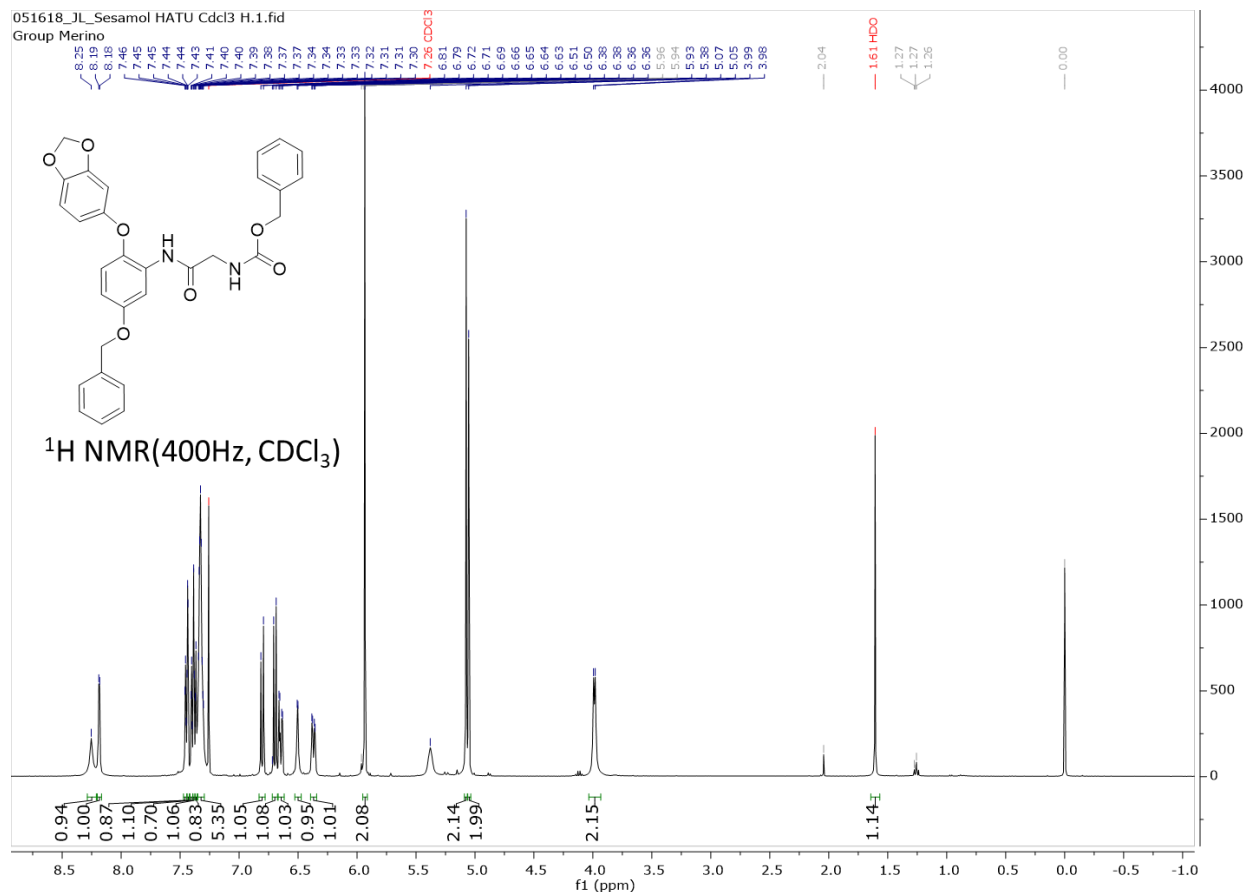


Synthesis of N-(2-(benzo[d][1,3]dioxol-5-yloxy)-5-(benzyloxy)phenyl)-2-(2-phenylacetamido)acetamide:

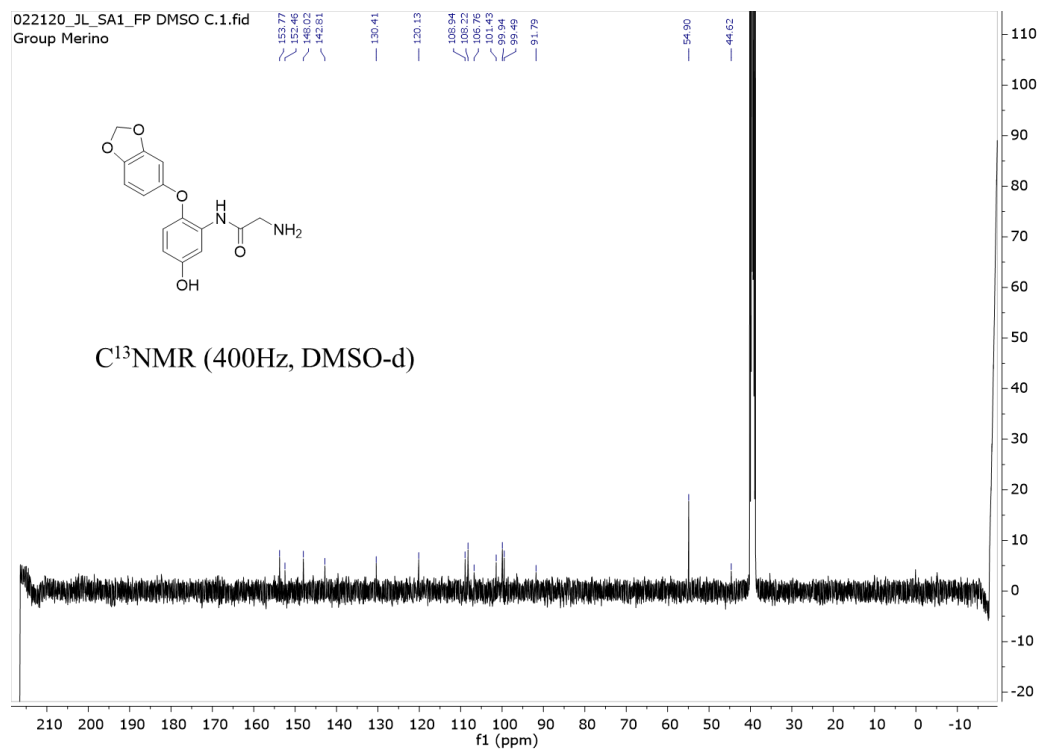
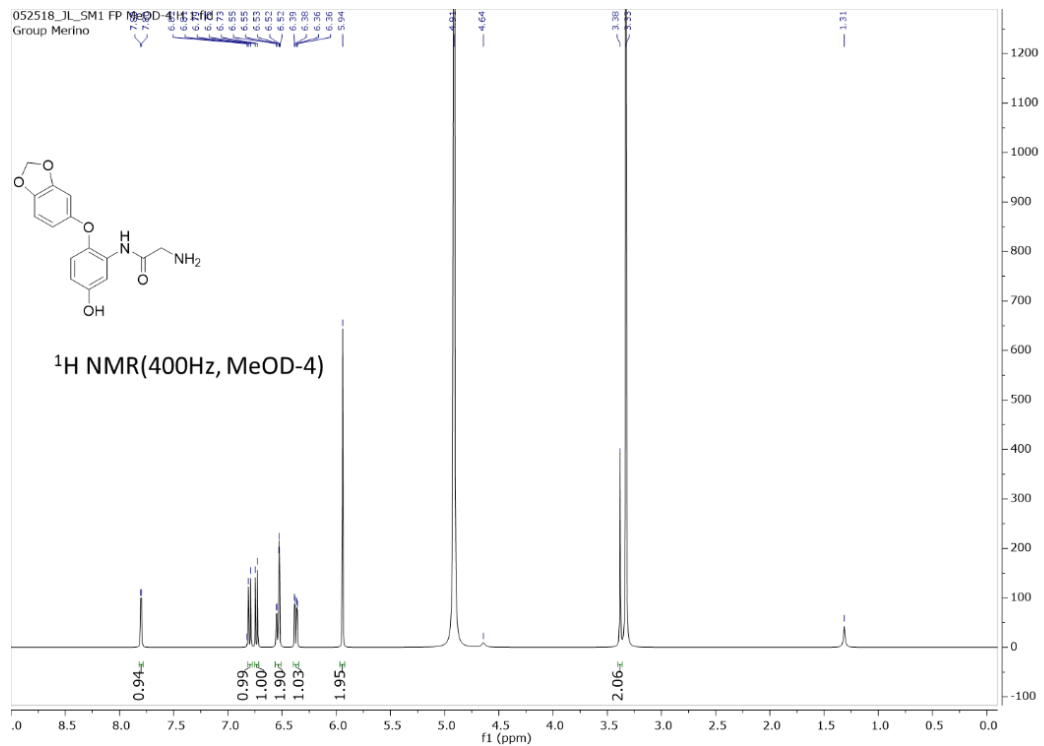
To a solution of the 2-(tert-butoxycarbonylmethylamino) acetic acid (1.675g, 5mmol) in DMF (5.0 mL) at room temperature was added HATU (2.1g, 5.5 mmol) and 2-(benzo[d][1,3]dioxol-5-yloxy)-5-(benzyloxy)aniline (0.91g, 5 mmol), after 30 mins, followed by the addition of DIPEA (1.8 mL,

10mmol). The resulting mixture was stirred at RT for 8 h, after which time the reaction mixture was diluted with H₂O and extracted with EtOAc. The organic layer was dried (Na₂SO₄) and concentrated in vacuo. The resulting material was purified by flash chromatography using ethyl acetate/hexane (1:1) as eluent to provide the product as a purple solid. [2.44g, 93%]¹H NMR (400 MHz, Chloroform-*d*) δ 8.25 (s, 1H), 8.19 (d, *J* = 3.0 Hz, 1H), 7.46 (d, *J* = 1.8 Hz, 1H), 7.44 (t, *J* = 1.4 Hz, 1H), 7.40-7.37 (dd, *J* = 1.6 Hz, 1H), 7.38 (d, *J* = 1.9 Hz, 1H), 7.33 (dq, *J* = 5.6, 2.5 Hz, 5H), 6.80 (d, *J* = 9.0 Hz, 1H), 6.70 (d, *J* = 8.4 Hz, 1H), 6.65 (dd, *J* = 9.0, 3.0 Hz, 1H), 6.50 (d, *J* = 2.6 Hz, 1H), 6.37 (dd, *J* = 8.5, 2.5 Hz, 1H), 5.93 (s, 2H), 5.07 (s, 2H), 5.05 (s, 2H), 3.99 (d, *J* = 5.8 Hz, 2H), 1.61 (s, 1H).

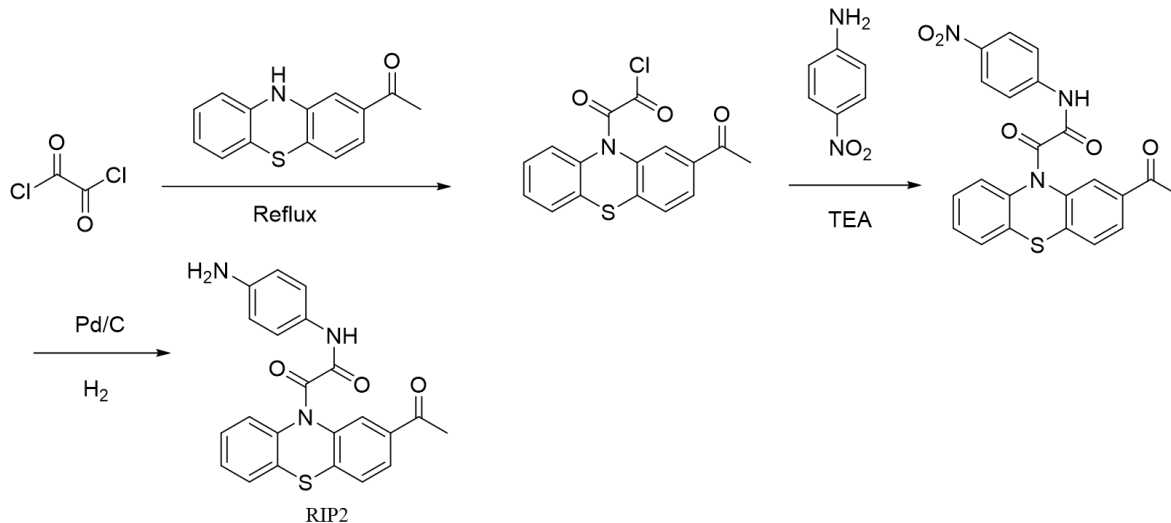
NMR for N-(2-(benzo[d][1,3]dioxol-5-yloxy)-5-(benzyloxy)phenyl)-2-(2-phenylacetamido)acetamide



NMR for 2-amino-N-(2-(benzo[d][1,3]dioxol-5-yloxy)-5-hydroxyphenyl)acetamide



3.2.1.2 Synthesis of compound RIP2



Scheme 11.4 The Synthesis route for RIP2.

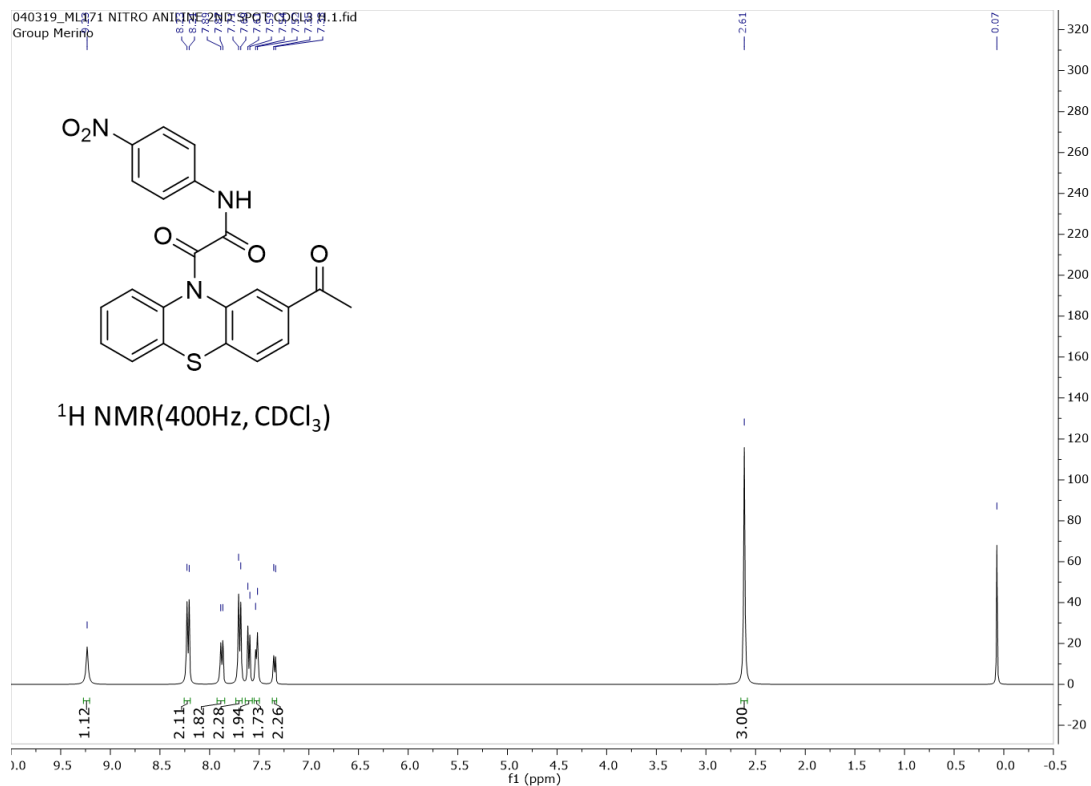
Synthesis of 2-(2-acetyl-10H-phenothiazin-10-yl)-2-oxoacetyl chloride:

To the compound of 1-(10H-phenothiazin-2-yl)ethanone (2.41g, 10mmol) add oxalyl chloride (8.58ml, 100mmol) and reflux for hours. The extra oxalyl chloride was removed by vacuo. The resulting material will be used for next synthesis without purification.

Synthesis of 2-(2-acetyl-10H-phenothiazin-10-yl)-N-(4-nitrophenyl)-2-oxoacetamide:

To a solution of 2-(2-acetyl-10H-phenothiazin-10-yl)-2-oxoacetyl chloride (1.98g, 6mmol) in *Tetrahydrofuran*(THF) added 4-nitro aniline(0.828g, 6mmol), after 30 mins, followed by the addition of TEA (2.09 mL, 15mmol). When the reaction was complete (TLC), typically complete within 12h, the solvent was removed under reduced pressure. The resulting material was purified through flash chromatography acetate/hexane (2:1) to provide the product as a yellowish solid. [1.3g, 50%.] ¹H NMR (400 MHz, Chloroform-*d*) δ 9.23 (s, 1H), 8.22 (d, $J = 8.7$ Hz, 2H), 7.88 (d, $J = 8.4$ Hz, 2H), 7.70 (d, $J = 8.8$ Hz, 2H), 7.60 (d, $J = 8.1$ Hz, 2H), 7.53 (d, $J = 7.5$ Hz, 2H), 7.34 (d, $J = 7.6$ Hz, 2H), 2.61 (s, 3H).

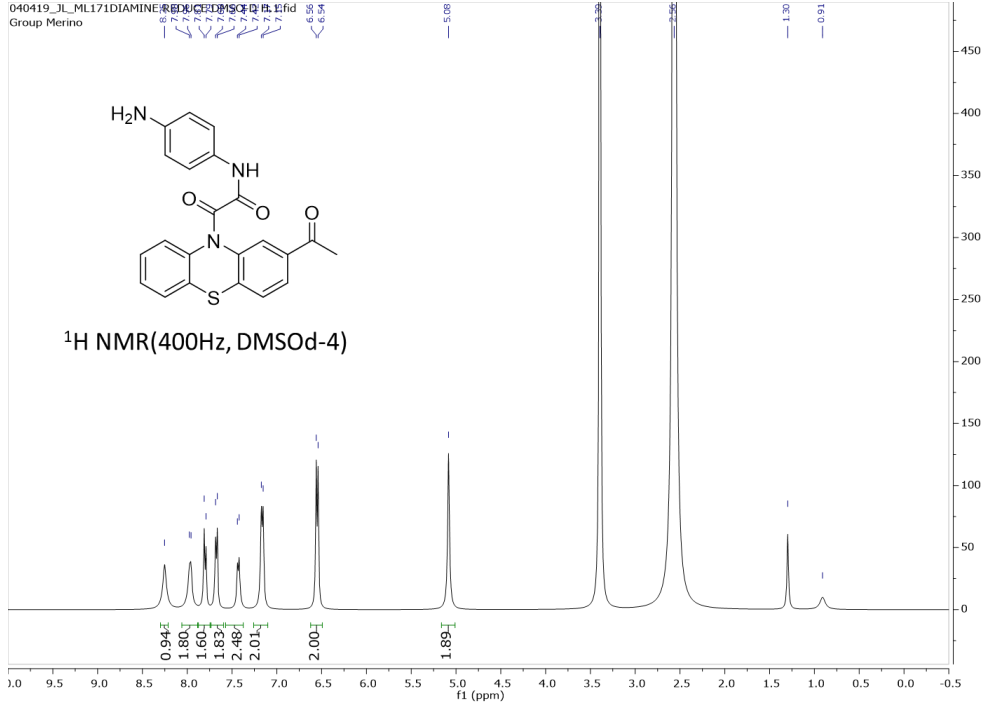
NMR for 2-(2-acetyl-10H-phenothiazin-10-yl)-N-(4-nitrophenyl)-2-oxoacetamide



Synthesis of 2-(2-acetyl-10H-phenothiazin-10-yl)-N-(4-aminophenyl)-2-oxoacetamide:

To a solution of 2-(2-acetyl-10H-phenothiazin-10-yl)-N-(4-nitrophenyl)-2-oxoacetamide (433mg, 1mmol) in dichloromethane (2mL) was added MeOH (5mL). The resulting mixture was stirred under Hydrogen(35psi), after which time the reaction mixture was filter with Celite and dried in vacuo. The resulting material was purified by flash chromatography using MeOH/DCM (1:9) as eluent to provide the product as a purple solid. [362.7mg, 90%] $^1\text{H NMR}$ (400 MHz, $\text{DMSO}-d_6$) δ 8.25 (s, 1H), 7.97 (d, $J = 7.3$ Hz, 2H), 7.80 (d, $J = 8.3$ Hz, 2H), 7.67 (d, $J = 7.7$ Hz, 2H), 7.43 (d, $J = 7.7$ Hz, 2H), 7.16 (d, $J = 8.1$ Hz, 2H), 6.55 (d, $J = 8.3$ Hz, 2H), 5.08 (s, 2H).

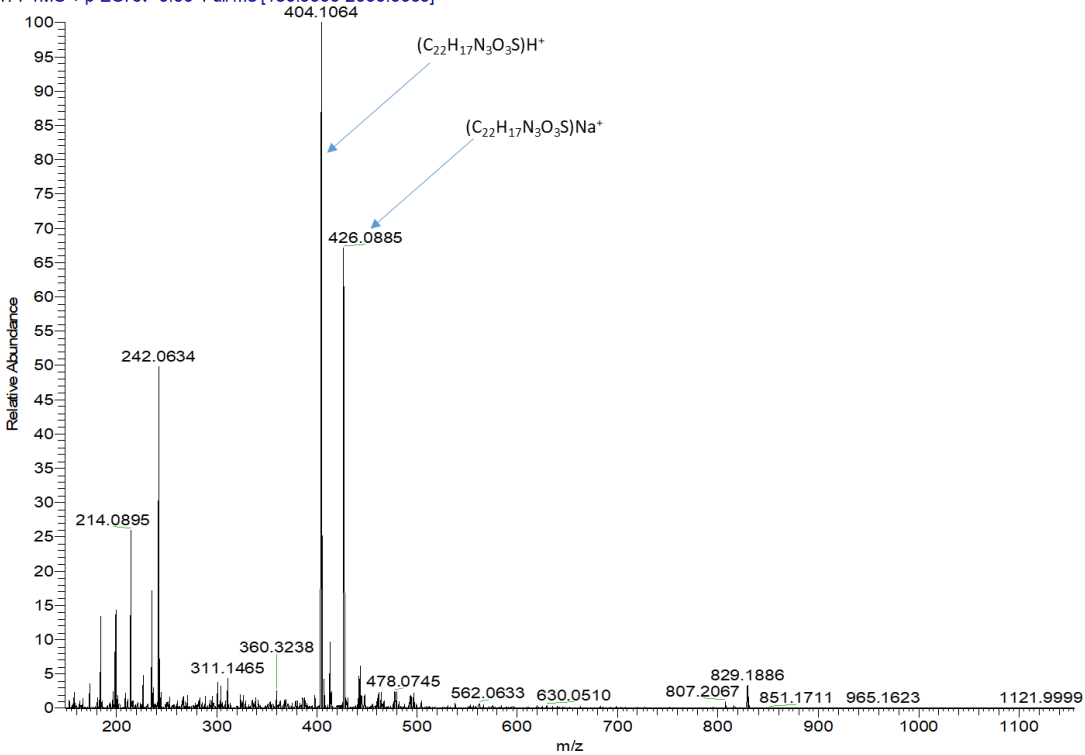
NMR for 2-(2-acetyl-10H-phenothiazin-10-yl)-N-(4-aminophenyl)-2-oxoacetamide



MS for 2-(2-acetyl-10H-phenothiazin-10-yl)-N-(4-aminophenyl)-2-oxoacetamide

Sample ID: RIP2 (Positive Ion Mode ESI-MS Data)

[RIP2] #129-200 RT: 0.33-0.71 AV: 72 NL: 3.41E7
T: FTMS + p ESI cv=0.00 Full ms [150,0000-2000,0000]



3.2.2 Oxidation study

H₂O₂ oxidation: A working solution (3mg **SA1** was dissolved in 20mL in 25 mM phosphate buffer mixing with 10% Acetonitrile, pH=7.0) was made. A 1mL sample was used as the control. The reaction was 1mL of working solution and 0.4 mM hydrogen peroxide. After 60 mins the reaction mixture was analyzed by HPLC to quantify the relative amounts of **SA1** and sesamol. Moles were calculated using a standard of each compound and yields were calculated using integration. All determinations were carried out in triplicate on different days. On each occasion and new standards and samples were made.

HRP oxidation: The above working solution was mixed with 1μL HRP-solution (0.5mg/ml 25mM phosphate buffer, pH 7.4) by centrifugation of HRP-solution placed on the cap of an Eppendorf tube. After 60mins of reaction, the reaction was processed as before.

Oxidation studies of compound **RIP2** were performed following the same procedure as **SA1**.

3.2.3 HPLC condition for oxidation studies

A Beckman Coulter's HPLC system consisting of a dual pump Model 126 with 32 Karat Software, a System Gold 168 detector, and a System Gold 508 Auto Sampler was used. A reverse phase C-18 column (Synergi™ 4μm Hydro-RP 80Å, LC Column 100×4.6mm, Ea.) was used. The mobile phase consisted of HPLC grade Acetonitrile (Fisher Scientific), LCMS grade formic acid (Fisher Scientific), and distilled water filtered through a Millipore Milli-Q water purification system. Solvent A for the mobile phase was 95% water, 5% Acetonitrile for all oxidation studies. Solvent B is 95% acetonitrile and 5% water. The gradient was 0% B for 4 minutes and 95% B over 16

minutes. Flow was 1ml/min. A detection wavelength of 250nm and 285nm was used for the oxidation study.

3.2.4 DCFDA assay by flow cytometry

SK-MET-2 cells were grown in 25 cm² tissue culture plates to 50% confluence. Then each plate was incubated with the listed compound for 18 hours. Cells were trypsinized and wash with HBSS twice. Each sample was irradiated, and then 5μM DCF-DA (Sigma Aldrich) was added. Incubation for 30 min, washing, and DCF fluorescence was obtained in using the BD FACS Canto flow cytometer by exciting at 485 nm and emission at 535nm after eliminating 7AAD positive cells. Percentage of cells with high DCF fluorescence were compared among different treatments. Data shown are the average of three biological replicates.

3.3 Results and Discussion

3.3.1 Compound SA1 could release sesamol as a prodrug.

The ROS-activated prodrug **SA1** was designed to release the sesamol as the antioxidant, as shown in **Figure 3.3A**. The phenol functional group of **SA1** attributes it to the biochemical property for ROS reduction. The attachment to a ROS-activated moiety with an ether will stabilize sesamol as a prodrug and only release it in the cell under oxidative stress. Compound SA1 was synthesized through 5 step synthesis with a net 37% yield.

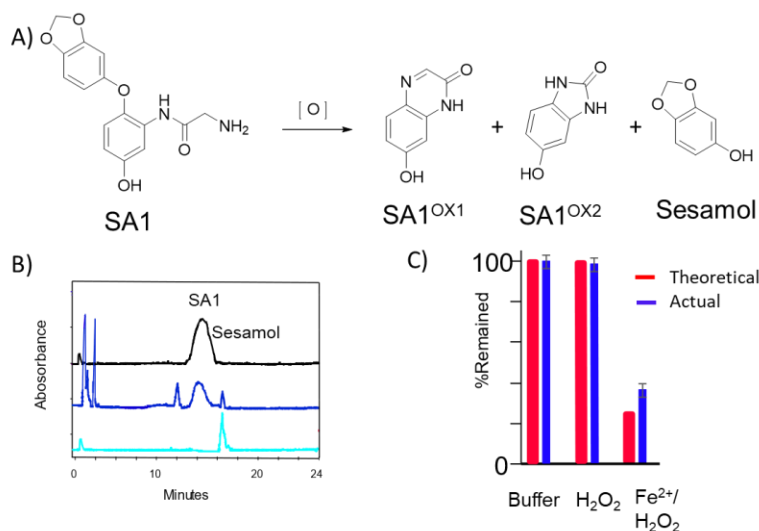


Figure 12.3 (A) Proposed reaction of **SA1** to release sesamol and generate **SA1^{OX}**. (B) HPLC analysis of **SA1** incubated in phosphate buffer (black trace) and under HRP conditions (blue trace). Pure sesamol sample was also analyzed (mint trace). (D) Sensitivities of **SA1** to various ROS forms.

In the beginning, the oxidation reaction of **SA1** was examined under only H₂O₂ conditions. It shows no reaction happened after 60mins with 0.4mM H₂O₂ existence indicate the stability of **SA1** under only H₂O₂ condition. Then, the oxidation reaction of **SA1** was examined (**Figure 3.3B**) under HRP conditions, which generate hydroxyl radicals. The HRP conditions were 0.01 mU of HRP enzyme and 0.4 mM H₂O₂ in pH 7.4 phosphate buffer and the concentration of **SA1** was 0.4 mM. The reaction mixture was analyzed by HPLC. Under our conditions, **SA1** eluted near 15 min with the HPLC condition as mobile phase A was 95% water, 5% Acetonitrile, and solvent B is 95% acetonitrile and 5% water gradient was 0% B for 4 minute and 95% B over 16 minutes. The pure sesamol bought from manufacture was analyzed as a control eluted near 17 min to verify the successful releasing of sesamol from **SA1** under HRP condition. Quantitative analysis of under these HRP conditions, 62% (+/- 2%) of **SA1** was oxidized to release sesamol (**Figure 3.3C**). This

is less to the expected yield (80%) based on the concentrations of SA1 and H₂O₂.

3.3.2 Compound RIP2 could release ML171 as a prodrug.

Another ROS-activated prodrug **RIP2** was designed to release the NOX1 inhibitor ML171, as shown in **Figure 4.4A**. The diphenylamine group of SA1 is the pivotal site to work as a NOX1 inhibitor⁵⁶. The attachment to a ROS-activated moiety with an oxalate linker will block the RIP2 as a NOX inhibitor and only release it in the cell under oxidative stress. Compound **RIP2** was synthesized through 3 step synthesis with a net 45% yield.

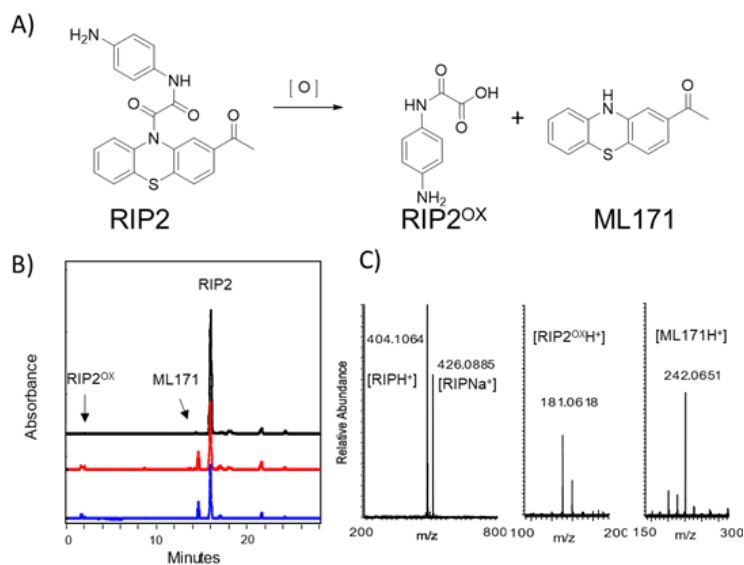


Figure 13.4 (A) Proposed reaction of **RIP2** to release ML171 and generate **RIP2^{OX}**. (B) HPLC analysis of **RIP2** incubated in phosphate buffer (black trace) with H₂O₂ (red trace) and under HRP conditions (blue trace). (C) MS of isolated products.

In the beginning, the oxidation reaction of **RIP2** was examined under only H₂O₂ conditions. It shows 52(+/-2%) RIP2 degrade after 3 hours of oxidation (**Figure 3.4B**). Under these conditions, **RIP2** eluted near 16 min with the HPLC condition as mobile phase A was 95% water, 5%

Acetonitrile, and solvent B is 95% acetonitrile and 5% water gradient was 0% B for 4 minute and 95% B over 16 minutes. And released ML171 and **RIP2^{ox}** eluted at 15mins and 2mins. Then each of the products was isolated and ran MS analysis confirmed expected product identities (**Figure 3.4C**).

Then, the oxidation reaction of **RIP2** was examined (**Figure 3.4B**) under HRP conditions, which generate hydroxyl radicals. The HRP conditions were 0.01 mU of HRP enzyme and 0.4 mM H₂O₂ in pH 7.4 phosphate buffer, and the concentration of **RIP2** was 0.4 mM. Under these HRP conditions, 64% (+/- 2%) of **RIP2** was oxidized to release ML171. This is shown **RIP2** has a higher sensitivity to HRP condition than only hydrogen peroxide.

3.3.3 RIP2 could reduce the ROS level in the cell.

Base on the common DCF-DA oxidative stress assay (**Figure 3.5**), the ROS inhibition potential as a NOX1 inhibitor of **RIP2** was further confirmed. Considering the known issue of DCF-DA assay, the ML171 with varies concentration was also analyzed with **RIP2** as a positive control.

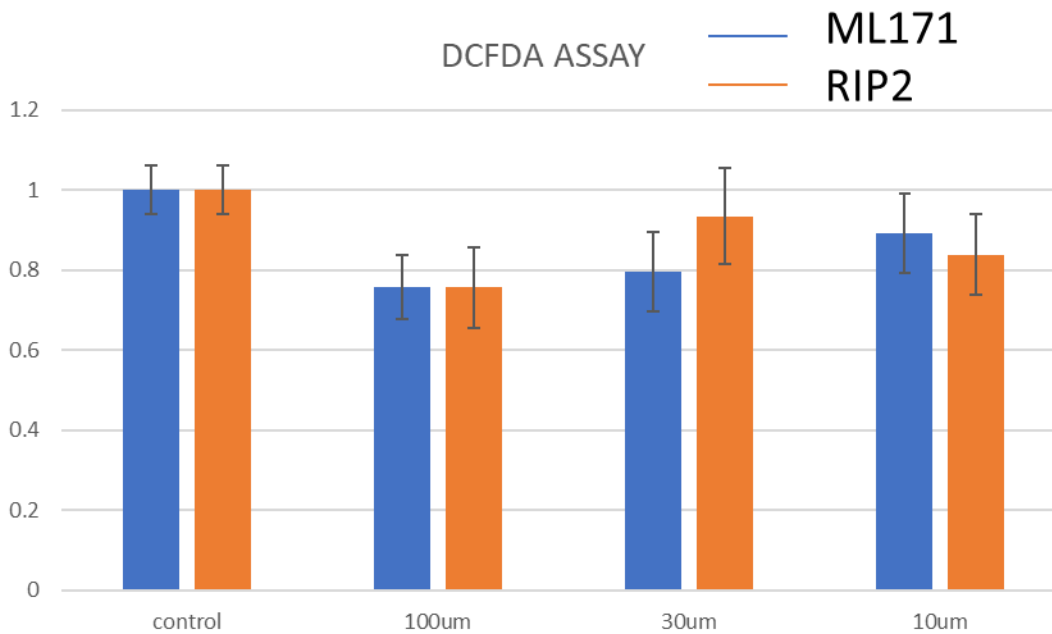


Figure 14.5 H₂O₂ inhibitor of RIP2 as a NOX1 inhibitor under Dichlorodihydrofluorescein diacetate fluorescence measurements

The ML171 was reported as a strong NOX1 inhibitor (IC_{50HT29} = 0.129 μM). It shows 24% (+/- 8%) hydrogen peroxide was inhibited with 100 μM ML171 pretreatment, and the RIP2 shows similar results with ML171. With decreasing the amount of NOX1 inhibitor, the ROS inhibition of both of ML171 and **RIP2** was getting lower. ML171 changed to 21% (+/- 10%) while RIP2 changed to 7% (+/- 12%) on 30 μM. Furthermore, ML171 changed to 11% (+/- 10%), while RIP2 changed to 17% (+/- 10%) on 10 μM. It indicates the **RIP2** may show less NOX1 inhibition as a prodrug under low ROS level comparing to ML171. To sum up, both of the ML171 and RIP2 inhibited the ROS production of SK-MET-2 cells. RIP shows less effect on it in normal cells because of the modification with a ROS-activated moiety.

3.4 Conclusions

In conclusion, we have designed and synthesized two ROS-activated antioxidants, **SA1** and **RIP2**, which release an antioxidant called sesamol and ML171 as a NOX inhibitor, respectively after the oxidative reaction. **SA1** was designed by attaching a ROS-activated moiety stated in chapter 2 to a key phenol to mute the antioxidant function. And SA1 was proved to oxidized and release sesamol under Fenton condition. **RIP2** was designed by coupling a proved NOX1 inhibitor ML171 with ROS-activated oxalate linker. Then the release of ML171 is proved by HPLC, and MS. DCF-DA assay further proves the ROS inhibition of cells from **RIP2**. Cell cytotoxicity and UV irradiation test in cells will be run to prove the application of these prodrugs in the future plan.

Chapter 4:
Novel ROS quantification technique based on
GCMS

4.1 Introduction

ROS are reactive oxygen species primarily produced from the metabolism procedure the oxygen participates in. Such as mitochondrial electron transport chain(ETC), NADPH oxidases, xanthine oxidase (XO). ROS play an important role in the proliferation, differentiation, senescence, and apoptosis of the cell. And the role of ROS as oxidative stress to affect the cell activity and relate to pathology is being widely studied by researchers.

Oxidative stress induced by ROS production plays a role in the immune system⁸², genomic stability⁸³, regulation of transcription⁷¹, and cancer. ROS on a low level will help with sustain proliferation and cell differentiation. However, high-level ROS lead cell apoptosis and gene mutation by oxidizing the protein, DNA, or lipids. It is important to quantify a certain ROS level for further research. However, the lifetime of them varies in biological systems ranges from nanoseconds to seconds up to different forms and antioxidant capacity⁸⁴. Given the high reactivity and low concentration⁸⁵, the quantification of ROS is a challenge to be overcome.

The general idea for ROS quantification in biological systems is to induce a reactive probe to react with ROS to produce a stable compound or signal to quantify. There are several probes used nowadays by releasing detectable products reflecting the formation of ROS. Use of 5,5-dimethyl-1-pyrroline-Noxide(DMPO) is one of the earliest methods⁸⁶ called spin trapping found to form a covalent bond with hydroxyl radical and NOO^\cdot . Electron paramagnetic resonance (EPR) will be used to detect the signals from the spin trap to quantify the ROS. This detection technique was widely used for studies of isolated enzymes and in chemical solutions⁸⁷. However, the reaction between trap and ROS is rather slower than the competitors in biological systems such as

superoxide dismutase(SOD) and ascorbate⁸⁸. More methods are developed for ROS detection to break through the limits, such as chemiluminescence methods⁸⁹, fluorescent probes⁹⁰. Both of the chemiluminescence methods, fluorescent probes share a similar idea to release detectable chemiluminescence or fluorescent signal after reacting with ROS produced in the cell. Dichlorodihydrofluoresceindiacetate (DCFHDA) is a fluorescence probe that is widely used for detecting intracellular H₂O₂. DCFHDA can penetrate the membrane and hydrolyze to DCFH, which will be catalyzed to be the fluorescence(DCF) under the existence of H₂O₂ in the cell.(**Figure 4.1**) This fluorescent probe was commonly used for its convenience to use, high sensitivity. However, its poor selectivity limits the potential. It could be oxidized not only by H₂O₂, but also several one-electron oxidizers, transition metals, cytochrome c, and heme peroxidases⁹¹.

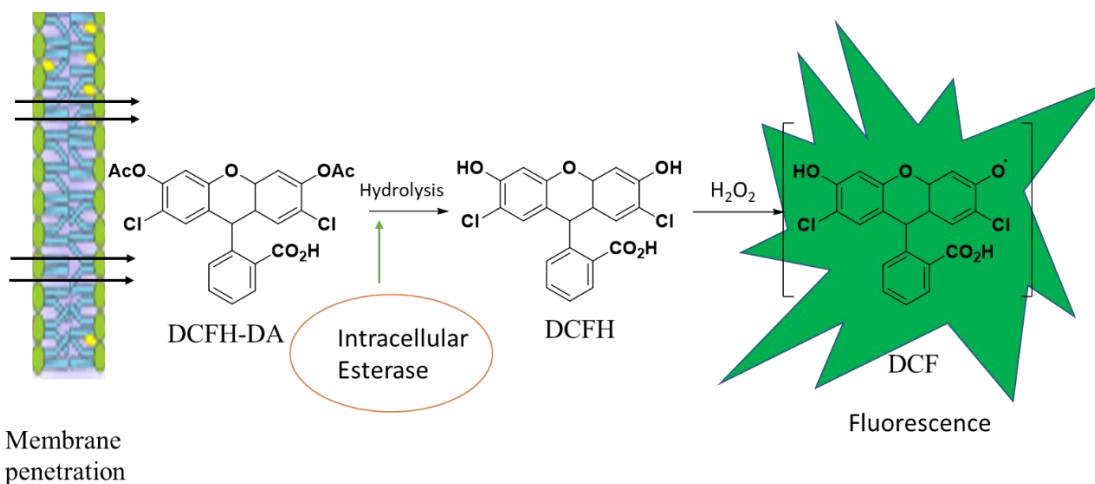


Figure 15.1 Dichlorodihydrofluoresceindiacetate (DCFHDA)intracellular reaction to release fluorescence

For better ROS quantification, new concepts and methods should be developed. The researcher set the goals for selectivity improvement and user-friendly detection for cell assay. The ROS-active linker which shows selectivity to H₂O₂, which could be a base for design a ROS sensitive probe⁹². For easing the procedure for quantification, gas chromatography-headspace-mass

spectrometry(GCHSMS) is the detector for quantification⁹³. So the probe connected with the ROS-activated moiety is decided to be diethylamine(DEA), which is a versatile small molecule that does not exist in the cells. (**Figure 4.2**)

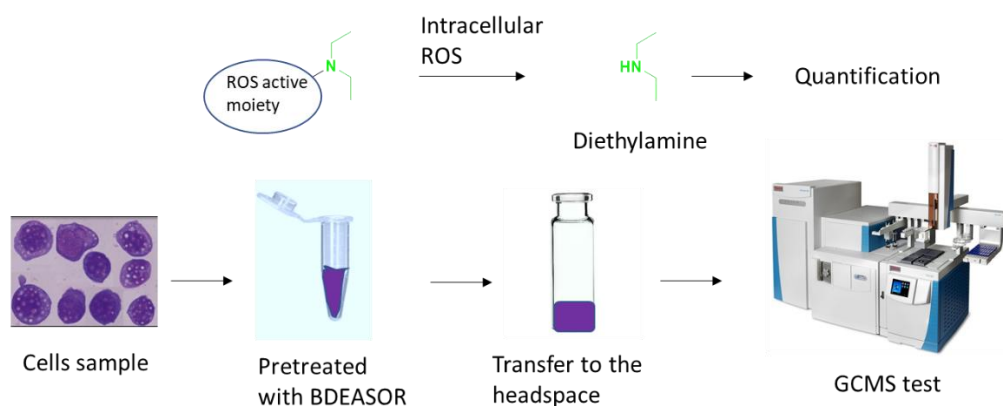


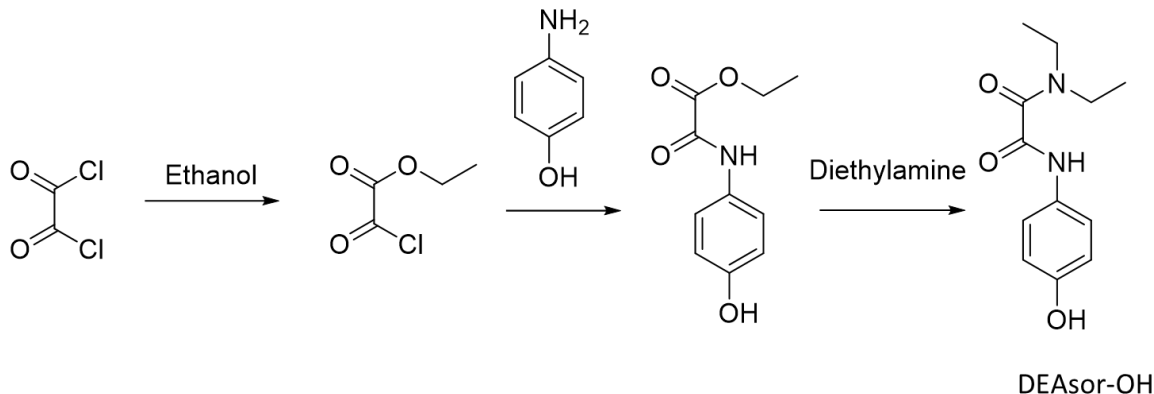
Figure 16.2 ROS quantification assay designed base on GCHSMS and a volatile amine

4.2 Experiment section

4.2.1 Synthesis and characterization

Boc-sarcosine, trifluoroacetic acid (TFA) and dimethylformamide, chloromethyl methyl ether were purchased from Sigma-Aldrich Chemical Co. (St. Louis, MO, USA). Sesamol, 4-floro-3nitro phenol, pladium on carborn, 4'-Hydroxyacetophenone, 1-Fluoro-2-nitrobenzene, Triethylsilane, HATU were purchased from Fisher scientific international, Inc. All solutions were prepared with water purified by a Milli-Q system (Millipore, Bedford, MA, USA). All reagents used for buffer preparation were of analytical grade.

4.2.1.1 Synthesis of compound DEASOR-OH



Scheme 17.3 The synthesis route of compound DEASOR-OH

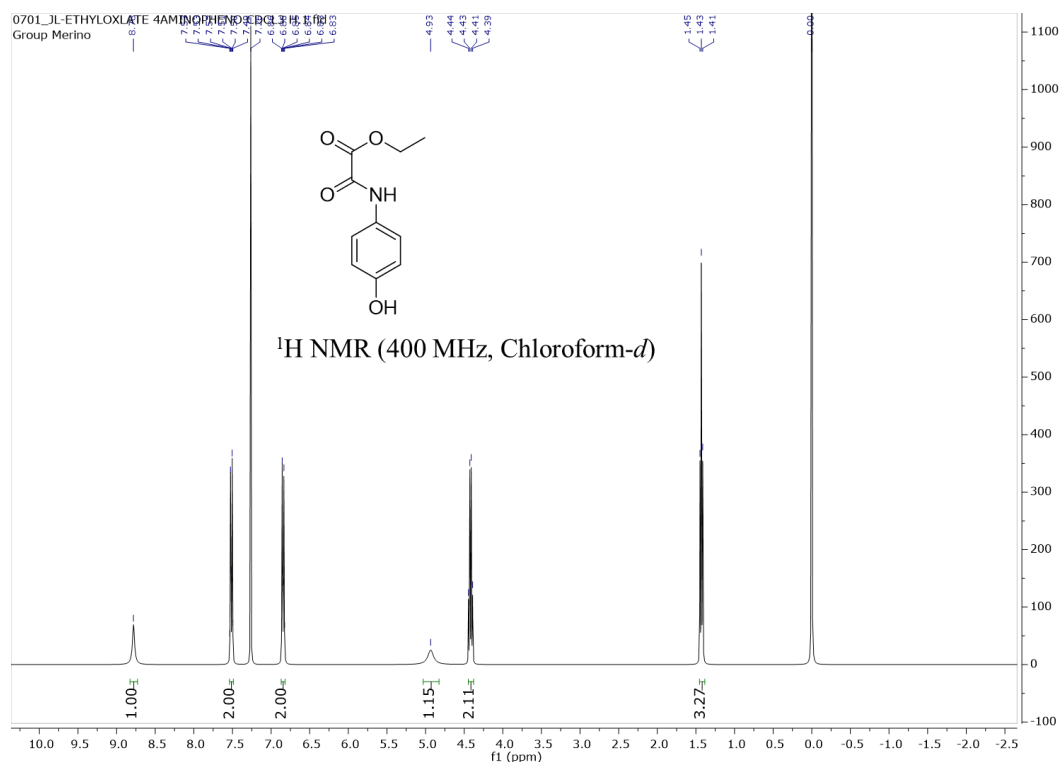
Synthesis of ethyl 2-chloro-2-oxoacetate:

To a solution of oxalate chloride (0.76g, 6mmol) in Diethylether added ethanol(0.28g, 6mmol). Stir for 3 hours. The solvent was removed under reduced pressure. The resulting material was used directly to the next step.

Synthesis of ethyl 2-(4-hydroxyphenylamino)-2-oxoacetate:

To a solution of ethyl 2-chloro-2-oxoacetate (0.816g, 6mmol) in Tetrahydrofuran(THF) added 4-amino phenol(0.654g, 6mmol), after 30 mins, followed by the addition of TEA (2.09 mL, 15mmol). When the reaction was complete (TLC), typically complete within 6h, the solvent was removed under reduced pressure. The resulting material was purified through flash chromatography acetate/hexane (2:1) to provide the product as a yellowish solid. [752.4mg, yield:60%] $^1\text{H NMR}$ (400 MHz, Chloroform-*d*) δ 8.78 (s, 1H), 7.58 – 7.45 (m, 2H), 6.88 – 6.79 (m, 2H), 4.93 (s, 1H), 4.42 (q, $J = 7.1$ Hz, 2H), 1.43 (t, $J = 7.1$ Hz, 3H).

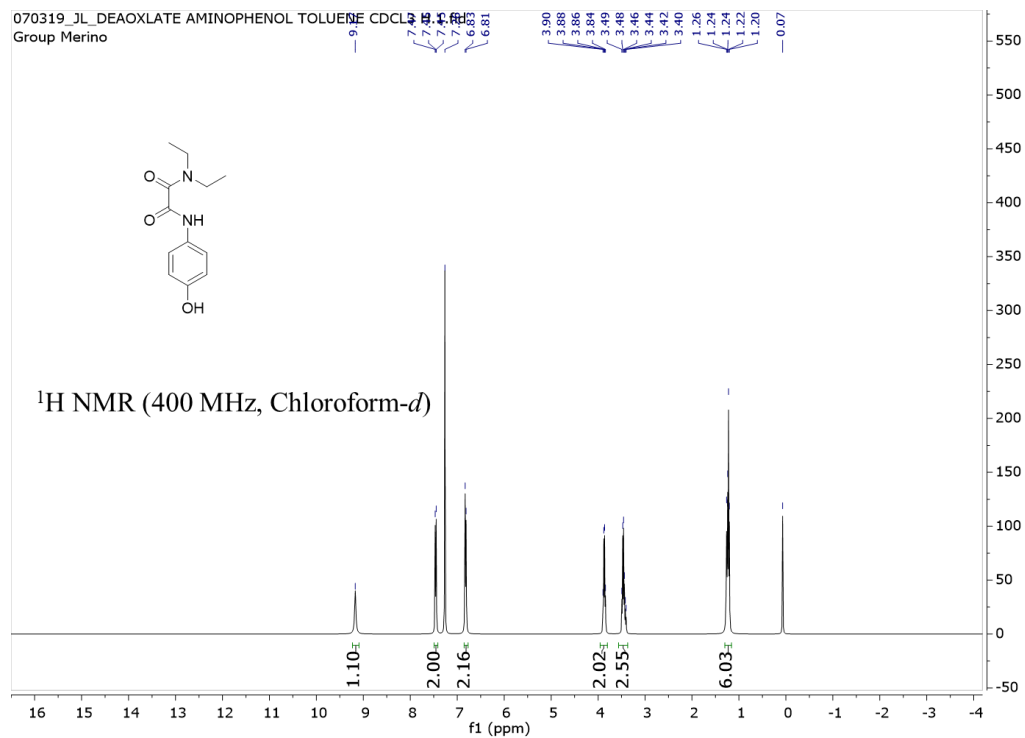
NMR for ethyl 2-(4-hydroxyphenylamino)-2-oxoacetate



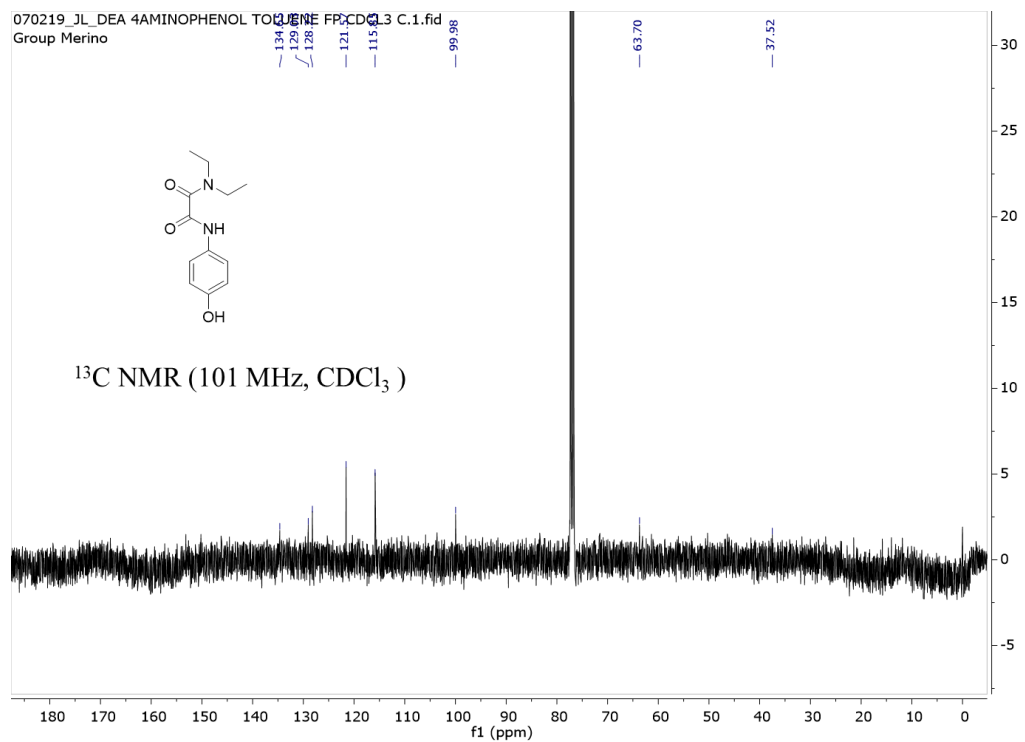
Synthesis of N1,N1-diethyl-N2-(4-hydroxyphenyl)oxalamide:

To a solution of ethyl 2-(4-hydroxyphenylamino)-2-oxoacetate (376mg, 3mmol) in THF (20mL) was added diethylamine (220mg, 3mmol). After 30 mins, , followed by the addition of TEA (1.05 mL, 7.5mmol). The resulting mixture was stirred for 4 hours, after which time the reaction mixture was dried in vacuo. The resulting material to provide the product as a yellow solid. [142mg, yield:99%] ¹H NMR (400 MHz, Chloroform-*d*) δ 9.17 (s, 1H), 7.46 (d, *J* = 8.7 Hz, 2H), 6.83 (d, *J* = 8.2 Hz, 2H), 3.87 (q, *J* = 7.1 Hz, 2H), 3.45 (dq, *J* = 10.7, 7.0 Hz, 2H), 1.42 – 1.11 (m, 6H). ¹³C NMR (101 MHz, CDCl₃) δ 134.65, 129.03, 128.22, 121.57, 115.85, 99.98, 63.70, 37.52.

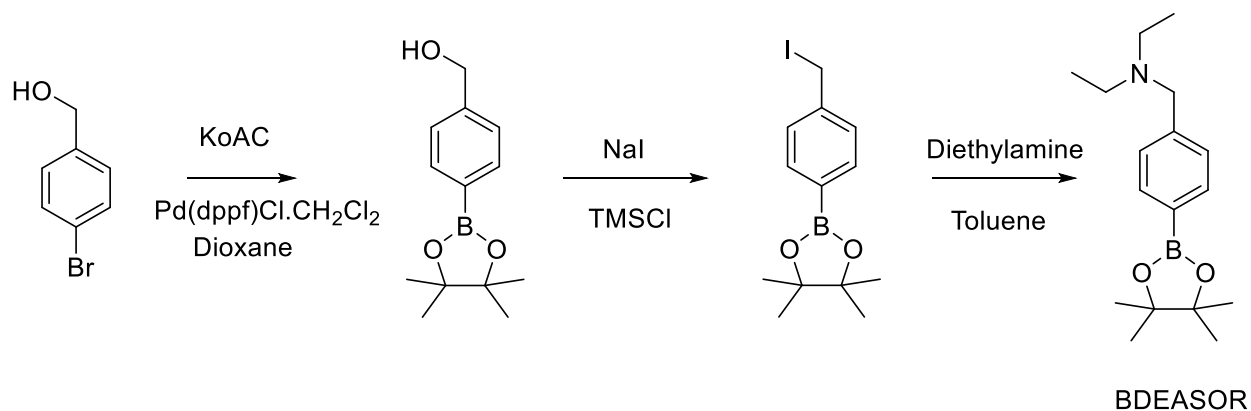
NMR for N1,N1-diethyl-N2-(4-hydroxyphenyl)oxalamide



^{13}C NMR for N1, N1-diethyl-N2-(4-hydroxyphenyl)oxalamide



4.2.1.2 Synthesis of compound BDEASOR

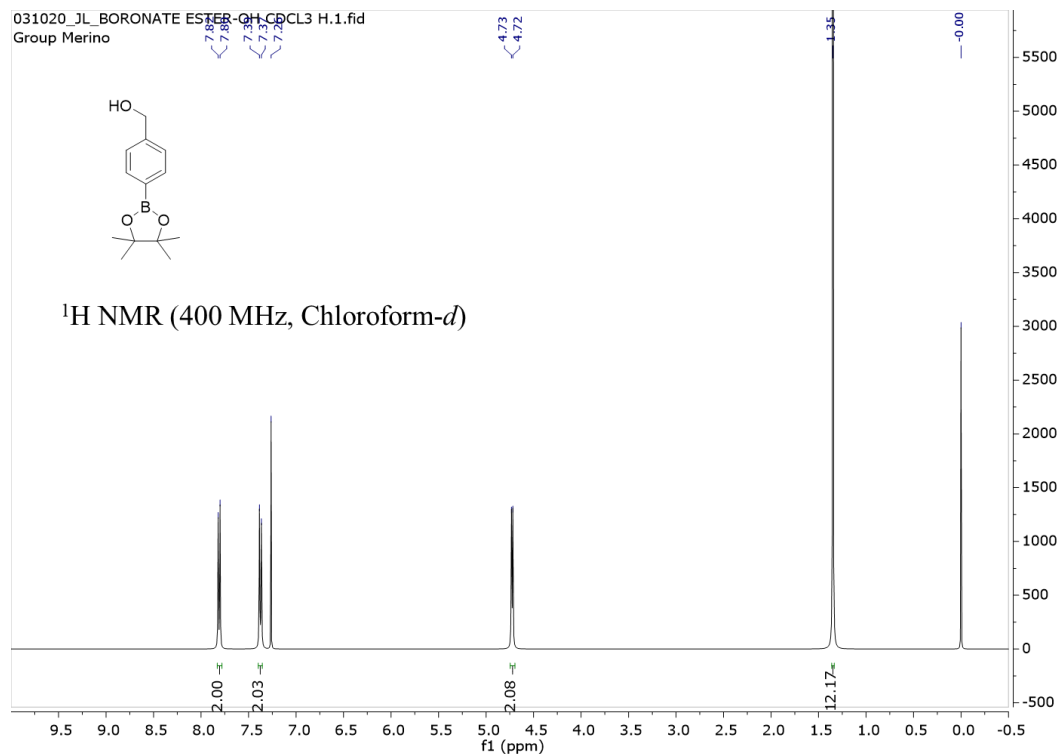


Scheme 18.4 The synthesis route of compound BDEASOR.

Synthesis of (4-(4,4,5,5-tetramethyl-1,3,2-dioxaborolan-2-yl)phenyl)methanol:

To a solution of the 4-Bromobenzyl alcohol (0.93g, 5mmol) in Dioxane (40ml) under argon protection was added 1,1'-Bis(diphenylphosphino)ferrocene]dichloropalladium(II) (0.81g, 1mmol), potassium acetate (1.47g, 15mmol) and Bis(pinacolato)diboron (1.897g, 7.5mmol). The resulting mixture was stirred at RT for 8 h, after which time the reaction mixture was filtered. The organic layer was concentrated in vacuo to provide the product as a white solid. [0.92g, yield:80%]
 $^1\text{H NMR}$ (400 MHz, Chloroform-*d*) δ 7.81 (d, $J = 8.0$ Hz, 2H), 7.38 (d, $J = 8.0$ Hz, 2H), 4.73 (d, $J = 5.9$ Hz, 2H), 1.35 (s, 12H).

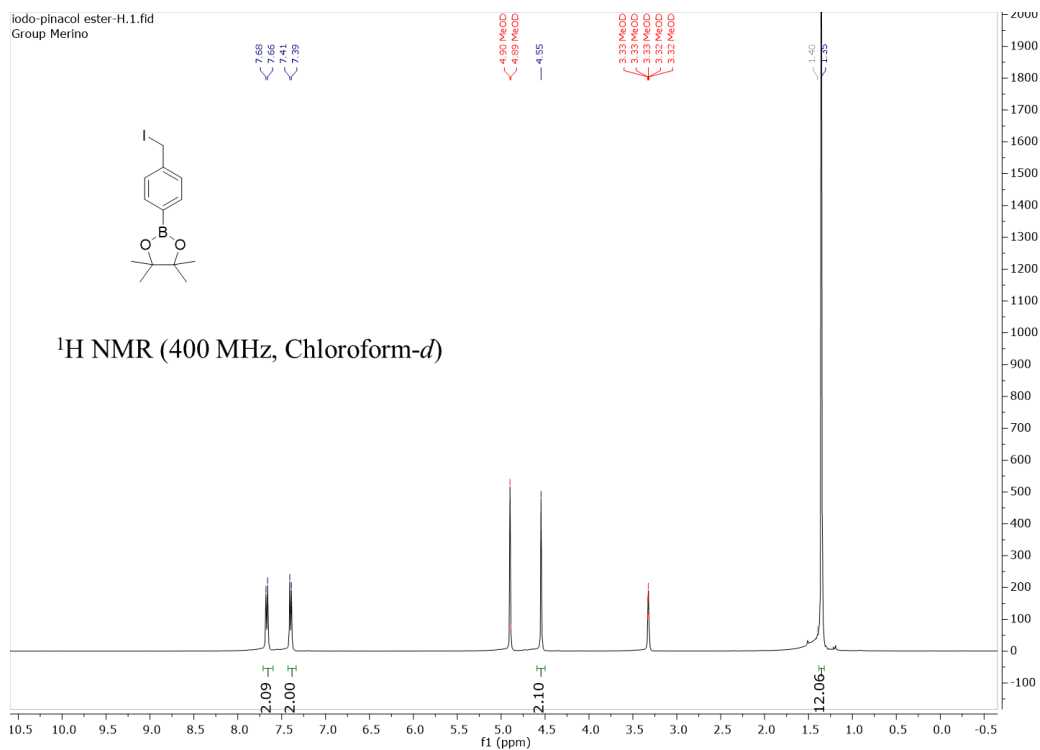
NMR for (4-(4,4,5,5-tetramethyl-1,3,2-dioxaborolan-2-yl)phenyl)methanol



Synthesis of 2-(4-(iodomethyl)phenyl)-4,4,5,5-tetramethyl-1,3,2-dioxaborolane:

To a solution of the (4-(4,4,5,5-tetramethyl-1,3,2-dioxaborolan-2-yl)phenyl)methanol (230mg, 1mmol) in ACN (6.0 mL) in an ice-water bath(0°C) was added sodium iodide (456mg, 3 mmol), after 15 mins, followed by the addition of TMSCl (0.372 mL, 3mmol). The resulting mixture was moved and stirred at RT for 8 h, after which time the reaction mixture was diluted with Na₂S₂O₃ saturated solution and extracted with EtOAc. The organic layer was dried (Na₂SO₄) and concentrated in vacuo to provide the product as a yellow solid. [204mg, 60%] ^1H NMR (400 MHz, Methanol-*d*₄) δ 7.67 (d, $J = 7.6$ Hz, 2H), 7.40 (d, $J = 7.6$ Hz, 2H), 4.55 (s, 2H), 1.35 (s, 12H). ^{13}C NMR (101 MHz, CDCl₃) δ 135.02, 129.07, 127.82, 83.86, 46.71, 42.55, 29.72, 24.88, 11.53.

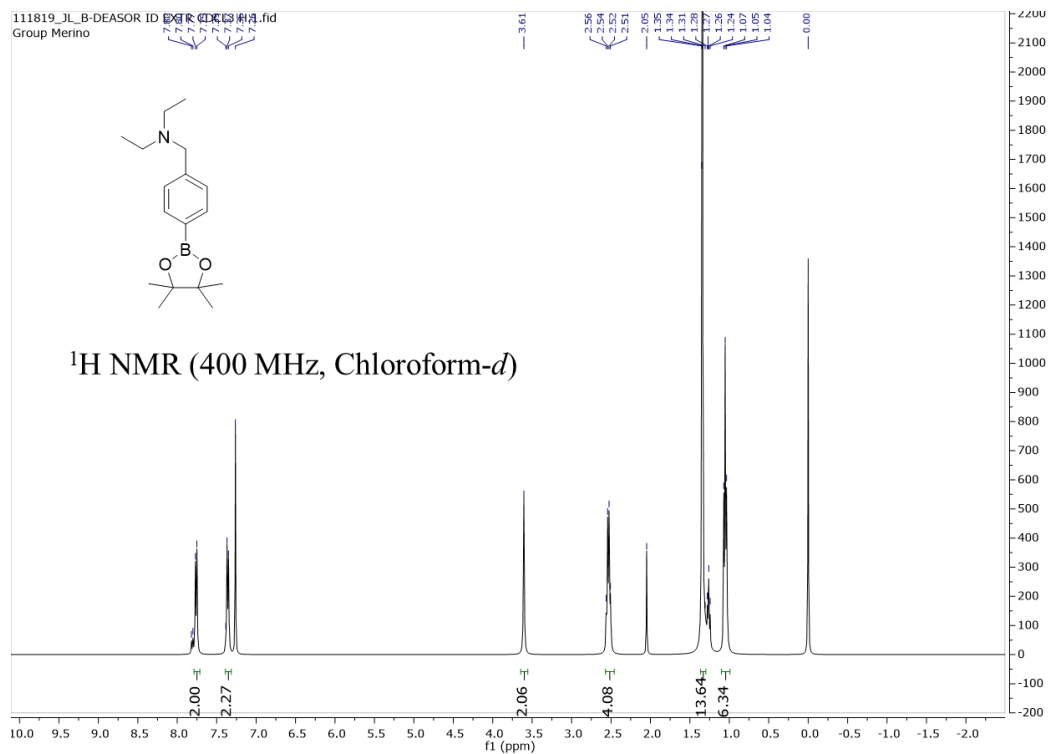
NMR for 2-(4-(iodomethyl)phenyl)-4,4,5,5-tetramethyl-1,3,2-dioxaborolane



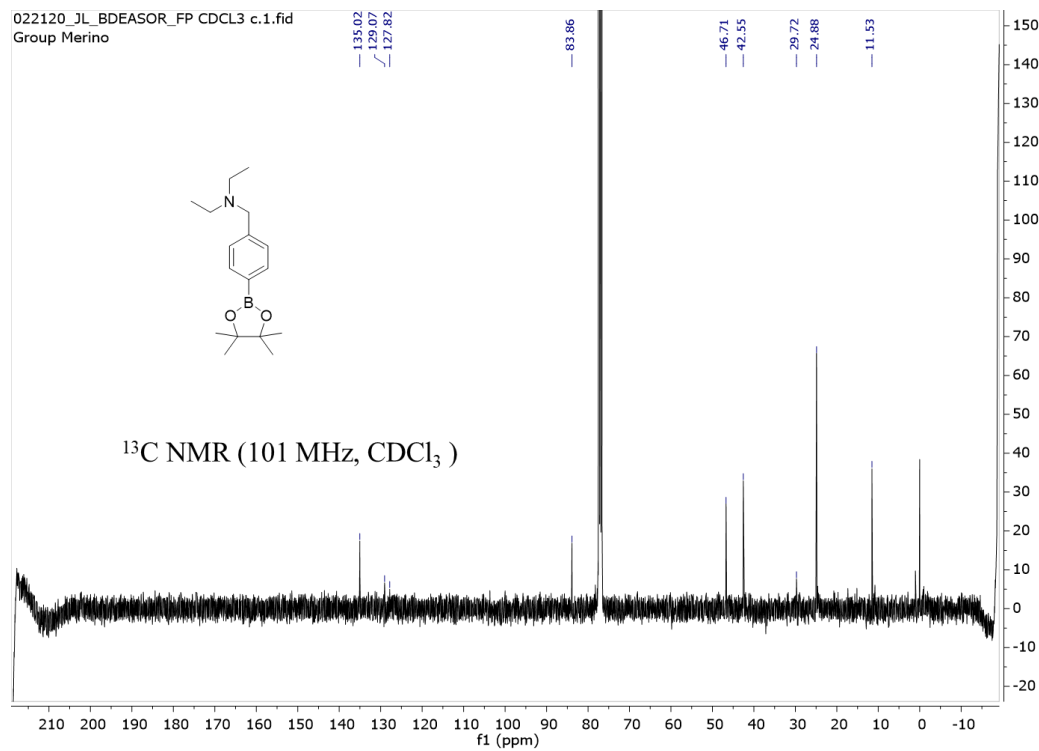
Synthesis of N-ethyl-N-(4-(4,4,5,5-tetramethyl-1,3,2-dioxaborolan-2-yl)benzyl)ethanamine:

To a solution of 2-(4-(iodomethyl)phenyl)-4,4,5,5-tetramethyl-1,3,2-dioxaborolane (170mg, 0.5mmol) in THF (1mL) was added excess diethylamine (3mL). The resulting mixture was stirred for 4 hours, after which time the reaction mixture was dried in vacuo. The resulting material to provide the product as a yellow solid. [142mg, yield:99%] ^1H NMR (400 MHz, Chloroform-*d*) δ 7.76 (d, $J = 7.6$ Hz, 2H), 7.36 (d, $J = 7.4$ Hz, 2H), 3.61 (s, 2H), 2.53 (q, $J = 7.1$ Hz, 4H), 1.34 (s, $J = 1.4$ Hz, 2H), 1.05 (t, $J = 7.1$ Hz, 6H).

NMR for N-ethyl-N-(4-(4,4,5,5-tetramethyl-1,3,2-dioxaborolan-2-yl)benzyl)ethanamine :



¹³C NMR for N-ethyl-N-(4-(4,4,5,5-tetramethyl-1,3,2-dioxaborolan-2-yl)benzyl)ethanamine



4.2.2 Oxidation study

HRP oxidation: A working solution (0.7mg DEASOR-OH was dissolved in 2mL DMSO with 0.5ml 25 mM phosphate buffer, pH=7.4) was made. A 1mL sample was used as the no enzyme control. The reaction was 1mL of working solution and 0.1U HRP and added H₂O₂ to make 0.4mM. After various time scale, 0.5ml NaOH(1N) was added. The result solution was analyzed by HPLC to quantify the relative amounts of DEASOR-OH. Moles were calculated using a standard of each compound and yields were calculated using integration. All determinations were carried out in triplicate on different days. On each occasion and new standards and samples were made.

4.2.3 HPLC condition for oxidation studies

A Beckman Coulter's HPLC system consisting of a dual pump Model 126 with 32 Karat Software, a System Gold 168 detector, and a System Gold 508 Auto Sampler was used. A reverse phase C-18 column (Synergi™ 4μm Hydro-RP 80Å, LC Column 100×4.6mm, Ea.) was used. The mobile phase consisted of HPLC grade Acetonitrile (Fisher Scientific), LCMS grade formic acid (Fisher Scientific), and distilled water filtered through a Millipore Milli-Q water purification system. Solvent A for the mobile phase was 95% water, 5% Acetonitrile for oxidation study of DEASOR-OH. Solvent B is 95% acetonitrile and 5% water. The gradient was 0% B for 4 minutes and 95% B over 16 minutes. The flow was 1ml/min. A detection wavelength of 250nm and 285nm was used for oxidation of DEASOR-OH.

4.2.4 GCMS assay

An Agilent Technologies 5977A MSD system and a System Agilent technologies 7697A headspace Sampler were used. An Agilent 19091S-433-5ms column(20m*250um*0.25um) was used. The flow rate of Helium as the carrier gas was set to 1.2ml/min. The pressure was set to 11 psi. The initial temperature was set to 45°C for 4mins and roused 70°C/mins until 250°C, then holding for 3minutes. The headspace oven was set to 80°C for 20minutes for equilibrium.

4.3 Results and Discussion

4.3.1 Diethylamine shows a good LOQ on GCMS

Diethylamine was selected as a small probe molecular detected by GCMS for its low boiling point. However, the availability of MS and method need to be confirmed base on the GCHSMS(**Figure 4.3A**). The designed assay should ask for 0.5ml of the phosphate buffer containing the cells needed to be tested. Then 2ml DMSO will be added to decrease the partial pressure of water from the sample to enhance diethylamine by increase partial pressure. Furthermore, 0.5ml of 1M NaOH should be added for breaking the hydrogen bond of diethylamine with water to increase the GCMS sensitivity further.

0.16mM of diethylamine was prepared with the solution mentioned and transferred to the headspace vial. The sample was then analyzed by the GCMS on headspace mode. Result shows as **Figure 4.3B**. Two characteristic peaks have identified the existence of diethylamine. One of the peaks ($m/z=73$) identified as the positively charged diethylamine, the other one($m/z=58$) produced when α -cleavage happens, and one ethyl group fall off.

At last, the calibration curve established from diethylamine with a series of various concentrations shown as **Figure 4.3C**. Limit of detection(LOD) and limit of quantification(LOQ) were calculated base on the equation of $LOD=3x(S/N)=8\mu M$ and $LOQ=10x(S/N)=24\mu M$. Considering the generation of oxidants in cells was about $2-3\text{ nmol } O_2^{\cdot-}/10^6\text{ cells-mins}^{94}$. After 24 hours of pretreatment of the cells mixing with the designed sensor, $28\mu M$ oxygen singlet should be released and react with the sensor to release quantifiable diethylamine for 10 million cells besides other different oxidants.

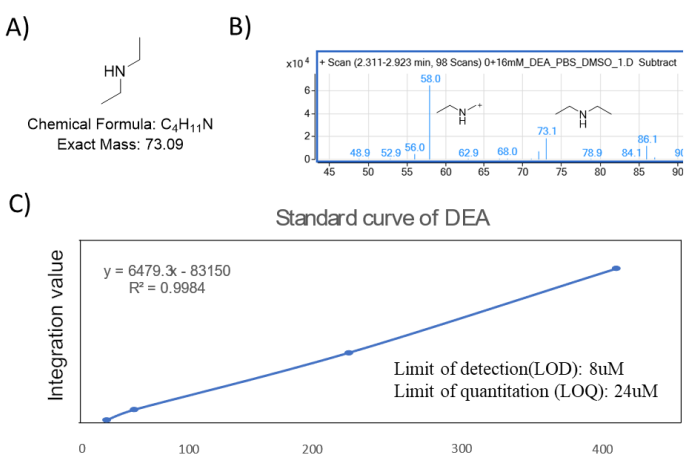


Figure 19.3 (A) Exact mass of Diethylamine (B) GCMS of Diethylamine (C) LOD and LOQ with the calibration curve.

After the confirmation of the MS of diethylamine on GCMS and LOD as $24\mu M$, which is an acceptable value for 10 million cell assay, two different DEA based sensors were designed and synthesized, which already stated in **4.2 section**.

4.3.2 Oxidation study of DEASOR-OH

Enlighten from the RIP2, DEASOR-OH was synthesized by attaching diethylamine on a ROS sensitive oxalate linker. It was made in three steps with a net 60% yield. Further study about

whether the designed compound could be oxidized to release diethylamine need to be further confirmed as the mechanism shown in **Figure 4.4A**.

The oxidation study of DEASOR-OH was analyzed by HPLC about its oxidation manner. The traces listed in **Figure 4.4B** from left to right are the remained DEASOR-OH on different time from 30 seconds to 3840 seconds. The remained DEASOR-OH change from 100% to 2% in 3840 seconds. The oxidation rate was analyzed by building chart DEASOR-OH% VS time, $\ln(\text{DEASOR-OH}\%)$ VS time, and $1/(\text{DEASOR-OH}\%)$ VS time to verify the reaction order and half-life of DEASOR-OH under HRP oxidation. The R^2 for $1/(\text{DEASOR-OH}\%)$ VS time chart calculated as 0.9859, which proves the reaction order as second order. Half-life is also calculated from the $1/\text{slope} * 100$ as 166 seconds.

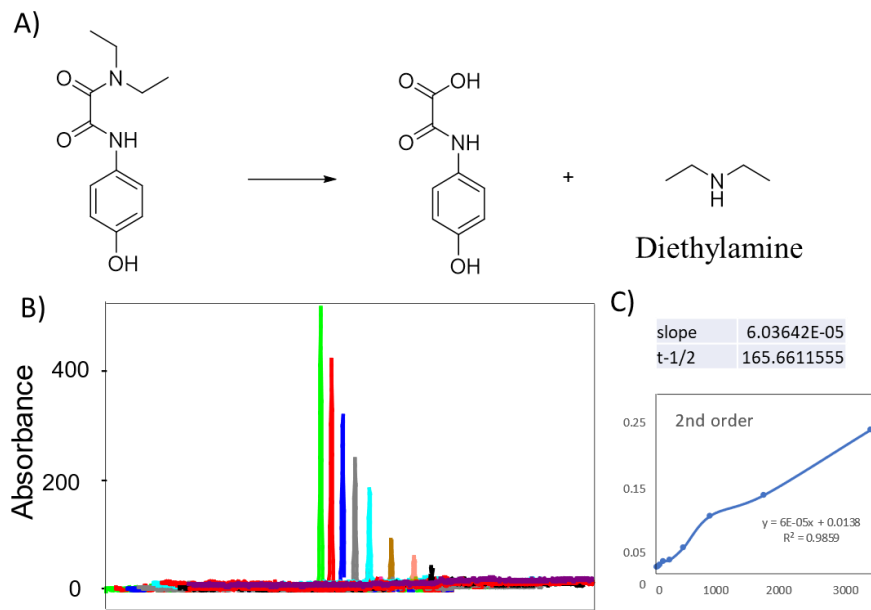


Figure 20.4 (A) Proposed reaction of DEASOR-OH to release diethylamine as the probe. (B) HPLC analysis of DEASOR-OH degradation on time scale in phosphate buffer under HRP conditions. (C) Reaction order of DEASOR-OH

To sum up, the degradation of DEASOR-OH following the second-order reaction as the rate under the HRP enzyme oxidation. It proved the potential use as an oxidant sensor under GCMS for further quantification.

4.3.3 GCMS study of BDEASOR

Another sensor was designed base on a boronate ester structure. This is proved to be a ROS-sensitive linker and degrade under hydrogen peroxide condition. The diethylamine was attached as a benzylamine with the boronate ester on the p position. The presumed mechanism started with the insertion of $[\cdot\text{OOH}]^-$. (**Figure4.5**) Then homologation happened with an alkyl group shifts from boron in a boronate to oxygen. At last, the diethylamine should be kicked off and released as the probe.

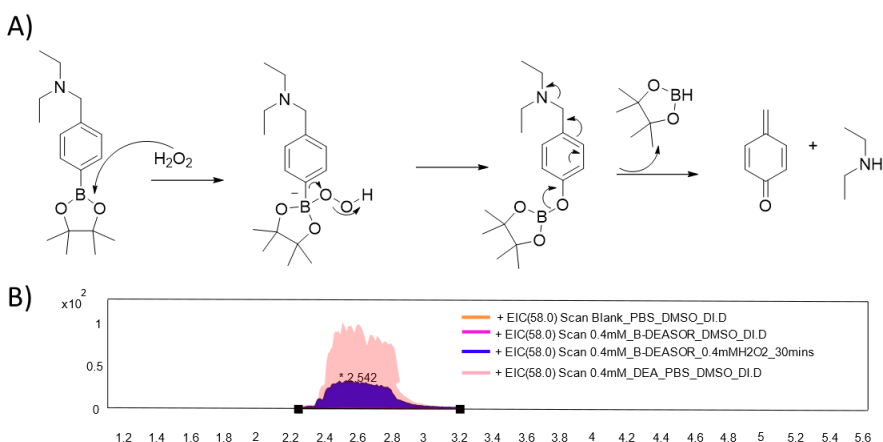


Figure 21.5 (A) Proposed mechanism of BDEASOR to release diethylamine as the probe. (B) GCHSMS analysis of BDEASOR under H_2O_2 condition (purple trace). Also, the pure Diethylamine is analyzed under the same condition (pink trace).

For further confirmation of the diethylamine releasing, GCHSMS was running. 0.4mM BDEASOR solution with 0.5ml PBS buffer, 2ml DMSO, and 0.5ml 1N NaOH solution was prepared as the working solution. Blank(orange trace) was run to make sure the background was

clean. (**Figure4.5**) Then the working solution(red trace) was to run without H₂O₂. It shows no diethylamine peaks the same as blank. It indicates the stability of BDEASOR without oxidants so that only release diethylamine under oxidative stress.

Afterward, the working solution was added with H₂O₂ to make concentration as 0.4mM. Mixing for 30 minutes for reaction and ran for the result. A peak (purple trace)belongs to diethylamine shown up at 2.6 minutes. A positive control prepared with diethylamine dissolved in the same solvent analyzed by GCMS shown the same retention time(pink trace) as a sample trace(purple). The integration of traces shows diethylamine released from BDEASOR is 40% of the positive control. It may because the 30mins are not enough for the compound to decompose and release all the diethylamine. However, the mechanism of BDEASOR is confirmed to kick off the diethylamine and quantified by GCMS. It is a promising molecular to applied to quantify the oxidative stress in a cell assay.

4.4 Conclusions

In this chapter, diethylamine is proved to be a small molecular that could be used for quantification of the oxidant in cells by GCHSMS technique. And two molecules are designed and synthesized to by attaching diethylamine on the ROS-activated moiety to be released only under oxidative stress conditions. Reaction rate verified by HPLC for DEASOR-OH. And a Boronat ester-based sensor shows proper releasing manner only under oxidative condition. Some more future studies about the oxidation rate about DEASOR need to be done to confirm the decent pretreatment time for fully releasing of the probe. And several cells will be run to value the application of the sensors.

Reference

1. Finkel, T., Signal transduction by reactive oxygen species. *Journal of Cell Biology* **2011**, *194* (1), 7-15.
2. Lambeth, J. D., NOX enzymes and the biology of reactive oxygen. *Nature Reviews Immunology* **2004**, *4* (3), 181-189.
3. Brand, M. D., The sites and topology of mitochondrial superoxide production. *Experimental gerontology* **2010**, *45* (7-8), 466-472.
4. Dannenmann, B.; Lehle, S.; Hildebrand, D. G.; Kübler, A.; Grondona, P.; Schmid, V.; Holzer, K.; Fröschl, M.; Essmann, F.; Rothfuss, O., High glutathione and glutathione peroxidase-2 levels mediate cell-type-specific DNA damage protection in human induced pluripotent stem cells. *Stem Cell Reports* **2015**, *4* (5), 886-898.
5. Ligtenberg, M. A.; Mougiakakos, D.; Mukhopadhyay, M.; Witt, K.; Lladser, A.; Chmielewski, M.; Riet, T.; Abken, H.; Kiessling, R., Coexpressed catalase protects chimeric antigen receptor–redirected T cells as well as bystander cells from oxidative stress–induced loss of antitumor activity. *The Journal of Immunology* **2016**, *196* (2), 759-766.
6. Cross, C. E.; HALLIWELL, B.; BORISH, E. T.; PRYOR, W. A.; AMES, B. N.; SAUL, R. L.; McCORD, J. M.; HARMAN, D., Oxygen radicals and human disease. *Annals of internal medicine* **1987**, *107* (4), 526-545.
7. Scharffetter-Kochanek, K.; Wlaschek, M.; Brenneisen, P.; Schauen, M.; Blandschun, R.; Wenk, J., UV-induced reactive oxygen species in photocarcinogenesis and photoaging. *Biological chemistry* **1997**, *378* (11), 1247-1258.
8. Armstrong, B. K.; Kricger, A., The epidemiology of UV induced skin cancer. *Journal of photochemistry and photobiology B: Biology* **2001**, *63* (1-3), 8-18.
9. Sage, E.; Girard, P.-M.; Francesconi, S., Unravelling UVA-induced mutagenesis. *Photochemical & Photobiological Sciences* **2012**, *11* (1), 74-80.
10. Narayanan, D. L.; Saladi, R. N.; Fox, J. L., Ultraviolet radiation and skin cancer. *International journal of dermatology* **2010**, *49* (9), 978-986.
11. Matés, J. M.; Sánchez-Jiménez, F. M., Role of reactive oxygen species in apoptosis: implications for cancer therapy. *The international journal of biochemistry & cell biology* **2000**, *32* (2), 157-170.
12. Denat, L.; Kadekaro, A. L.; Marrot, L.; Leachman, S. A.; Abdel-Malek, Z. A., Melanocytes as instigators and victims of oxidative stress. *The Journal of investigative dermatology* **2014**, *134* (6), 1512-1518.
13. Beers, R. F.; Sizer, I. W., A spectrophotometric method for measuring the breakdown of hydrogen peroxide by catalase. *J Biol chem* **1952**, *195* (1), 133-140.
14. Wondrak, G. T.; Jacobson, M. K.; Jacobson, E. L., Endogenous UVA-photosensitizers: mediators of skin photodamage and novel targets for skin photoprotection. *Photochemical & photobiological sciences* **2006**, *5* (2), 215-237.
15. Bossi, O.; Gartsbein, M.; Leitges, M.; Kuroki, T.; Grossman, S.; Tennenbaum, T., UV irradiation increases ROS production via PKC δ signaling in primary murine fibroblasts. *Journal of cellular biochemistry* **2008**, *105* (1), 194-207.
16. Meyskens Jr, F. L.; Farmer, P.; Fruehauf, J. P., Redox regulation in human melanocytes and melanoma. *Pigment cell research* **2001**, *14* (3), 148-154.
17. Nakabeppu, Y., Cellular levels of 8-oxoguanine in either DNA or the nucleotide pool play pivotal roles in carcinogenesis and survival of cancer cells. *International journal of molecular sciences* **2014**, *15* (7), 12543-12557.
18. Siegel, R. L.; Miller, K. D.; Jemal, A., Cancer statistics, 2019. *CA: a cancer journal for clinicians* **2019**, *69* (1), 7-34.
19. Beeby, A.; Jones, A. E., The Photophysical Properties of Menthyl Anthranilate: A UV-A Sunscreen. *Photochemistry and photobiology* **2000**, *72* (1), 10-15.

20. Suzuki, T.; Kitamura, S.; Khota, R.; Sugihara, K.; Fujimoto, N.; Ohta, S., Estrogenic and antiandrogenic activities of 17 benzophenone derivatives used as UV stabilizers and sunscreens. *Toxicology and applied pharmacology* **2005**, *203* (1), 9-17.
21. Janjua, N. R.; Mogensen, B.; Andersson, A.-M.; Petersen, J. H.; Henriksen, M.; Skakkebaek, N. E.; Wulf, H. C., Systemic absorption of the sunscreens benzophenone-3, octyl-methoxycinnamate, and 3-(4-methyl-benzylidene) camphor after whole-body topical application and reproductive hormone levels in humans. *Journal of Investigative Dermatology* **2004**, *123* (1), 57-61.
22. Cole, C.; Shyr, T.; Ou-Yang, H., Metal oxide sunscreens protect skin by absorption, not by reflection or scattering. *Photodermatology, photoimmunology & photomedicine* **2016**, *32* (1), 5-10.
23. Shaath, N. A., Ultraviolet filters. *Photochemical & Photobiological Sciences* **2010**, *9* (4), 464-469.
24. Smijs, T. G.; Pavel, S., Titanium dioxide and zinc oxide nanoparticles in sunscreens: focus on their safety and effectiveness. *Nanotechnology, science and applications* **2011**, *4*, 95.
25. Karlsson, I.; Hillerström, L.; Stenfeldt, A.-L.; Mårtensson, J.; Börje, A., Photodegradation of dibenzoylmethanes: potential cause of photocontact allergy to sunscreens. *Chemical research in toxicology* **2009**, *22* (11), 1881-1892.
26. Gaspar, L.; Campos, P. M., Evaluation of the photostability of different UV filter combinations in a sunscreen. *International Journal of pharmaceutics* **2006**, *307* (2), 123-128.
27. Hanson, K. M.; Gratton, E.; Bardeen, C. J., Sunscreen enhancement of UV-induced reactive oxygen species in the skin. *Free Radical Biology and Medicine* **2006**, *41* (8), 1205-1212.
28. Tovar-Sánchez, A.; Sánchez-Quiles, D.; Basterretxea, G.; Benedé, J. L.; Chisvert, A.; Salvador, A.; Moreno-Garrido, I.; Blasco, J., Sunscreen products as emerging pollutants to coastal waters. *PLoS One* **2013**, *8* (6).
29. Downs, C. A.; Kramarsky-Winter, E.; Segal, R.; Fauth, J.; Knutson, S.; Bronstein, O.; Ciner, F. R.; Jeger, R.; Lichtenfeld, Y.; Woodley, C. M., Toxicopathological effects of the sunscreen UV filter, oxybenzone (benzophenone-3), on coral planulae and cultured primary cells and its environmental contamination in Hawaii and the US Virgin Islands. *Archives of environmental contamination and toxicology* **2016**, *70* (2), 265-288.
30. Danovaro, R.; Bongiorno, L.; Corinaldesi, C.; Giovannelli, D.; Damiani, E.; Astolfi, P.; Greci, L.; Pusceddu, A., Sunscreens cause coral bleaching by promoting viral infections. *Environmental health perspectives* **2008**, *116* (4), 441-7.
31. Wiench, K.; Wohlleben, W.; Hisgen, V.; Radke, K.; Salinas, E.; Zok, S.; Landsiedel, R., Acute and chronic effects of nano-and non-nano-scale TiO₂ and ZnO particles on mobility and reproduction of the freshwater invertebrate *Daphnia magna*. *Chemosphere* **2009**, *76* (10), 1356-1365.
32. McCoshum, S. M.; Schlarb, A. M.; Baum, K. A., Direct and indirect effects of sunscreen exposure for reef biota. *Hydrobiologia* **2016**, *776* (1), 139-146.
33. Sporn, M. B.; Dunlop, N.; Newton, D.; Smith, J. In *Prevention of chemical carcinogenesis by vitamin A and its synthetic analogs (retinoids)*, Federation proceedings, 1976; pp 1332-1338.
34. Steward, W.; Brown, K., Cancer chemoprevention: a rapidly evolving field. *British journal of cancer* **2013**, *109* (1), 1-7.
35. Premi, S.; Brash, D. E., Chemical excitation of electrons: A dark path to melanoma. *DNA repair* **2016**, *44*, 169-177.
36. Markovic, S. N.; Erickson, L. A.; Rao, R. D.; McWilliams, R. R.; Kottschade, L. A.; Creagan, E. T.; Weenig, R. H.; Hand, J. L.; Pittelkow, M. R.; Pockaj, B. A. In *Malignant melanoma in the 21st century, part 1: epidemiology, risk factors, screening, prevention, and diagnosis*, Mayo Clinic Proceedings, Elsevier: 2007; pp 364-380.
37. Godic, A.; Poljšak, B.; Adamic, M.; Dahmane, R., The role of antioxidants in skin cancer prevention and treatment. *Oxidative medicine and cellular longevity* **2014**, *2014*.
38. Hsieh, T.-c.; Wang, Z.; Hamby, C. V.; Wu, J. M., Inhibition of melanoma cell proliferation by resveratrol is correlated with upregulation of quinone reductase 2 and p53. *Biochemical and biophysical research communications* **2005**, *334* (1), 223-230.

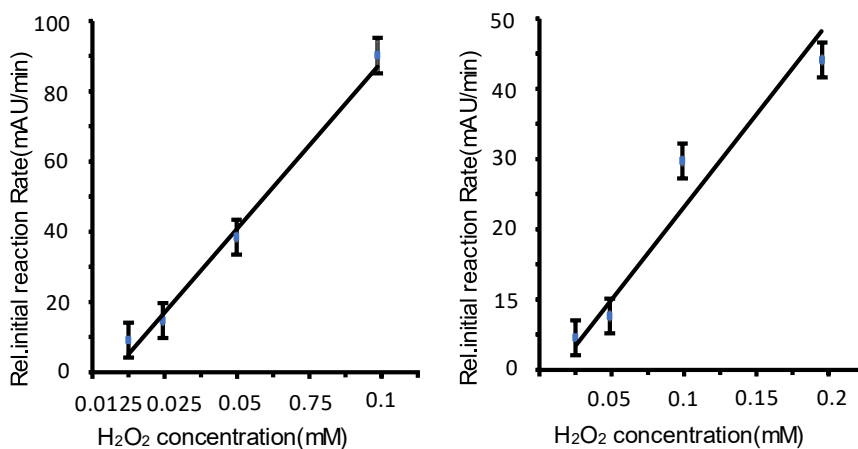
39. Ighodaro, O.; Akinloye, O., First line defence antioxidants-superoxide dismutase (SOD), catalase (CAT) and glutathione peroxidase (GPX): Their fundamental role in the entire antioxidant defence grid. *Alexandria Journal of Medicine* **2018**, *54* (4), 287-293.
40. Birben, E.; Sahiner, U. M.; Sackesen, C.; Erzurum, S.; Kalayci, O., Oxidative stress and antioxidant defense. *World Allergy Organization Journal* **2012**, *5* (1), 9-19.
41. Traikovich, S. S., Use of topical ascorbic acid and its effects on photodamaged skin topography. *Archives of otolaryngology-head & neck surgery* **1999**, *125* (10), 1091-1098.
42. Stahl, W.; Krutmann, J., Systemic photoprotection through carotenoids. *Der Hautarzt; Zeitschrift für Dermatologie, Venerologie, und verwandte Gebiete* **2006**, *57* (4), 281-285.
43. Wu, Y.; Liu, F., Targeting mTOR: evaluating the therapeutic potential of resveratrol for cancer treatment. *Anti-Cancer Agents in Medicinal Chemistry (Formerly Current Medicinal Chemistry-Anti-Cancer Agents)* **2013**, *13* (7), 1032-1038.
44. Jung, Y. D.; Ellis, L. M., Inhibition of tumour invasion and angiogenesis by epigallocatechin gallate (EGCG), a major component of green tea. *International journal of experimental pathology* **2001**, *82* (6), 309-316.
45. Srivastava, A. K.; Bhatnagar, P.; Singh, M.; Mishra, S.; Kumar, P.; Shukla, Y.; Gupta, K. C., Synthesis of PLGA nanoparticles of tea polyphenols and their strong in vivo protective effect against chemically induced DNA damage. *International journal of nanomedicine* **2013**, *8*, 1451.
46. Liu, Y.; Fiskum, G.; Schubert, D., Generation of reactive oxygen species by the mitochondrial electron transport chain. *Journal of neurochemistry* **2002**, *80* (5), 780-787.
47. Vásquez-Vivar, J.; Kalyanaraman, B.; Martásek, P.; Hogg, N.; Masters, B. S. S.; Karoui, H.; Tordo, P.; Pritchard, K. A., Superoxide generation by endothelial nitric oxide synthase: the influence of cofactors. *Proceedings of the National Academy of Sciences* **1998**, *95* (16), 9220-9225.
48. Zangar, R. C.; Davydov, D. R.; Verma, S., Mechanisms that regulate production of reactive oxygen species by cytochrome P450. *Toxicology and applied pharmacology* **2004**, *199* (3), 316-331.
49. Ty, M. C.; Zuniga, M.; Götz, A.; Kayal, S.; Sahu, P. K.; Mohanty, A.; Mohanty, S.; Wassmer, S. C.; Rodriguez, A., Malaria inflammation by xanthine oxidase-produced reactive oxygen species. *EMBO molecular medicine* **2019**, *11* (8).
50. Bedard, K.; Krause, K.-H., The NOX family of ROS-generating NADPH oxidases: physiology and pathophysiology. *Physiological reviews* **2007**, *87* (1), 245-313.
51. Sumimoto, H.; Miyano, K.; Takeya, R., Molecular composition and regulation of the Nox family NAD (P) H oxidases. *Biochemical and biophysical research communications* **2005**, *338* (1), 677-686.
52. Kang, M.; So, E.; Simons, A.; Spitz, D.; Ouchi, T., DNA damage induces reactive oxygen species generation through the H2AX-Nox1/Rac1 pathway. *Cell death & disease* **2012**, *3* (1), e249-e249.
53. Leto, T. L.; Morand, S.; Hurt, D.; Ueyama, T., Targeting and regulation of reactive oxygen species generation by Nox family NADPH oxidases. *Antioxidants & redox signaling* **2009**, *11* (10), 2607-2619.
54. Takac, I.; Schröder, K.; Zhang, L.; Lardy, B.; Anilkumar, N.; Lambeth, J. D.; Shah, A. M.; Morel, F.; Brandes, R. P., The E-loop is involved in hydrogen peroxide formation by the NADPH oxidase Nox4. *Journal of Biological Chemistry* **2011**, *286* (15), 13304-13313.
55. Aldieri, E.; Riganti, C.; Polimeni, M.; Gazzano, E.; Lussiana, C.; Campia, I.; Ghigo, D., Classical inhibitors of NOX NAD (P) H oxidases are not specific. *Current drug metabolism* **2008**, *9* (8), 686-696.
56. Gianni, D.; Taulet, N.; Zhang, H.; DerMardirossian, C.; Kister, J.; Martinez, L.; Roush, W. R.; Brown, S. J.; Bokoch, G. M.; Rosen, H., A novel and specific NADPH oxidase-1 (Nox1) small-molecule inhibitor blocks the formation of functional invadopodia in human colon cancer cells. *ACS chemical biology* **2010**, *5* (10), 981-993.
57. Gorin, Y.; Block, K.; Hernandez, J.; Bhandari, B.; Wagner, B.; Barnes, J. L.; Abboud, H. E., Nox4 NAD (P) H oxidase mediates hypertrophy and fibronectin expression in the diabetic kidney. *Journal of Biological Chemistry* **2005**, *280* (47), 39616-39626.

58. Rey, F.; Cifuentes, M.; Kiarash, A.; Quinn, M.; Pagano, P., Novel competitive inhibitor of NAD(P)H oxidase assembly attenuates vascular O₂⁻ and systolic blood pressure in mice. *Circulation research* **2001**, *89* (5), 408-414.
59. Csányi, G.; Cifuentes-Pagano, E.; Al Ghoulleh, I.; Ranayhossaini, D. J.; Egaña, L.; Lopes, L. R.; Jackson, H. M.; Kelley, E. E.; Pagano, P. J., Nox2 B-loop peptide, Nox2ds, specifically inhibits the NADPH oxidase Nox2. *Free Radical Biology and Medicine* **2011**, *51* (6), 1116-1125.
60. Valencia, A.; Kochevar, I. E., Nox1-based NADPH oxidase is the major source of UVA-induced reactive oxygen species in human keratinocytes. *Journal of Investigative Dermatology* **2008**, *128* (1), 214-222.
61. Ueyama, T.; Geiszt, M.; Leto, T. L., Involvement of Rac1 in activation of multicomponent Nox1- and Nox3-based NADPH oxidases. *Molecular and cellular biology* **2006**, *26* (6), 2160-2174.
62. Bickers, D. R.; Athar, M., Oxidative stress in the pathogenesis of skin disease. *Journal of Investigative Dermatology* **2006**, *126* (12), 2565-2575.
63. Rothenberg, M. L.; Carbone, D. P.; Johnson, D. H., Improving the evaluation of new cancer treatments: challenges and opportunities. *Nature Reviews Cancer* **2003**, *3* (4), 303-309.
64. M Huttunen, K.; Rautio, J., Prodrugs-an efficient way to breach delivery and targeting barriers. *Current topics in medicinal chemistry* **2011**, *11* (18), 2265-2287.
65. AbdulSalam, S. F.; Gurjar, P. N.; Zhu, H.; Liu, J.; Johnson, E. S.; Kadekaro, A. L.; Landero-Figueroa, J.; Merino, E. J., Self-Cyclizing Antioxidants to Prevent DNA Damage Caused by Hydroxyl Radical. *Chembiochem : a European journal of chemical biology* **2017**, *18* (20), 2007-2011.
66. Martin, J. R.; Gupta, M. K.; Page, J. M.; Yu, F.; Davidson, J. M.; Guelcher, S. A.; Duvall, C. L., A porous tissue engineering scaffold selectively degraded by cell-generated reactive oxygen species. *Biomaterials* **2014**, *35* (12), 3766-3776.
67. Van de Bittner, G. C.; Dubikovskaya, E. A.; Bertozzi, C. R.; Chang, C. J., In vivo imaging of hydrogen peroxide production in a murine tumor model with a chemoselective bioluminescent reporter. *Proceedings of the National Academy of Sciences* **2010**, *107* (50), 21316-21321.
68. Halliday, G. M., Inflammation, gene mutation and photoimmunosuppression in response to UVR-induced oxidative damage contributes to photocarcinogenesis. *Mutation Research/Fundamental and Molecular Mechanisms of Mutagenesis* **2005**, *571* (1-2), 107-120.
69. Halliday, G. M., Common links among the pathways leading to UV-induced immunosuppression. *Journal of Investigative Dermatology* **2010**, *130* (5), 1209-1212.
70. Bosch, R.; Philips, N.; Suárez-Pérez, J. A.; Juarranz, A.; Devmurari, A.; Chalensouk-Khaosaat, J.; González, S., Mechanisms of photoaging and cutaneous photocarcinogenesis, and photoprotective strategies with phytochemicals. *Antioxidants* **2015**, *4* (2), 248-268.
71. Tsukagoshi, H.; Busch, W.; Benfey, P. N., Transcriptional regulation of ROS controls transition from proliferation to differentiation in the root. *Cell* **2010**, *143* (4), 606-616.
72. Simon, H.-U.; Haj-Yehia, A.; Levi-Schaffer, F., Role of reactive oxygen species (ROS) in apoptosis induction. *Apoptosis* **2000**, *5* (5), 415-418.
73. Ziech, D.; Franco, R.; Pappa, A.; Panayiotidis, M. I., Reactive Oxygen Species (ROS)—Induced genetic and epigenetic alterations in human carcinogenesis. *Mutation Research/Fundamental and Molecular Mechanisms of Mutagenesis* **2011**, *711* (1-2), 167-173.
74. Bandarchi, B.; Ma, L.; Navab, R.; Seth, A.; Rasty, G., From melanocyte to metastatic malignant melanoma. *Dermatology research and practice* **2010**, *2010*.
75. Aggarwal, V.; Tuli, H. S.; Varol, A.; Thakral, F.; Yerer, M. B.; Sak, K.; Varol, M.; Jain, A.; Khan, M.; Sethi, G., Role of Reactive Oxygen Species in Cancer Progression: Molecular Mechanisms and Recent Advancements. *Biomolecules* **2019**, *9* (11), 735.
76. Gloire, G.; Legrand-Poels, S.; Piette, J., NF- κ B activation by reactive oxygen species: fifteen years later. *Biochemical pharmacology* **2006**, *72* (11), 1493-1505.
77. Karin, M., Nuclear factor- κ B in cancer development and progression. *Nature* **2006**, *441* (7092), 431-436.

78. Ueda, Y.; Richmond, A., NF- κ B activation in melanoma. *Pigment cell research* **2006**, *19* (2), 112-124.
79. Payne, A. S.; Cornelius, L. A., The role of chemokines in melanoma tumor growth and metastasis. *Journal of Investigative Dermatology* **2002**, *118* (6), 915-922.
80. Srisayam, M.; Weerapreeyakul, N.; Barusrux, S.; Kanokmedhakul, K., Antioxidant, antimelanogenic, and skin-protective effect of sesamol. *J cosmet Sci* **2014**, *65* (2), 69-79.
81. Wu, X.-L.; Liou, C.-J.; Li, Z.-Y.; Lai, X.-Y.; Fang, L.-W.; Huang, W.-C., Sesamol suppresses the inflammatory response by inhibiting NF- κ B/MAPK activation and upregulating AMP kinase signaling in RAW 264.7 macrophages. *Inflammation Research* **2015**, *64* (8), 577-588.
82. Droge, W., Free radicals in the physiological control of cell function. *Physiological reviews* **2002**, *82* (1), 47-95.
83. Naka, K.; Muraguchi, T.; Hoshii, T.; Hirao, A., Regulation of reactive oxygen species and genomic stability in hematopoietic stem cells. *Antioxidants & redox signaling* **2008**, *10* (11), 1883-1894.
84. Dickinson, B. C.; Chang, C. J., Chemistry and biology of reactive oxygen species in signaling or stress responses. *Nature chemical biology* **2011**, *7* (8), 504.
85. Cadenas, E.; Davies, K. J., Mitochondrial free radical generation, oxidative stress, and aging. *Free Radical Biology and Medicine* **2000**, *29* (3-4), 222-230.
86. Finkelstein, E.; Rosen, G. M.; Rauckman, E. J., Spin trapping of superoxide and hydroxyl radical: practical aspects. *Archives of biochemistry and biophysics* **1980**, *200* (1), 1-16.
87. Suzen, S.; Gurer-Orhan, H.; Saso, L., Detection of reactive oxygen and nitrogen species by electron paramagnetic resonance (EPR) technique. *Molecules* **2017**, *22* (1), 181.
88. Zhao, H.; Joseph, J.; Fales, H. M.; Sokoloski, E. A.; Levine, R. L.; Vasquez-Vivar, J.; Kalyanaraman, B., Detection and characterization of the product of hydroethidine and intracellular superoxide by HPLC and limitations of fluorescence. *Proceedings of the National Academy of Sciences* **2005**, *102* (16), 5727-5732.
89. Agarwal, A.; Allamaneni, S. S.; Said, T. M., Chemiluminescence technique for measuring reactive oxygen species. *Reproductive BioMedicine Online* **2004**, *9* (4), 466-468.
90. Soh, N., Recent advances in fluorescent probes for the detection of reactive oxygen species. *Analytical and bioanalytical chemistry* **2006**, *386* (3), 532-543.
91. Kalyanaraman, B.; Hardy, M.; Podsiadly, R.; Cheng, G.; Zielonka, J., Recent developments in detection of superoxide radical anion and hydrogen peroxide: Opportunities, challenges, and implications in redox signaling. *Archives of biochemistry and biophysics* **2017**, *617*, 38-47.
92. Sun, X.; Xu, Q.; Kim, G.; Flower, S. E.; Lowe, J. P.; Yoon, J.; Fossey, J. S.; Qian, X.; Bull, S. D.; James, T. D., A water-soluble boronate-based fluorescent probe for the selective detection of peroxynitrite and imaging in living cells. *Chemical science* **2014**, *5* (9), 3368-3373.
93. Sponring, A.; Filipiak, W.; Ager, C.; Schubert, J.; Miekisch, W.; Amann, A.; Troppmair, J., Analysis of volatile organic compounds (VOCs) in the headspace of NCI-H1666 lung cancer cells. *Cancer Biomarkers* **2010**, *7* (3), 153-161.
94. Palazzolo-Ballance, A. M.; Suquet, C.; Hurst, J. K., Pathways for intracellular generation of oxidants and tyrosine nitration by a macrophage cell line. *Biochemistry* **2007**, *46* (25), 7536-7548.

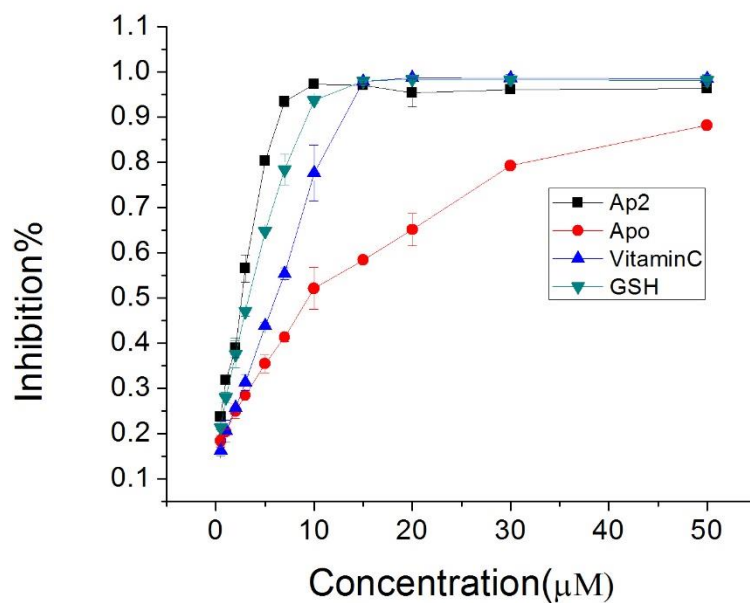
Appendices

Appendices S1: Reagent 1 reaction with Fenton generated hydroxyl radical is diffusion controlled.



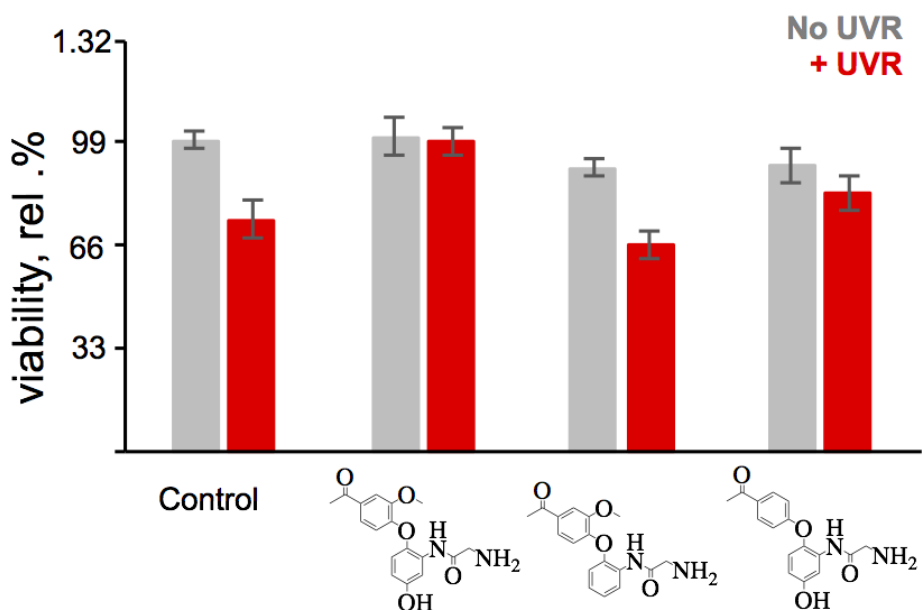
Appendices S1: Compound 1 reaction with hydroxyl radical is a diffusion-controlled reaction. Reaction rate increases with increase in concentration of hydroxyl radical generating Fenton system components, Fe²⁺ or peroxide. Thus, the reaction of the compound with hydroxyl radical is fast. Reaction can hardly happen on low level hydroxyl radical condition such as normal cells condition.

Appendices S2: ABTS Inhibition Study



Appendices S2: Compound 1 had an EC_{50} value of 2.4 (± 0.1) μ M, whereas the EC_{50} of 2 is 60 (± 1) μ M. Apocynin, catalase, glutathione, and vitamin C had EC_{50} values of 11.7 (± 0.4), 0.7 (± 0.1), 3.5 (± 0.2), and 7 (± 0.1) μ M, respectively.

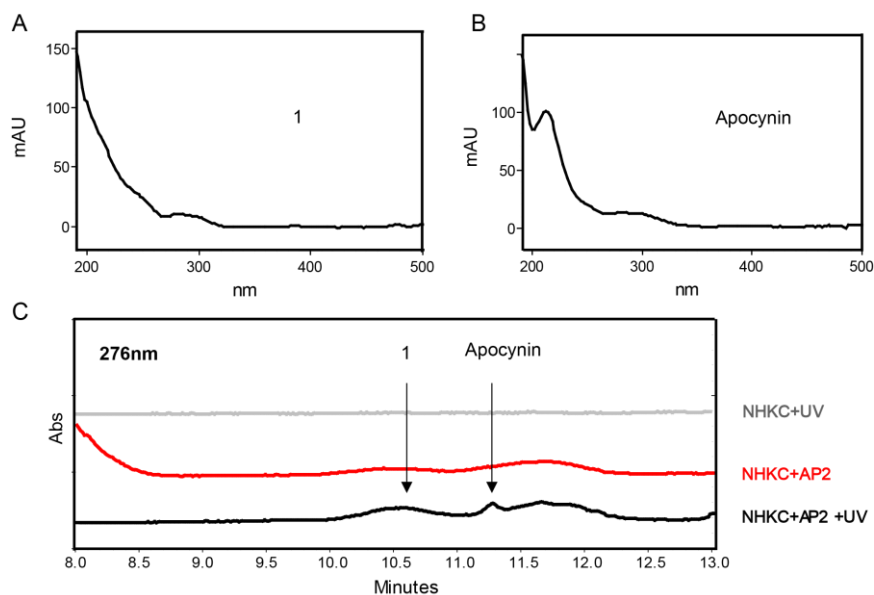
Appendices S3: The effect of compound 2 and a compound lacking apocynin release on viability and UVR rescue



Appendices S3: Viability of primary keratinocytes without (gray bars) and with 10 SED UVR (red bars) in the presence of the indicated compounds. UVR reduces viability while compound 1 (2nd from left) recues some cells. A derivative incapable of oxidation (compound 2, 3rd from left) and a compound lacks apocynin ejection (4th from left) fail to rescue cells from UVR treatment.

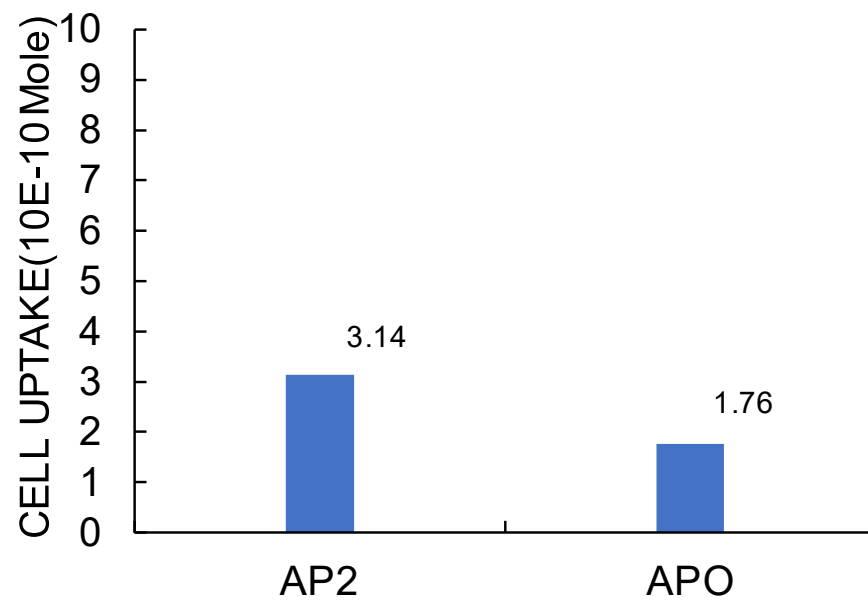
Appendices S4: Compound releasing in Neonatal human

keratinocytes cell (NHKC) after irradiation



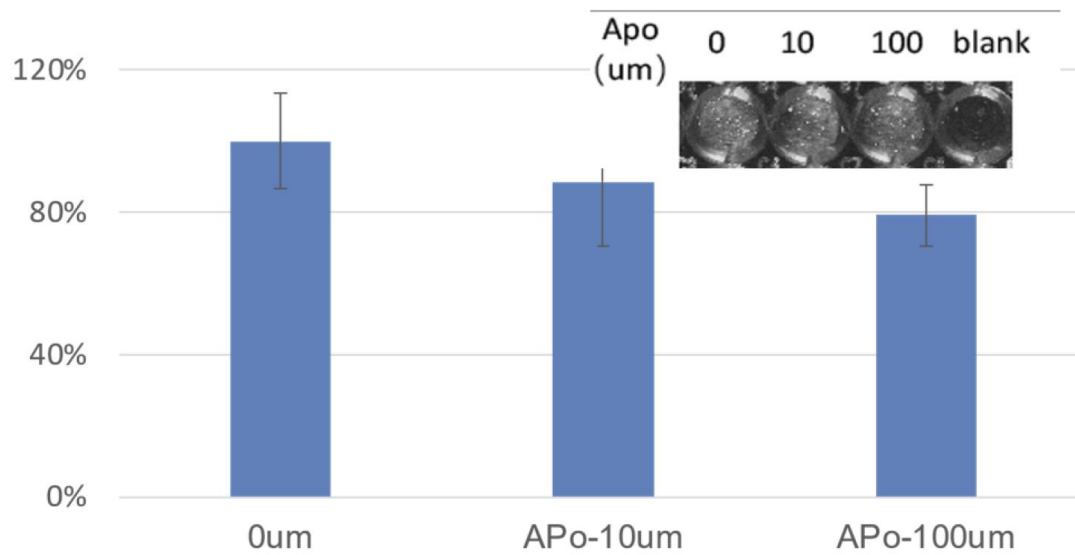
Appendices S4: For the aim of protecting cell from irradiation. **1** can quench ROS by reacting with it and release the effective compound apocynin. The profile for **1** (S2. B) and apocynin (S2.A) agree with the standard. HPLC show that the Control group which is just the NHKC cell release no apocynin nor AP2. Comparing to the sample pretreated with AP2 but not UC irradiation, **1** peak is detected in the sample which dosed with ap2 and irradiated with 10SED.

Appendices S5: Uptake of 1 and apocynin by cells.



Appendices S5: There is about 3.14×10^{-10} moles AP2 up taken by cells There is about 1.75×10^{-10} moles apocynin by for cells. The ratio for uptake of AP2 to apocynin is 9:5. So the amount of AP2 which remain in the cells is comparable to Apocynin.

Appendices S6: Western blot for Apocynin.



Appendices S6: The western blot and the bar plot of phosphorylation of Akt at Ser483 relative to the total Akt signal. The inhibitory effect of apocynin on Akt signaling pathway by inhibiting the NADPH oxidases (NOX). [1]10uM of apocynin inhibit 11% (+/-18%) Akt. 100uM of apocynin inhibit 21%(+/-9%) Thus apocynin inhibits NOX1 activity.

Abbreviations List

ROS--Reactive oxygen species

UVR--Ultraviolet radiation

DNA--Deoxyribonucleic acid

NOX--Nicotinamide adenine dinucleotide phosphate oxidase

NADPH--Nicotinamide adenine dinucleotide phosphate

HPLC--High-performance liquid chromatography

MS--Mass spectrometry

DCFDA--Dichlorofluorescein diacetate

CPD--Cyclobutane pyrimidine dimers

GCHSMS--Gas chromatography-headspace-mass spectrometry

LOD--Limit of detection

LOQ--limit of quantification

PKC--Protein kinase C

8-oxo-dG--8-oxo-7,8-dihydro-2'deoxyguanosine

GSH--Glutathione

EFGR--Growth factor receptor

ETC--Electrons transport chain

NOS--Nitric oxide synthase

XO--Xanthine oxidase

FAD--Flavin adenine dinucleotide

SOD--Superoxide dismutase

PGE2--Prostaglandin E2